Design of an Air-Breathing Electric Thruster for CubeSat Applications

1 author:

Stephen Wade Jackson
University of Colorado Boulder
2 PUBLICATIONS **2** CITATIONS

Some of the authors of this publication are also working on these related projects:

Project   Air-breathing Electric Thrusters View project

Design of an Air-Breathing Electric Thruster for CubeSat Applications

by

Stephen W. Jackson

B.S., University of Colorado, Colorado Springs, 2010

A thesis submitted to the

Faculty of the Graduate School of the

University of Colorado in partial fulfillment

of the requirements for the degree of

Masters of Science

Department of Aerospace Engineering Science

2017

This thesis entitled:
Design of an Air-Breathing Electric Thruster for CubeSat Applications
written by Stephen W. Jackson
has been approved for the Department of Aerospace Engineering Science

_____
Prof. Robert Marshall

_____
Prof. Lakshmi Kantha

_____
Prof. Scott Palo

Date _____

The final copy of this thesis has been examined by the signatories, and we find that both the content and the form meet acceptable presentation standards of scholarly work in the above mentioned discipline.

Jackson, Stephen W. (M.S., Aerospace Engineering)

Design of an Air-Breathing Electric Thruster for CubeSat Applications

Thesis directed by Prof. Robert Marshall

The altitude range between 120 and 300 km is relatively unexplored with regard to space weather, atmospheric models, climate observations, the global electric circuit, remote sensing, and intelligence gathering. This altitude range is not conducive to to in situ measurements due to the high magnitudes of drag that are experienced by satellites at these altitudes. The concept of air-breathing propulsion systems have been proposed to counteract drag. These propulsion systems produce thrust through electrostatic propulsion by ionizing the background neutral atmospheric particles. The atmospheric neutral particles that are the cause of drag at these altitudes are used as the fuel source for these air-breathing thrusters. Systems have been conceptually designed for larger satellites, but in this work we show that is possible for CubeSats to employ similar systems. CubeSats are a relatively new technology that have allowed low cost satellites to be built by a variety of entities including universities and private companies at low cost and with rapid development cycles. Due to current restrictions, CubeSats are not allowed to carry propellant. This limits CubeSats from maneuvering, formation flying, orbit raising, drag make-up, and deorbiting. However, this has not prevented the study and design of propulsion systems for CubeSats, with the anticipation of the propellant restrictions being lifted.

In this research, a concept for an air-breathing ion thruster is designed for the use in 3U, 6U, 12U, and 27U Cubesats. The design is created to be modular to this system, and each component is discussed separately. An analysis is conducted to determine the best inlet shape for capturing atmospheric particles. This analysis is conducted using a 3D Monte Carlo simulator. The ionization of atmospheric particles is investigated, and issues with ionization of the particles given the design of the system are discussed. Based on the expected inlet capture efficiency and ionization efficiency, the thrust capabilities of the system are projected for the various CubeSat standard sizes in LEO

altitudes (80 km to 600 km). Analysis of the thrust based on CubeSat size, voltage, solar activity, and ionization efficiency is also conducted herein. This work shows that it is possible to build air-breathing propulsion systems for CubeSats with thrust exceeding the local drag in LEO altitudes.

Dedication

> "Imagination is more important than
> knowledge. For knowledge is limited,
> whereas imagination embraces the
> entire world, stimulating progress,
> giving birth to evolution."
>
> *Albert Einstein, 1929*

I dedicate this work to my God, who created the heavens above, who loved me first, whose grace abounds, and who gave me the wisdom and knowledge to accomplish this task. No matter where I go, your hand shall lead me and your right hand shall hold me.

Acknowledgements

Firstly, I would like to thank my adviser, Dr. Bob Marshall. He took me on as a graduate student in his first year at CU, and gave me the latitude to do research in a focus area that is very important to me. I'm grateful for his guidance, support, and expertise in plasma physics and electrical engineering without which this work would not have been possible. I would also like to thank my committee members. I would like to thank Dr. Lakshmi Kantha for kindling my passion for rocket and space propulsion and supporting my efforts herein. I would also like to thank Dr. Scott Palo for his expertise with respect to CubeSats and sharing his wealth of knowledge in support of this paper.

I would also like to thank my parents for their constant love and support. I want to thank my brother and sister-in-law for housing me for more than a year during this time. You gave me mental and emotional support throughout this process, and I'll be forever grateful for it. To the rest of my family, big and small, thank you for your support during this time. Thank you to my friends, especially the K's and the Y's, for making sure I took breaks and had fun outside of research.

Contents

Chapter

Tables

Table

Figures

Figure

Chapter 1

Introduction

1.1   Motivation and Proposal

The region of the atmosphere and ionosphere between 120 km to 300 km is relatively unexplored [*Voss et al.*, 2015]. CubeSats have the potential to be a cost effective platform to observe this region of the atmosphere if equipped with a propulsion system to counteract drag effects at these lower altitudes. Currently, CubeSats are restricted to use in altitudes below 600 km with missions below 250 km lasting only a matter of hours due to the large drag that the CubeSat would experience [*Oltrogge and Leveque*, 2011]. CubeSats have become increasingly popular for their low cost and short production time compared to larger satellites. The most commonly used sizes of CubeSats are the 1U (10 cm × 10 cm × 10 cm), 3U (10 cm × 10 cm × 30 cm), and 6U (10 cm × 20 cm × 30 cm) with the 6U being the largest launchable size allowed. CubeSats are not allowed to have an on board propulsion systems [*NASA*, 2014]. Propulsion systems have the potential to both decrease the orbit degradation at lower altitudes, extend mission lifetime, and allow for orbit maneuvers, formation flying, orbit raising, and de-orbiting. Larger CubeSats (6U, 12U, and 27U) will be cleared for launch on NASA's SLS once it is operational. These larger CubeSats will give a larger platform for a propulsion system to be implemented.

There are many traditional systems that could be used for propulsion in CubeSats such as cold gas thrusters, monopropellants, and solid propulsion [*Burkhardt et al.*, 2002]. Cold gas thrusters are simple and reliable, but commonly have low specific impulse (Isp) and only moderate impulse capabilities. Monopropellants are a proven technology with a wide thrust range, but also

have low Isp and commonly use toxic fuel [*Burkhardt et al.*, 2002]. A solid rocket motor has been designed and tested for nanosatellite applications [*Faber*, 2013]. Solid-rocket motors are highly reliable; however testing is still being done in order to reduce the particulates expelled from the exhaust in this application. Such particles would only add to the current orbital debris concerns [*Lücking et al.*, 2012]. Solid propulsion systems also have the disadvantage of lasting for only one use unlike chemical or electric propulsion systems [*Burkhardt et al.*, 2002]. Propellant-less concepts have been researched as well. Solar radiation pressure augmentation for small satellites is one such idea that has been recently proposed specifically for deorbiting. Using a deployable sail or balloon made of a reflective surface, this sail, directed towards the sun, would increase the area-to-mass ratio of the satellite and in turn produce enough aerodynamic drag to deorbit the satellite [*Lücking et al.*, 2012]. This design is promising for propulsion in general, but such solar sails can be very fragile and susceptible to destruction by space debris. Electromagnetic tethers are another option considered for propulsion on satellites. The tether, stored in the CubeSat, would deploy and a small amount of power would be used to generate an electric current through the tether which would produce thrust via the Lorentz force. A major advantage of this technique is the mass savings because it wouldn't require propellant [*Pardini et al.*, 2006]. However, concerns with this concept is the length of the tether which could potentially be severed by space debris thus creating more space debris, and the tether could possibly impact other larger space objects.

Research has begun over the past 15 years regarding air-breathing electric propulsion (ABEP), sometimes referred to as atmosphere-breathing electric propulsion or ram-electric propulsion (RAM-EP), with the primary interest being drag make-up and mission extension for extremely low earth orbit (ELEO) satellites. Traditional systems could be used, but the amount of propellant that would have to be stored to extend the lifetime by any significant amount would be prohibitive. Instead of storing propellant, air-breathing thrusters use the atmosphere in low earth orbit (LEO) as propellant.

Conley [1995] proposed the idea of a deployable ionization chamber with acceleration grids. The chamber deploys from a larger satellite operating at or below 200 km. The actually size of

the propulsion system would be 5 m wide and 15 m in radius and use about 2.9 kW of power to operate. Using ambient gas, the particles would be ionized by the satellite's trailing rings, and then accelerated through the subsequent acceleration grids as shown in Figure 1.1.
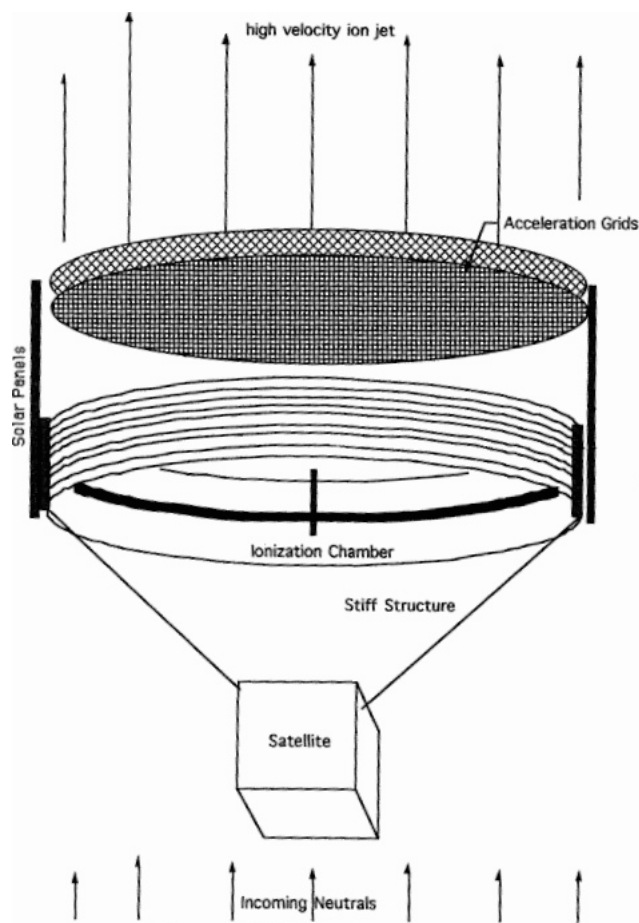
Figure 1.1: The LEO ion thruster concept uses a deployable ionization chamber and grid system that allows the ambient neutral particles to flow through the system, be ionized, and then accelerated through a grid [*Conley*, 1995].

Conley effectively proved that the drag make-up using such a system was feasible at these altitudes; however, the size makes his design unfeasible for application. Conley understood this, and suggested that if slow ions could be contained in the ionization cavity with the circulating electrons, the density could be increased thus allowing for a smaller more efficient thruster [*Conley*, 1995].

Unlike Conley's design, *Dressler* [2006] proposed an ion engine with a similar open system that uses the ambient ionosphere at altitudes less than 1000 km. Dressler claimed that such a system could not only be used for drag make-up operations and orbit changes, but might also serve as a station keeping system on the ISS. Figure 1.2 shows an example of Dressler's Ambient Atmosphere Ion Thruster (AAIT). The system uses two or more electrically charged grids, separated by some distance. Unlike conventional ion thrusters, the grids used in Dressler's concept would have large holes to "minimize the amount of gas flux blocked from entering and exiting the volume contained between the 'grids' " [*Dressler*, 2006]. Like Conley's concept ion thruster, Dressler's concept would also need to be very large in order to counteract the aerodynamic drag.
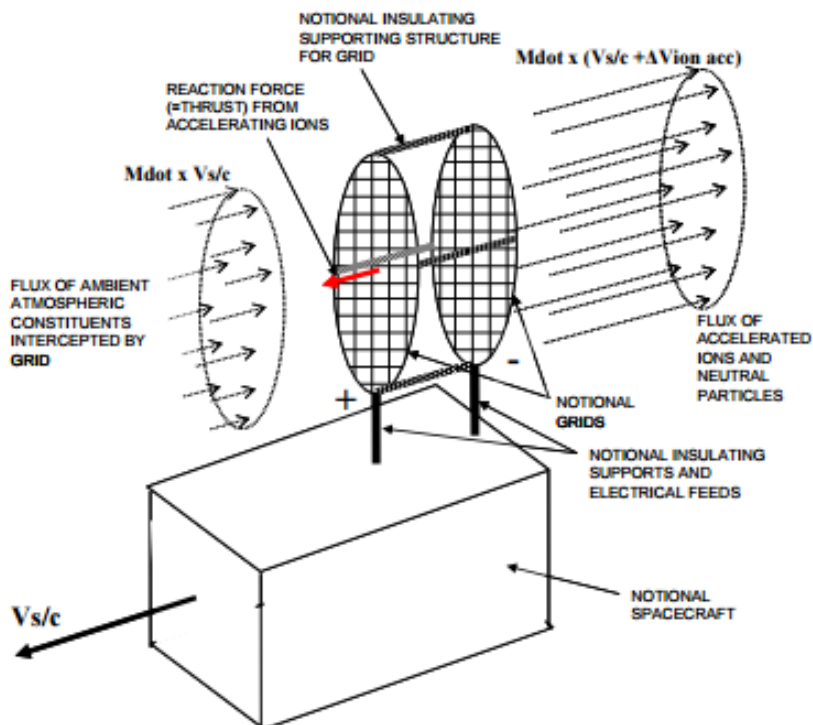
Figure 1.2: The ambient atmosphere ion thruster uses a deployable ionization chamber and grid system that allows the ambient neutral particles to flow through the system, be ionized, and then accelerated through a grid [*Dressler*, 2006].

According to [*Singh and Walker*, 2015], Dressler's design relied on two major assumptions that ultimately limited the accuracy of the AAIT's analysis. Firstly, Dressler assumes a drag

coefficient of 2 where it is known that the coefficient of drag exceeds 2 in most cases and also varies with orbit altitude. Secondly, the local space potential is ignored [*Singh and Walker*, 2015]. The major problem occurs in the second assumption because by the nature of Dressler's design, the local space potential and the potential of the neutrals are equal which means that the voltage potential between the grids does not produce any acceleration. The incoming ions would need to have an increase potential above the local space charge in order for ions to be accelerated in the grids. Followup research conducted by *King et al.* [2014] on Dressler's model, removed this simplifying assumptions, and did show that with additional ionization of the flow and a proper coefficient of drag, that drag compensation via "atmospheric propulsion" was possible with a compressing inlet [*Singh and Walker*, 2015].

During this same period of time, Japanese researchers were working on RAM-EP designs as well. *Nishiyama* [2003] proposed the concept of an ion thruster with a similar methodology; however, instead of a deployable grid, the system would be attached on the outside of a satellite vehicle. The proposed system would have long narrow tubes to capture the particles, and then an electron cyclotron resonance (ECR) microwave discharge to ionize the incoming particles before being accelerated through a grid. For this thruster, two critical assumptions are made. Firstly, that the thermal velocity of incoming particles are much slower than the velocity of the space vehicle, and secondly that the mean free path of the particles is much greater than the length of the inlet [*Singh and Walker*, 2015]. Figure 1.3 shows the concept of what Nishiyami calls the air-breathing ion engine (ABIE). The collimator proposed by Nishiyami is one of two well-known, proposed methods for atmospheric particle collection. With the collimator, there is a higher capture of incoming air with a low amount of loss for particles trying to escape [*Singh and Walker*, 2015].
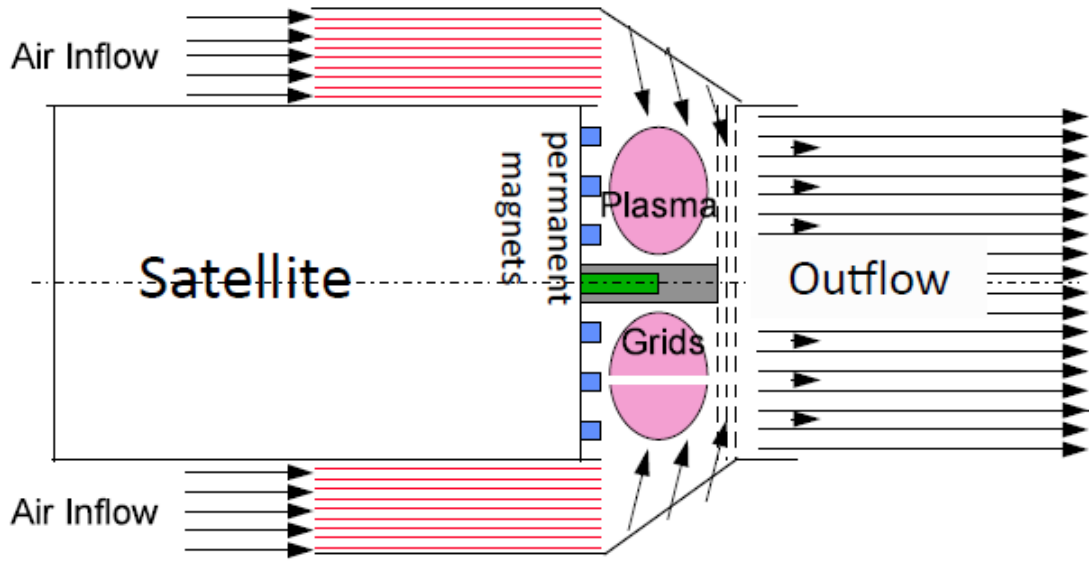
Figure 1.3: The air-breathing ion engine design forces the neutral particles to enter long narrow tubes before being ionized in order to increase particle capture and prevent losses back out of the inlet due to diffuse deflection [*Nishiyama*, 2003].
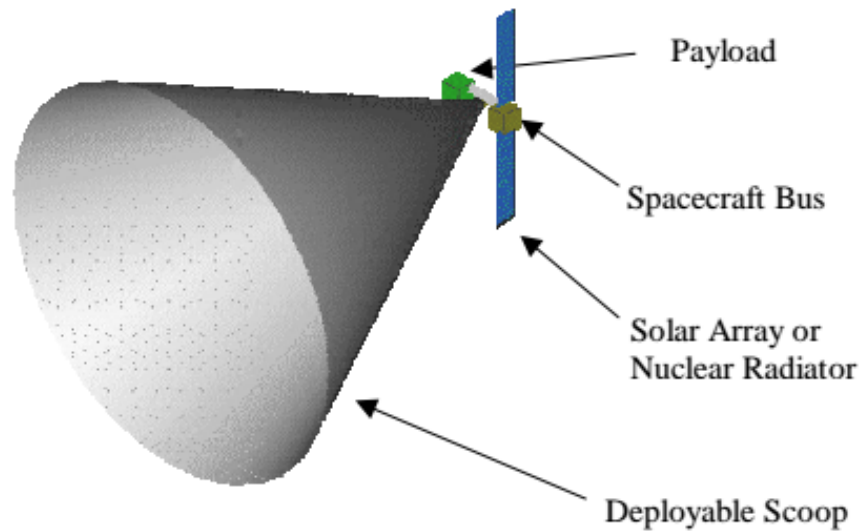
Figure 1.4: McGuire's Scoop Inlet Concept is depicted as very large conical scoop with respect to the satellite here; however his research shows that the scoop would not have to be as large as expected to get the intended particle capture [*McGuire*, 2001].

In contrast to Conley's and Dressler's passive capture approach, and as an alternative to Nishiyama's collimated capture method, a "scoop" collection concept was proposed by *McGuire* [2001]. For this concept, it is assumed the given space vehicle is operating below 200 km and more desirably at 100 km. At these altitudes, the scoop must be modeled for use in the transition region where the flow goes from continuum to free molecular, and shocks forming at the front of the scoop must also be taken into account [*McGuire*, 2001]. Figure 1.4 shows the proposed scoop deployed from a satellite. McGuire's and Nishiyama's methods have competing views on the behavior of the flow; however, they both conclude that the smaller the inlet the greater the capture percentage [*Singh and Walker*, 2015]. McGuire's method is preferable when the flow has the potential of transitioning into hypersonic continuum flow which is highly likely given McGuire's intended application of skirting the lower atmosphere with this conical collector. The difference of the two is that Nishiyama desires to stay in ELEO whereas McGuire's inlet designed for use in LEO and possibly even geosynchronous equatorial orbit (GEO).

Hall thrusters have also been studied for air-breathing systems as well. *Pigeon and Whitaker* [2004] first proposed the Hall thruster for air-breathing propellant, and it was similar to that of Dressler's and Conley's that used an "open" system. This first attempt at such a Hall Thruster did not produce enough thrust to be considered feasible for use in drag make-up scenarios [*Singh and Walker*, 2015]. Similar to the design of Dressler, *Pekker and Keidar* [2012] proposed a concept that brought the incoming flow directly into a Hall acceleration chamber. This system was determined to be ideal between 90 km and 95 km, but Pekker and Keidar's conclusion was that if the pressure of the flow were raised it might have uses at higher altitudes [*Pekker and Keidar*, 2012]. The limiting factor with this design was determined to be the power requirements which were unrealistic under normal operations [*Singh and Walker*, 2015].

Also of note are the works of Diamant and Shabshelowitz who have both analyzed the use of a 2-stage Hall Effect Thruster (HET). The two stages are the ionization stage and the HET used for acceleration. Diamant, like Nishiyama, chose an ECR for ionization [*Diamant*, 2010] while Shabshelowitz also uses a magnetic field along with an antenna to ionize the incoming neutrals

[*Shabshelowitz*, 2013]. Figure 1.5 shows the two-stage HET as realized by Shabshelowitz which has little difference from a standard Hall effect thruster [*Singh and Walker*, 2015]. Much like the Ion thruster, the HET would require little to no modification in order to use the ambient atmosphere as a propellant.
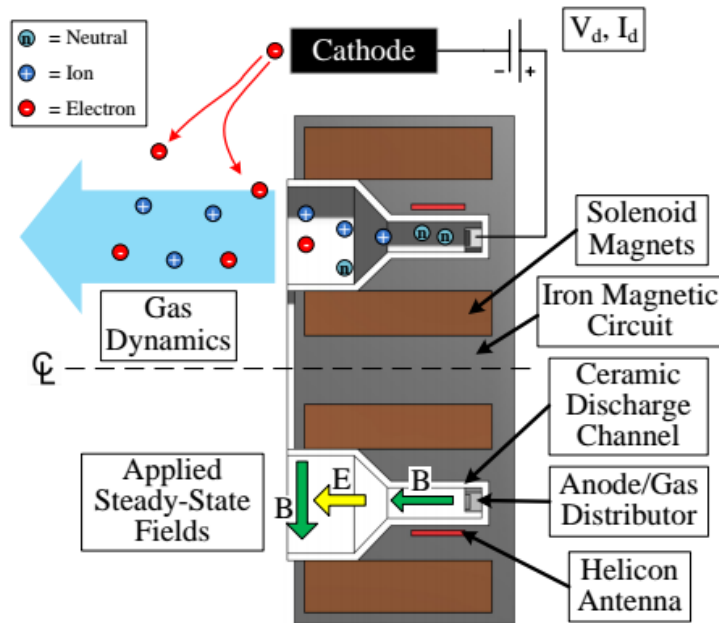
Figure 1.5: The 2-stage Hall-effect thruster first stage uses an axial magnetic field and antenna for ionization and the second stage uses a traditional HET for acceleration of the ionized particles [*Shabshelowitz*, 2013].

1.2   Research Contribution

These above listed air-breathing thrusters are designed for medium to large satellites (500-1000 kg). The intent and purpose of this paper is to show that these air-breathing thrusters are a viable option for use on a CubeSat, in order to extend their operations in LEO for drag make-up.

Although air-breathing thrusters are under development for CubeSats [e.g., *Voss et al.*, 2015], there has yet to be an extensive analytical study on the subject. Along with this analysis of the

thrust of a system this size, the structure will be discussed with specific focus on the inlet whose design is vital to the operation of such a system.

This work seeks to answer the following questions regarding air-breathing systems for CubeSat applications:

- **Are air-breathing systems a viable option for drag make-up on CubeSats of 3U, 6U, 12U, and 27U sizes?**

  The 6U, 12U, and 27U CubeSat sizes are not currently cleared for any current launch system; however, once NASA's SLS is online, these CubeSats will become part of the standard sizes of CubeSats allowed. These size CubeSats are also more capable than their smaller predecessors to have propulsion systems on-board. This research attempts to show how effective air-breathing systems would be for these CubeSats.

- **For an internally housed air-breathing thruster, what is the best inlet design?**

  Most of the previous air-breathing designs have relied on deployable or external satellite structures for the system to operate. The proposed design detailed in this research is for an internally housed thruster that fits within the CubeSat frame. The inlet is an essential part of the air-breathing system as the more particles are captured, the better the thruster performance. This research will analyze viable shapes (some previously proposed), and highlight a unique solution to the inlet.

1.3   Overview

Following this introduction, Chapter 2 will give a history of electric propulsion (EP), an overview of electric propulsion types, an analysis of why the ion thruster was the EP type chosen for this research, and a brief overview of the proposed system and its complexities.

In Chapter 3, the orbital and atmospheric factors that will impact the air-breathing system and its design are discussed in detail with a particular focus on the rarefied nature of the atmosphere and gas-surface interactions.

Chapter 4 will detail the inlet design of the proposed system, showing an analysis of different types of inlet shapes. The particular issues concerning air-breathing systems and rarefied flow are discussed next, along with proposed solutions to certain issues.

Chapter 5 focuses on ionization and ion confinement. The plasma physics involved are out of the scope of this paper, and an entire PhD thesis could be centered on the development of a feasible ion confinement sysstem in an air-breathing thruster. However, a broad overview of the ionization process and potential options for this system regarding ion confinement are discussed.

In Chapter 6, the analysis of the thrust of the proposed air-breathing CubeSat thruster system is detailed. The performance of different sizes and configurations of this air-breathing system are compared. These thrust outputs are evaluated against drag, and the power requirements of this system are discussed.

Chapter 7 summarizes the findings of this paper and the accomplishments made; some recommendations for future work are discussed.

Chapter 2

Electric Propulsion

RAM-EP is a thruster concept that utilizes the neutral particles in Earth's orbit as a propellant. This chapter will briefly discuss the history of electric propulsion, the types of EP, and give a brief overview of the proposed air-breathing system.

2.1   Electric Propulsion: A Brief History

Electric propulsion was first conceived in the early 20th century. The matter of who first proposed it is up for debate, but this seems trivial in comparison to the momentous advancement of science that occurred just by the mere proposal of the concept. Robert Hutchings Goddard and Konstantin Eduardovitch Tsiolkovsky were men on the opposite sides of the world both daring to explore the possibility that atomic particles could produce large velocities for propulsion purposes [*Choueiri*, 2004]. Both of these men were working with early studies on electrons and electricity. The idea that ions could be used was not immediately considered because the underlying physics for production of electron-ions pairs was yet to be fully defined. As the science developed so did the capabilities of such a system, and Goddard proposed the world's first documented electrostatic thruster in 1920 [Figure 2.1; *Choueiri*, 2004].
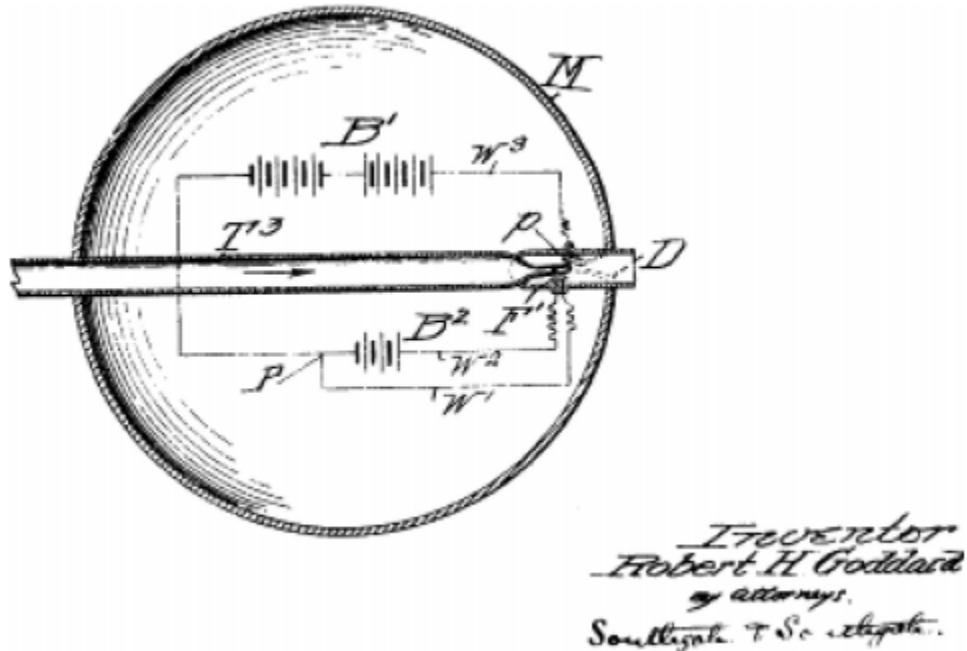
Figure 2.1: The world's first documented electrostatic thruster was patented by Robert Goddard. It was the third variant of the original 1917 invention [*Choueiri*, 2004].

However, Goddard's and Tsiolkovsky's work was seen by very few until decades later. Electric propulsion wasn't seriously pursued for application until after World War II. This hiatus in EP development was due to several factors. Firstly, chemical rockets were not yet capable of launching spacecraft from Earth. Creating better chemical rockets became the primary focus before EP was to be considered further. Secondly, EP systems are of little use in wartime, and with World War II in full swing, most if not all propulsion research was centered on rockets for military uses. Thirdly, electric thrusters required the vacuum of space to operate. Such laboratories and testing facilities at the time were incapable of simulating such an environment for testing of EP [*Choueiri*, 2004].

The next 10–20 years after the end of World War II began to see a resurgence in EP research and studies. If the previous generation of researchers were the visionaries, this new generation were the developers who built upon the earlier works. In this time before Sputnik launched, several key components that govern electric propulsion today were established [*Choueiri*, 2004]:

- The need for a high atomic weight propellant to make the most of the acceleration of the particles

- The necessity of beam neutralization via injecting electrons into the outlets' plume

- The use of two grids placed a small distance apart to produce the electric potential

With the first in-depth and detailed EP system outlined in 1954 by Ernst Stuhlinger [*Choueiri*, 2004], EP has since continued to grow in its application. The first tests of EP systems in space began in the early 1960s by both the United States and the Soviet Union. These systems were used and still are for station keeping. In the modern era, EP systems have been adopted for commercial use as well for station keeping, and electric propulsion has more recently been used for orbit insertion as well.

2.2 Electric Propulsion Types

2.2.1 Electrostatic Propulsion

In electrostatic propulsion, a suitable propellant is ionized, and ions are then accelerated to high velocities via an electric field [*Kantha*, 2017]. The ions are passed through perforated grids that have a voltage differential. The outgoing plume is then neutralized with an electron stream to prevent charge buildup. Common propellants for electrostic systems are cesium, argon, and xenon [*Kantha*, 2017].

The Field Emission Electric Propulsion (FEEP), Ion, and Hall-effect Thrusters (HETs) are examples of electrostatic propulsion. In FEEP thrusters, ions or charged droplets are extracted from conductive liquids, funneled through small needles, and electrostatically accelerated through biased, aligned openings [*Goebel and Katz*, 2008]. FEEP thrusters generate very low thrust. Ion thrusters are known for using a variety of plasma generation techniques to ionize a significant portion of the propellant. Biased grids (surfaces with many apertures) are used to electrostatically accelerate the extracted ions [*Goebel and Katz*, 2008]. Ion thrusters have the highest efficiency and

have a very high specific impulse compared with other electric thrusters [*Goebel and Katz*, 2008]. HETs generate plasma via a cross-field discharge described by the Hall effect. An electric field aligned perpendicular to the magnetic field accelerates the ions while a transverse magnetic field prevents electron motion from shorting out the electric field [*Goebel and Katz*, 2008]. HETs have less efficiency and a lower specific impulse compared to ion thrusters; but their thrust-to-power ratio is higher, they are simpler in design, and require fewer power supplies to operate [*Goebel and Katz*, 2008]. Figure 2.2a and Figure 2.2b show the common geometry for ion and Hall Effect thrusters, respectively. Both the ion thruster and HET have been scaled down to smaller sizes for use in small and power-limited satellites. For eaxmple, a micro-HET was developed by *Ito et al.* [2006] that operates in the 10–40 W range with an outer diameter of 4 mm.
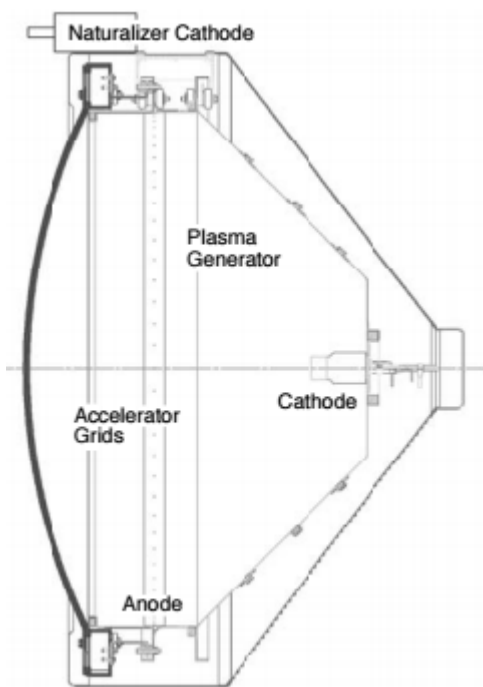
(a) Ion thruster geometry [*Goebel and Katz*, 2008]
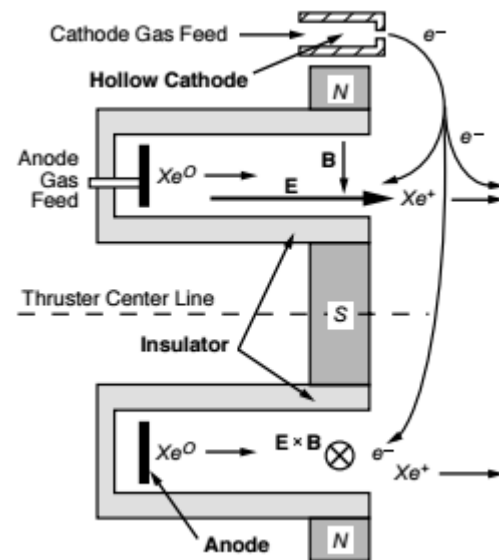
(b) Hall thruster geometry [*Goebel and Katz*, 2008]

2.2.1.1   Micro-Ion Thrusters

The miniaturization of ion thrusters has its challenges, but over the past 40 years, they have been successfully scaled in order to meet specific mission parameters. "Micro" ion thrusters are usually less than 3 cm in diameter, and produce thrust in the mN to sub-mN range [*Wirz*, 2015]. Figure 2.3a shows the MiXi thruster designed by a Caltech/JPL/UCLA collaboration which is 3 cm in diameter, has thrust in the range of 0.1 to 1.5 mN, and a specific impulse between 1764–3184 s [*Wirz*, 2015]. The thruster in Figure 2.3b, developed by the Japan Aerospace Exploration Agency, has a 2 cm diameter, a thrust of about 0.3 mN, and a specific impulse of about 1400 s [*Wirz*, 2015].
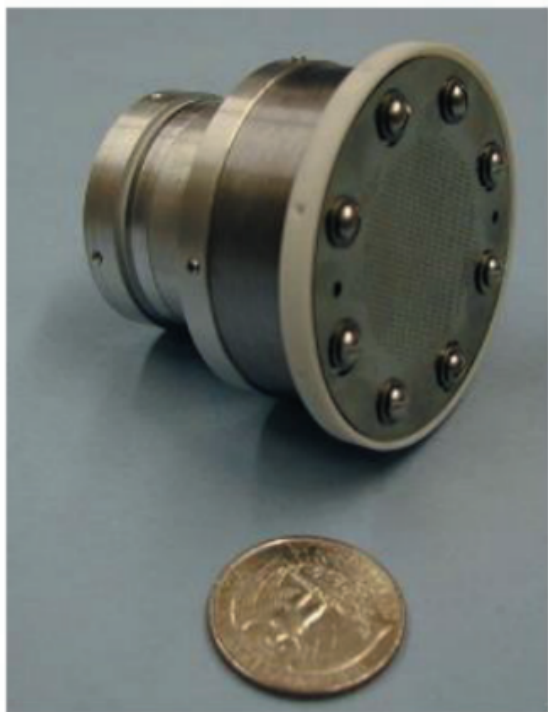
(a)   (b)

Figure 2.3: Examples of micro ion thrusters. (a) MiXi thruster (b) μ1 thruster [*Wirz*, 2015]

The ion beam's interaction with the spacecraft and contamination is generally a concern for ion thrusters. However due to their low beam divergence half-angle ($5 - 15°$) and quiet electrical operation, micro ion thrusters' beams interact less with the spacecraft [*Wirz*, 2015]. These scaled

thrusters are also capable of a higher Isp which is another advantage they have compared to their larger counterparts.

2.2.2   Electromagnetic Propulsion

Unlike electrostatic thrusters, the working propellant for electromagnetic EP is a plasma, "a collection of various charged particles that are free to move in response to fields they generate or fields that are applied to the collection" [*Goebel and Katz*, 2008]. In such a system the plasma is created by heating the initial propellant to high temperatures (> 5000 K) [*Kantha*, 2017]. The plasma acts as an electrical conductor, and with the magnetic field perpendicular to the current, the Lorentz Force acts on ions. A common propellant for these systems is xenon.

The Pulsed Plasma Thruster (PPT) and Magnetoplasmadynamic (MPD) engines are examples of electromagnetic propulsion. The PPT uses an pulsed electrical discharge to ablate a solid propellant source into a plasma arc [*Goebel and Katz*, 2008]. The electromagnetic effects in the pulse accelerate the ions. The thrust level is determined by the pulse rate [*Goebel and Katz*, 2008]. The MPD use a very high current arc to ionize a large portion of the available propellant. Then the electromagnetic forces (Lorentz forces) in the plasma discharge in turn accelerating the ionized propellant [*Goebel and Katz*, 2008]. The plasma discharge in these systems, commonly generate both the current and the magnetic field. This requires MPDs to consume a lot of power in order to produce the high specific impulse and high thrust compared to most other EP systems [*Goebel and Katz*, 2008]. Figure 2.4 shows a schematic detailing how the MPD thruster works.
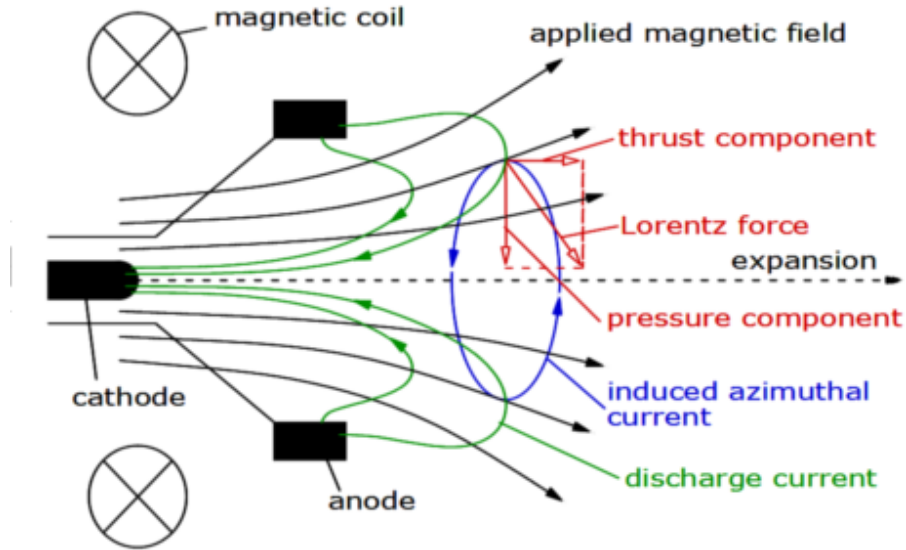
Figure 2.4: Magnetoplasmadynamic thruster schematic [*Institute for Space Travel Systems, University of Stuttgart*, 2016]

2.2.2.1   New Applications

The Electrodeless Lorentz Force (ELF) thruster is important to mention as it is employs technology that may be useful to future RAM-EP concepts. The ELF thruster generates a high-density, magnetized plasmoid by use of a rotating magnetic field. An axial magnetic field gradient is generated, and this in turn accelerates the plasmoid [*Slough and Kirtley*, 2015]. Slough and Kirtly's work on this ELF thruster relies on the argument that the molecular weight of the propellant is directly proportional to the thruster's efficiency. The key feature then of the ELF thruster involves injecting neutral particles downstream of the already ionized neutrals. This in turn generates newly ionized particles at no cost and thus increases efficiency. Currently this system has only been tested using neon [*Singh and Walker*, 2015]. Figure 2.5a shows the constructed ELF thruster undergoing testing.
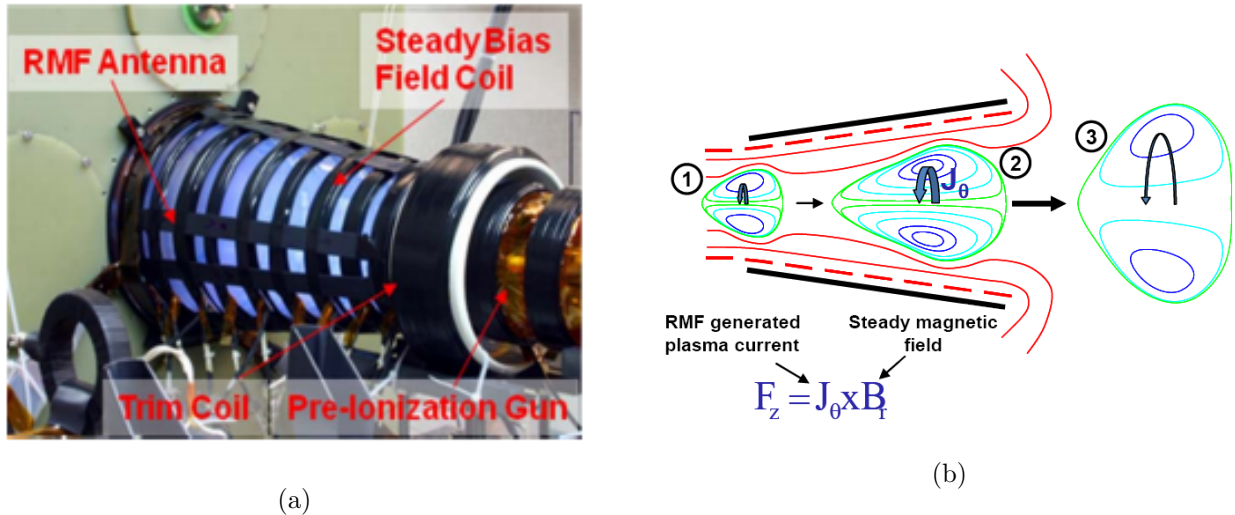
Figure 2.5: (a) The ELF Thruster (b) ELF Thruster Operation: (1) Rotating Magnetic Fields (RMF) form high-density, Field Reversed Configuration (FRC) plasmoid (2) FRC grows and accelerates driven by RMF generated currents and steady field (3) FRC expands as ejected, converting any remaining thermal energy into directed energy [*Slough and Kirtley*, 2015]

The VASIMR engine being developed by NASA is another electromagnetic thruster worth mentioning for air-breathing applications. VASIMR stands for Variable Specific Impulse Magneto-plasma Rocket and is shown in Figure 2.6. It is being created for quick travel to Mars; however, it also has the potential to be used as an OTV (Orbital Tow Vehicle). VASIMR uses radio waves to ionize the gas propellant, and then a powerful magnetic field generated by superconducting magnets accelerates the plasma. Unlike ion thrusters and HETs, the VASIMR does not use electrodes, which erode over time; and therefore has a longer engine life. The VASIMR can operate on a variety of gases (hydrogen, helium, argon) as well. An important element of this system, with regards to the topic of this paper, is that it runs on hydrogen which is relatively abundant within Earth's atmosphere. The developers of the VASIMR engine state that it could be refueled without assistance which implies that this technology could potentially be using some sort of air-breathing system [*NASAexplores*, 2013]. The downside to the VASIMR though is that its magnetic field is

very strong (1–2 Teslas) meaning it could affect other systems or payloads, and in turn, it has very high power demands [*Kantha*, 2017].
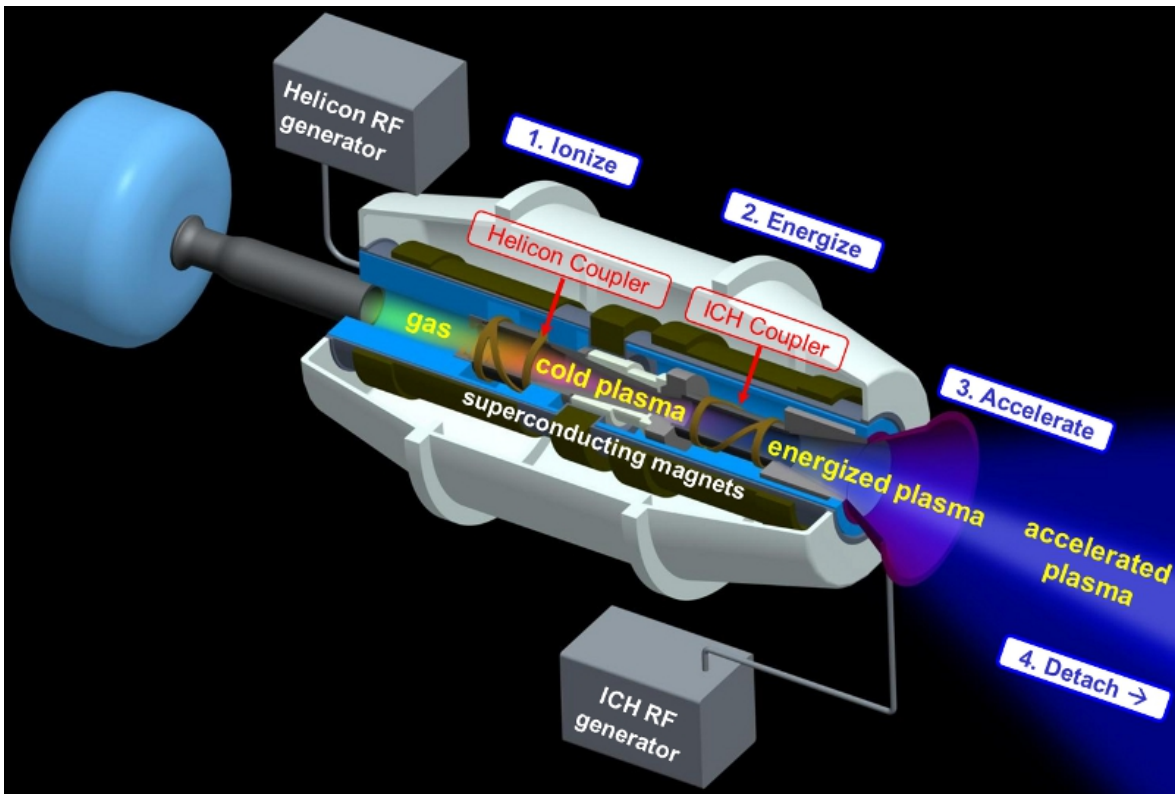
Figure 2.6: VASIMR engine detailed cut-away view

2.2.3   Electrothermal Propulsion

The two most common applications of electrothermal propulsion are the resistojet and arcjet thrusters. In a resistojet, the propellant is heated by either passing over a resistively heated element or through a resistively heated chamber before moving through a nozzle downstream [*Goebel and Katz*, 2008]. The thrust for electrothermal propulsion systems is generated by the heating of the propellant. Resistojets commonly use hydrazine and have a thruster efficiency of 65-85% [*Kantha*, 2017]. The arcjet differs from the resistojet thruster in that it uses a high current arc on-axis with the nozzle feed system to heat the propellant [*Goebel and Katz*, 2008]. Both of these systems have very low Isp in comparison to the aforementioned thrusters [*Burkhardt et al.*, 2002].

2.3   Components of Electric Thrusters

Electric thrusters can be broken down into three main components: ionization chamber, acceleration, and neutralization. In this section, the ionization chamber and the acceleration grids will be discussed as they apply to Ion Thrusters. The neutralizer cathode will be briefly discussed; however, its operation will be assumed to be fairly standard on the proposed air-breathing system.

2.3.1   Ionization Chamber

Also referred to as plasma generators, the ionization chamber ionizes the propellant before reaching the acceleration grids. For most standard electric thrusters xenon is the preferred propellant of choice due to its high molecular mass and the fact that it does not need cryogenic storage [*Kantha*, 2017]. There are three common methods used in electric propulsion to generate plasma from a neutral gas:

(1) direct current (DC) electron discharge

(2) radio frequency (RF) discharge

(3) microwave discharge

The basics of any ionization chamber includes a neutral particle inlet and some electron source. This basic structure is shown in Figure 2.7 which also shows the accelerator grids that follow the chamber.
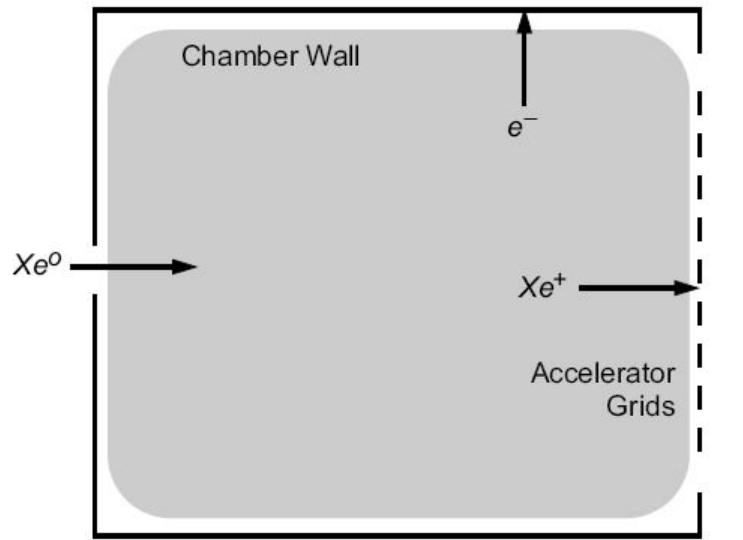
Figure 2.7: Basic Ionization Chamber for a DC-discharge electron bombardment ion thruster [*Goebel and Katz*, 2008]

2.3.1.1   DC Discharge

A DC discharge ionization chamber uses a hollow cathode tube electron source and an anode potential discharge chamber. The neutral propellant is injected into the discharge chamber and also through the hollow cathode. The extracted electrons from the cathode enter the discharge chamber, collide with the neutral particles, and ionize the propellant. Surrounding the discharge chamber are permanent magnets which are primarily used to confine the electrons. This improves the length of time before the electrons hit the anode wall and are lost, and in turn, this increases the ionization probability [*Goebel and Katz*, 2008]. The percentage of neutral propellant ionized is dependant on the energy expended. Since not all of the neutrals are ionized, they can absorb energy from the ions and in turn defocus the beam [*Kantha*, 2017]. The key component in this design is the placement of the magnetic field to confine the electrons and ions in the chamber to ultimately produce uniform plasmas. The first design for the magnetic fields used a solenoidal or mildly divergent magnetic field still used in Kaufman thrusters. Today the permanent magnet ring-cusp thruster designed by Sovey is the most widely used thruster design [*Goebel and Katz*, 2008].
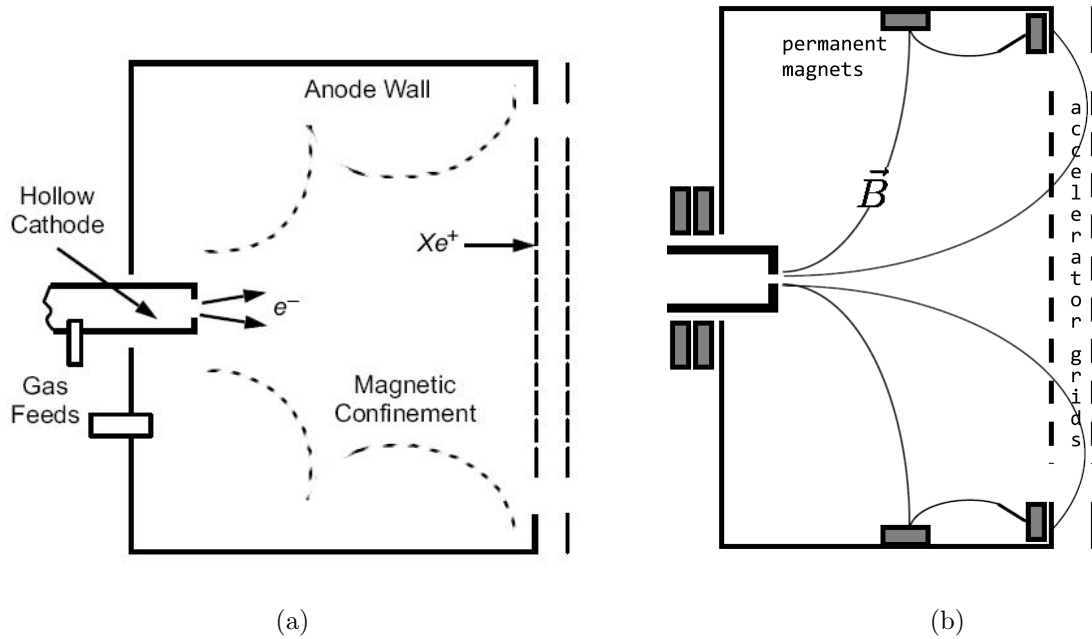
Figure 2.8: Ion thruster chamber layout: (a) DC-discharge used for ion generation (b) ring-cusp type magnetic fields [*Goebel and Katz*, 2008, chapter 4]

2.3.1.2   RF Discharge

An alternate method to the DC discharge applies a low frequency RF voltage to an antenna around or inside of the plasma. The simplest implementation of this method is wrapping the RF coil around the ionization chamber. This method heats the plasma electrons which subsequently ionizes the injected particles. Figure 2.9 shows this design. Unlike the DC-discharge, the RF coil does not require an applied magnetic field, although one can be implemented to improve performance [*Goebel and Katz*, 2008].
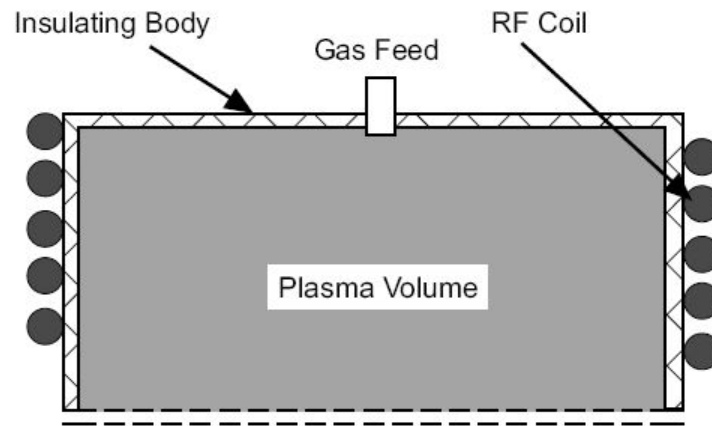
Figure 2.9: Ion thruster using RF discharge via a RF coil wrapped around the insulating chamber [*Goebel and Katz*, 2008]

With this method the lack of free electrons can prevent the ionization from occurring unlike the DC-discharge which forces free electrons into the ionization chamber. To counter this, a spark generator or cathodes are used to "seed" the plasma volume in order to start the plasma discharge. Electrons are injected into the discharge chamber (with the voltage on the accelerator grids turned off). This gives the RF electric fields more electrons to interact with once the system is started and ionization of the propellant begins.

2.3.1.3   Microwave Discharge

The last common method for ionization involves using electromagnetic fields at microwave frequencies. This ionization technique experiences less mechanical breakdown than the DC-discharge which can experience breakdowns in the hollow cathode and sputter erosion. However, the electromagnetic fields have specific conditions under which they are capable of being absorbed in the plasmas. In general if the microwave frequency is too high and plasma density too low, this technique does not perform as well as the DC or RF discharge methods.
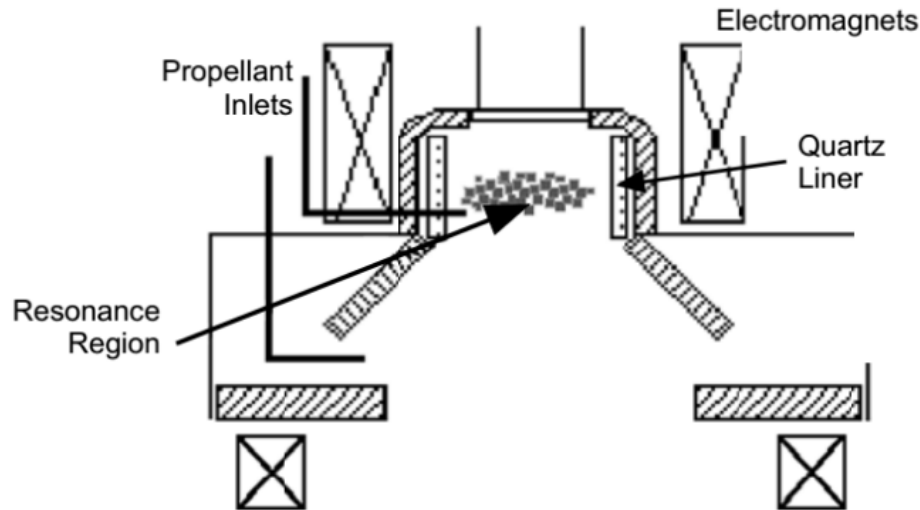
Figure 2.10: Microwave ion source schematic [*Goebel and Katz*, 2008]

2.3.2   Accelerator Grids

For ion thrusters, ions are extracted from the plasma generator and electrostatically acceler-
ated in order to produce thrust. This acceleration is generated by multi-aperture grids that have an
electric potential difference between them. The grid design in and of itself is critical to the thrusters
operation consisting of a fine balance between size, life, and performance. Given the impact of ions
on the grids, the life of a grid is usually the limiting factor to the thrusters operation. The design
and placement of this grid factors into how well the beam is focused through the apertures of the
acceleration grid, how well the beam is focused over a range of plasma densities, the losses due to
ion impingement on the screen grid, the mass utilization efficiency, and beam divergence which can
reduce thrust if too high [*Goebel and Katz*, 2008].

The accelerator grids are comprised of the screen grid and the acceleration grid. The screen
grid is primarily used to protect the acceleration grid from erosion by "aligning" the ions with the
apertures of the acceleration grid. Without the screen grid, ions that are off axis to the acceleration
grid would impact the grid at high energy and erode it quickly. The screen grid will get impacted
by other off axis ions, and so the screen grid is allowed to "float electrically" or is biased with
respect to the cathode of the plasma chamber in order that the ions will impact the screen grid

at a relatively low energy [*Goebel and Katz*, 2008]. Figure 2.11 shows a three grid system which includes a deceleration grid downstream of the acceleration grid. The function of the deceleration grid to keep the exhaust velocities at an optimum value which is determined for each specific mission [*Kantha*, 2017].
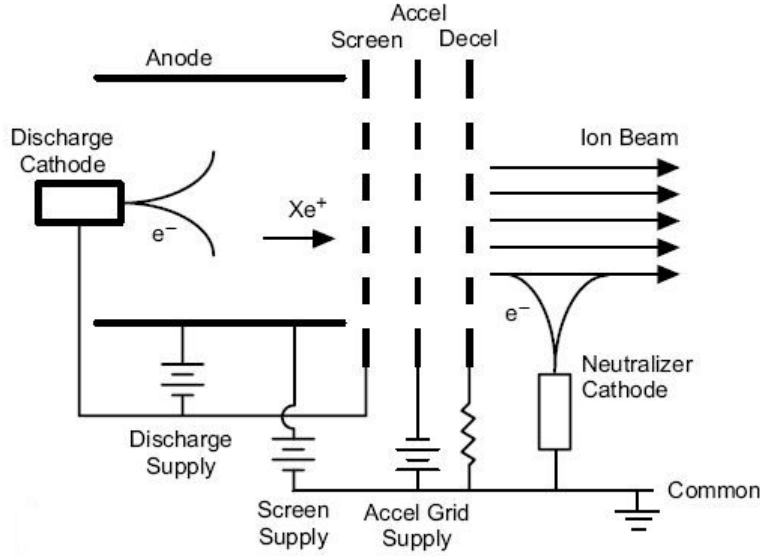
Figure 2.11: Electrical schematic of a 3-grid ion thruster system [*Goebel and Katz*, 2008]

A crucial phenomenon that effects the size of the grids and hence the size of the thruster is the space charge. According to the Child-Langmuir law, the rate at which ions can be extracted from the plasma and accelerated through the grids is limited due to space-charge buildup between the grids [*Kantha*, 2017]. This in turn means that the ion current obtainable by each aperture of the grid is limited by the space charge [*Goebel and Katz*, 2008]. Therefore to increase thrust, the number of apertures is increased which can effect the grid size.

This understanding of the space-charge-limit leads to a very simple calculation for the maximum thrust per unit area of the thruster that is independent of the ions used. This equation only depends on the voltage difference between the grids and the distance between them [*Kantha*, 2017]:

$$\left.\frac{F}{A}\right|_{max} = \frac{8\epsilon}{9}\left(\frac{V_a}{d}\right)^2 \tag{2.1}$$

From the equation, it can be seen that the smaller the gap and the higher the voltage differential the greater the thrust will be. However, there are obvious limitations to how large the differential can be and how small the gap size between the grids can be. The voltage differential is clearly limited by the spacecraft power supply. The smaller the grid gap size the greater the potential of distorting the electric field and the possibility of arcing across the grids.

2.3.2.1   Thrust Equations

Although Equation 2.1 is entirely valid to understand the max thrust capable for a given thruster; in order to assess the performance of the thruster, it is necessary to take into account the ion mass and density. Starting with the basic thrust equation:

$$T = \dot{m}_p v_{ex} \approx \dot{m}_i v_i \tag{2.2}$$

where $\dot{m}$ is the mass flow rate, v is the velocity, the subscript p is for "propellant", the subscript ex is for "exit", the subscript i is for "ion". The ion exhaust velocity is given by

$$v_i = \sqrt{\frac{2qV_b}{M}} \tag{2.3}$$

where q is the charge, V_b is the beam voltage, and M is the molecular mass of the particles. The beam voltage is usually related to, but slightly less than, the actual applied voltage. Usually the propellant, and therefore the incoming ions, have a high density when they reach the accelerator grids. This high density can disrupt the electric field in turn lowering the actual voltage experienced at the grids. For this application since the density is so low, there is assumed to be negligible losses in voltage.

The mass flow rate of the ions is calculated from the beam current:

$$\dot{m}_i = \frac{I_b m_i}{q} \tag{2.4}$$

where the beam current is calculated as follows:

$$I_b = \frac{1}{2} n_i \, q \, v_a A \, T_g \tag{2.5}$$

where n_i is the ion particle density, v_a is the ion acoustic velocity, A is assumed to be the grid area, and T_g is the grid transparency. According to *Goebel and Katz* [2008], a common value for the grid transparency is between 70% and 80%. The acoustic velocity can only be applied in high density flows, therefore to account for this variable, the velocity of the ions through the grid gap was determined. The equation of motion in terms of the charge and the electric field was integrated with respect to time in order to get the time for a single ion to cross the grid gap.

$$d = \iint \frac{q\vec{E}}{m_i} dt^2 \tag{2.6}$$

where d is the known grid gap distance and $\vec{E}$ is the electric field. The velocity through the grid gap is then

$$v = \frac{qV_b}{m_i d} t \tag{2.7}$$

Using Equation 2.7 to calculate beam voltage, and then substituting Equation 2.3 and Equation 2.4 into Equation 2.2, the equation for the thrust can be calculated by

$$T = \sqrt{\frac{2m_i}{q}} I_b \sqrt{V_b} \tag{2.8}$$

The energy imparted per ion is the kinetic energy of an ion plus its potential (the charge) which can be written as

$$E = 0.5 m_i v^2 + e_{ion} \tag{2.9}$$

where e_{ion} is equal to $q \times 1V$. Dividing Equation 2.9 by the impulse

$$J = m_i v \tag{2.10}$$

gives the Power to Thrust ratio

$$\frac{P}{T} = \frac{0.5m_i v^2 + e_{ion}}{m_i v} \tag{2.11}$$

Using Equation 2.8, the, the power can then be determined by [$Kantha$, 2017]:

$$P = \frac{0.5m_i v^2 + e_{ion}}{m_i v} T \tag{2.12}$$

The specific impulse is calculated by:

$$I_{sp} = \frac{1}{g_0} \sqrt{\frac{2q}{m_i} V_b} \tag{2.13}$$

where g_0 is the acceleration due to gravity. (If the deceleration grid is used, V in this equation is the voltage of the deceleration grid.)

However, since this is an air-breathing system, the thruster will experience ram drag similar to a turbofan engine. The drag is produced by a velocity differential between the incoming particle velocity and the velocity of the particles at the exit of the system. The thrust therefore will be reduced by a factor of:

$$\epsilon_{ram} = \frac{g_0 I_{sp} - v_{rel}}{g_0 I_{sp}} \tag{2.14}$$

where v_{rel} is the orbital velocity of the space vehicle.

From Equation 2.8, it's clear that increasing voltage increases thrust. Thrust's dependence on the ion's mass and the particle density also explains why xenon is commonly used for these types of systems. The parameters used to determine the beam current along with the beam voltage are the primary factors in thrust. The beam current shows that thrust is directly dependant on the particle density, the electric potential the neutrals are brought to, the grid area, and the velocity through the grid gap. Assuming the particles will only brought to the first potential, the primary variables are then particle density, the grid area, and velocity. The velocity is impacted by the grid gap size. The smaller the gap, the greater the velocity and the greater the beam current. However,

as mentioned previously, the closer the grids are to each other the greater the chance the electric field will break down. The beam voltage is the other key factor in thrust. It is influenced by the particle density. The higher the particle density, the more the electric field is disrupted which impacts the voltage experienced by the particles between the grids. Therefore increasing density will negatively impact the beam voltage, thus presenting another trade-off in performance.

It is also important to note the calculation for I_{sp}. The standard equation for I_{sp} relies on the mass flow rate and the thrust. In this equation for I_{sp}, it would appear that the density (either mass or particle) is of no consequence to the efficiency of the system. However, the beam voltage depends on the density of the propellant. So although density doesn't directly factor into I_{sp}, it does impact its value.

2.3.3 Other Considerations

2.3.3.1 Neutralizer Cathode & Plume Characteristics

The final stage in the system is the neutralizer cathode. Shown in Figure 2.2a, this cathode is positioned outside of the thruster to produce electrons in order to neutralize ions in the exhaust plume. This prevents a charge imbalance from being generated with the spacecraft. In the case of the an air-breathing system, a propellant-less field emission cathode would be needed, unless a propellant bypass channel were to be incorporated into the design in order to feed the neutralizer cathode. This design is out of scope for this paper, and so it will be assumed that the design for the moment uses the propellant-less option. Such a propellant-less system has been designed by Busek called a carbon nanotube field emission (CNTFE) cathode [*Wirz*, 2015].

The ion beam, which is also the thruster plume, is important to study in order to understand how the outgoing ions will interact with the spacecraft. Plume impingement on the surface of the satellite or on deployed systems (such as solar arrays) is a significant issue when using electrostatic thrusters [*Goebel and Katz*, 2008]. Ions can potentially backflow into the thruster or move radially and hit the spacecraft and its systems [*Goebel and Katz*, 2008]. The plume itself is composed of

ions and electrons of various energies and some neutrals. The neutrals are a combination of both un-ionized particles coming from the thruster and ions neutralized by the neutralizer. Determining how the thruster plume will interact with the spacecraft is essential in determining where the thruster is located amongst other considerations which usually requires a trade-off between thrust efficiency and the life of other subsystems, mainly solar arrays [*Goebel and Katz*, 2008]. The plume interaction can either have immediate effects, such as momentum transfer, or slower effects, such as erosion or contamination of surfaces [*Goebel and Katz*, 2008]. Today 3D models of the plume are generated in order to visualize how the plume will interact with the satellite and its subsystems. Figure 2.12a shows a 3D plot of an ion thruster plume, and Figure 2.12b shows the a plot of the plume ion density profile with respect to a satellite.

(a)

(b)
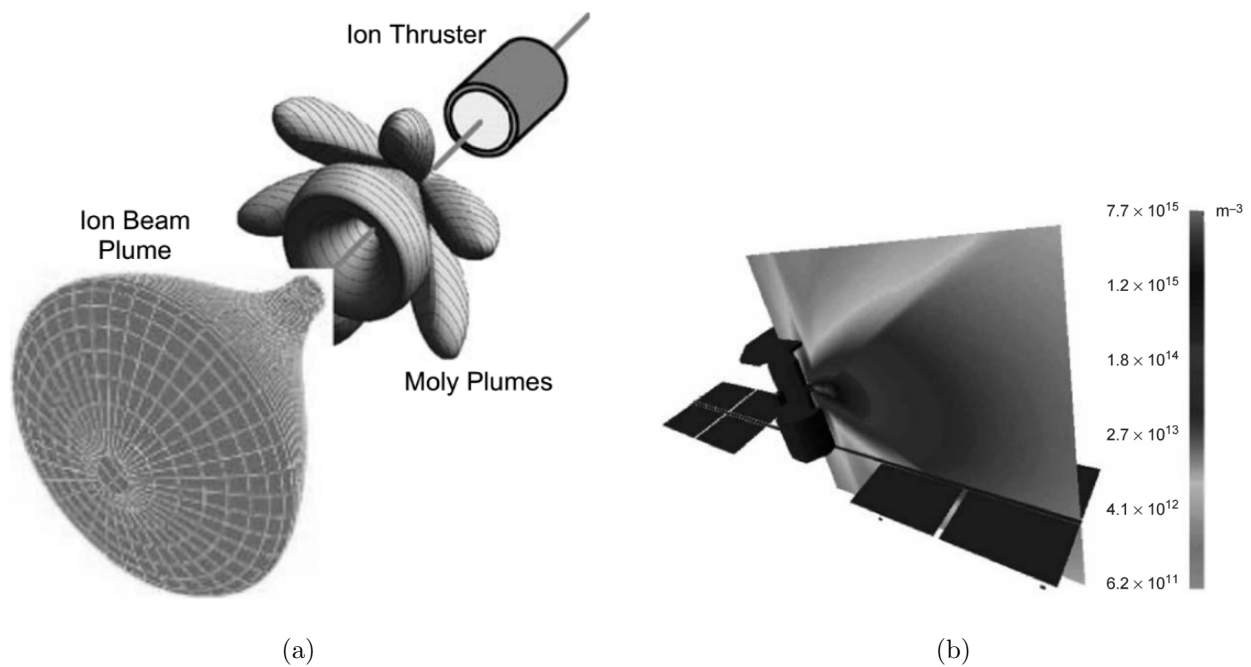
Figure 2.12: Plots of thruster plume interactions (a) 3-D plot fo an ion thruster plume (b) plot of plume ion density with respect to a satellite [*Goebel and Katz*, 2008]

2.4 Proposed Air-Breathing Electric Thruster

2.4.1 Thrust Type

Given the discussion above and the comparison of different types of electric thrusters, it is necessary to determine the best type of EP for the proposed application. As mentioned, the Hall and ion thrusters are both capable of being scaled to the size of the CubeSat, but the ion thruster is commonly suggested for air-breathing applications. To understand why, it is important to look at the full spectrum of EP systems.

Figure 2.13 shows a comparison of the thrust for these various propulsion systems. Higher thrust is commonly obtained by chemical and solid propellant systems, and electric propulsion systems tend to have a low thrust as shown. However, the lower the thrust the greater the Isp and the less propellant that is required to produce the required ΔV for a given mission. Therefore given the low density of the propellant for air-breathing systems, a higher Isp is desirable. As stated in Section 2.3.2.1, the greater the density of incoming particles the lower the beam voltage. So although thrust might increase slightly since thrust is directly proportional to density and to the square root of voltage, the total voltage applied must increase as density increases, which leads to more power consumption. Figure 2.14 shows a comparison of the Isp for various electric propulsion systems.
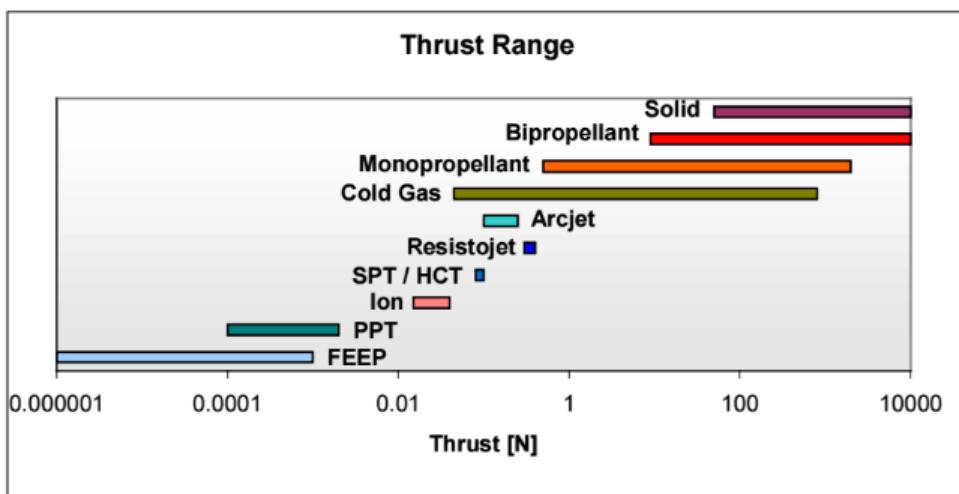
Figure 2.13: Comparison of the thrust output of various satellite propulsion systems [*Burkhardt et al.*, 2002]
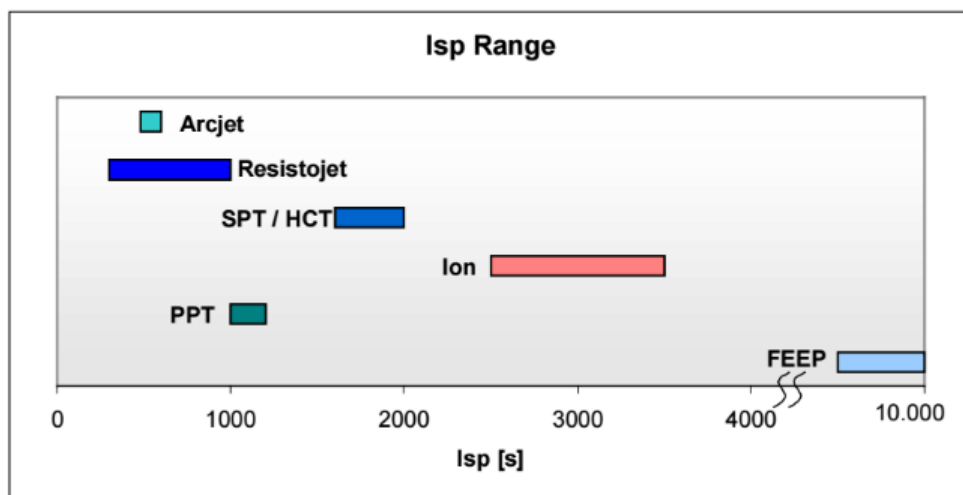
Figure 2.14: Comparison of the specific impulse of various electric satellite propulsion systems [*Burkhardt et al.*, 2002]

The choice of thruster depends on the mission parameters and constraints. For the thruster being designed in this paper, a few constraints can easily be defined:

- Low power usage is required

- High Isp is necessary

- Must be able to use ionized atmospheric particles as propellant

From the previous figures, the arcjet and FEEP style EP systems can be ignored as the arcjet has too low of an Isp for practicality and the FEEP's thrust is too low. Furthermore, neither could operate (as of now) on the propellant type being considered. This then leaves four options. These options are weighed in Table 2.1 based on the above constraints.

Table 2.1: Electric propulsion system comparison [*Burkhardt et al.*, 2002]

	Resisto/EHT	SPT/HCT	Ion Thruster	PPT
Thrust level (mN)	300–400	80–100	5–40	0.1–2
Specific impulse (s)	300 (1000 at most)	1600–2000	2500–3800	>1000
Overall efficiency (%)	80–90	50	≤60	<20(*)
Mass (kg)	0.3–0.8	3–5	2	~1(*)
Power demands (W)	500–600	1300–1500	500–800	10–100

Numbers marked by (*) are estimates.

The Resistojet/EHT (Electrothermal [Hydrogen] Resistance Thruster), although lightweight and efficient, has too low of an Isp for this application. The SPT/HCT (Stationary Plasma Thrusters / Hall Current Thruster) is a good candidate for its high Isp, but its mass and power demands are high with respect to the other options. The PPT is an excellent candidate for such a system; however, the PPT has a low efficiency and is best suited for solid propellant types.

The ion thruster is overall a practical option. It doesn't outperform other systems in one particular area, but it meets the criteria. Ion thrusters are also simple in design and capable of handling the mixture of atmospheric ions as propellant. Although this evaluation is looking at EP systems in general (not necessarily micro-EP thrusters), the important factor for the ion thruster is that it has been successfully scaled for CubeSat applications. It has a slightly higher Isp and

thus lower thrust than its larger counterparts [*Wirz*, 2015]; but the fact remains that scaling this type of thruster would not be an issue.

2.4.2 Structure

Although the structure of this system and its components will be discussed in detail in Chapters 4–6, the structure of this design will receive a brief overview here. The 6U, 12U, and 27U CubeSats are all 0.36 m in length. There are two proposed suggestions as to the orientation, and hence, the structure of the system.

The "long" configuration places the inlet in the RAM direction of the satellite (which is presumably the side with the smallest surface area) with an intermediate channel running between the inlet and the accelerator grids. This orientation presents a challenging problem to the ionization that will be discussed in Chapter 5. This configuration uses multiple inlets that channel into a single set of accelerator grids. Such a configuration would allow each section (inlet, channel, thruster) to be 1U modular components without having to resize for the different sized CubeSats. A mock-up of such a system is shown in Figure 2.15.

1U 1U 1U

Ionization

Ion Containment
Region

Accelerator Grids
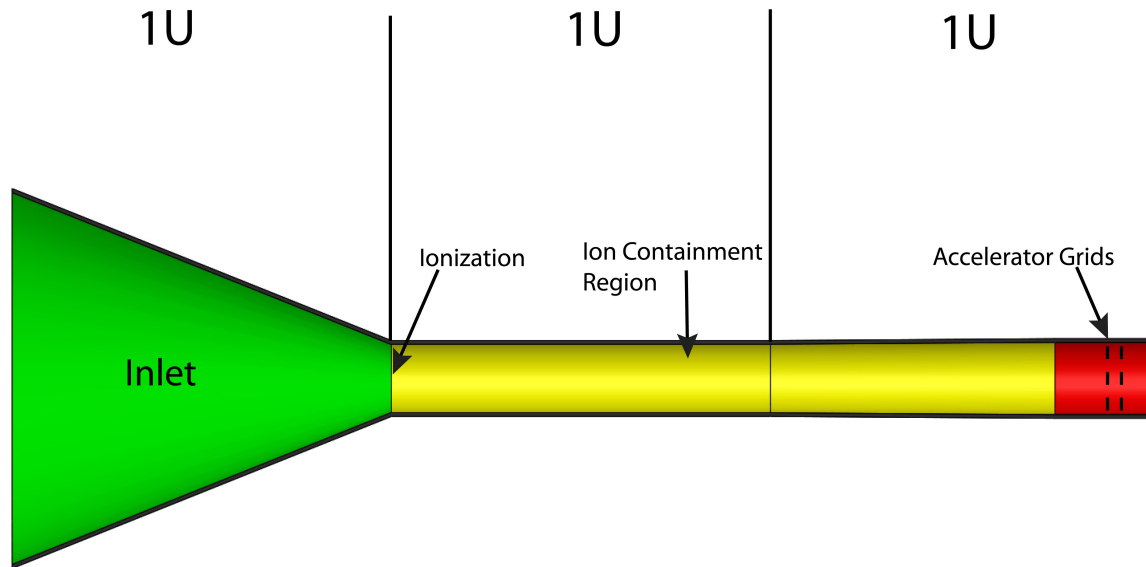
Inlet

Figure 2.15: Example of the proposed structure of the air-breathing systems with inlet, ioniza-tion/containment area, and the accelerator grids

The "short" configuration would orient the thrusters on axis with the broad-side of the CubeSat. This configuration would increase the drag experienced by the satellite, but this could be offset by the ability to use more than one thruster on certain sizes. For example, the 6U CubeSat, instead of only having 2 inlets and 1 set of accelerator grids in the long configuration, could have at most 4 full thrusters systems (the system could handle 6 thrusters with regard to size however this would leave no room for other subsystems or payloads). The advantage to the short configuration is that at least for the 6U and 12U configurations, the channel between the inlet and accelerator grids is either shortened or eliminated altogether. These different configurations will be discussed further in Chapters 5 and 6. Figure 2.16 shows an example of a 3U CubeSat in the "long" configuration. Figure 2.17 shows a 6U CubeSat in one possible variation on the "short" configuration that only uses two thrusters.
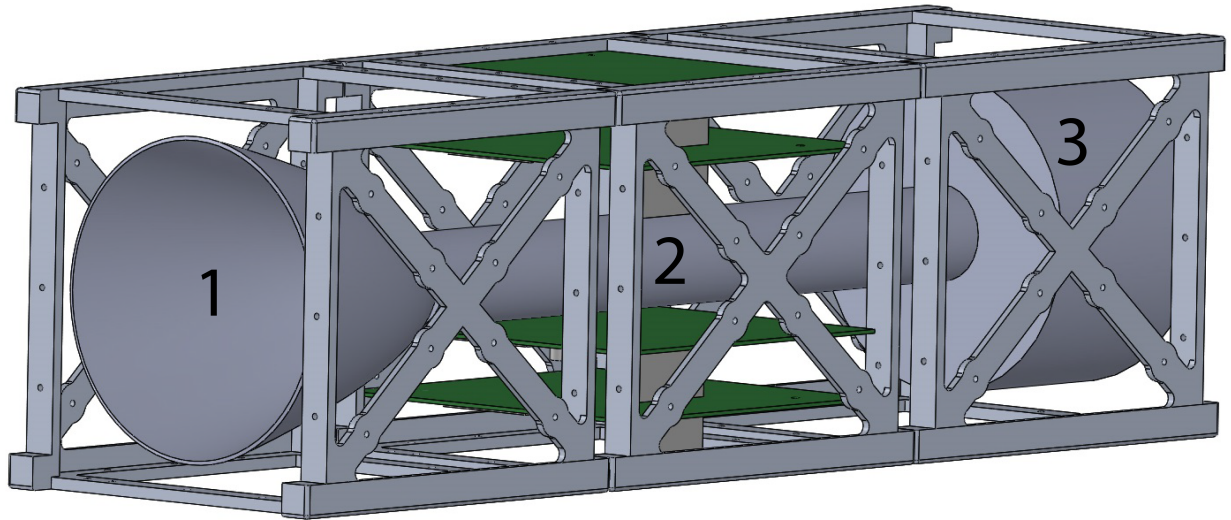
Figure 2.16: 3U CubeSat with the thruster running the length of the CubeSat (the "long" configuration). (1) Thruster's parabolic inlet. (2) Ionization/Ion Confinement channel. (3) Acceleration grids and subsystems to the accelerator grids represented by the large cylinder.
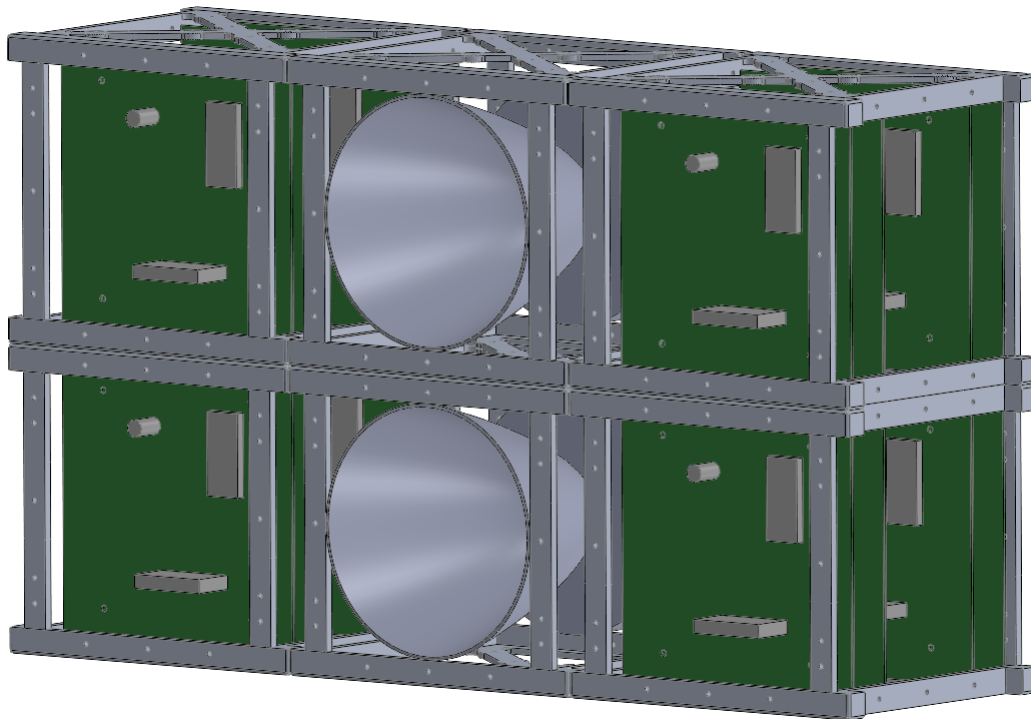
Figure 2.17: 6U CubeSat with two thrusters on the broadside

2.4.3   Volume and Mass Considerations

Integrating a propulsion system inside of the CubeSat framework has the potential to limit the space used for other subsystems and payload. Since the air-breathing propulsion system proposed here must extend the length of the CubeSat in order to ingest the neutral particles and subsequently propel the ions, the actual volume used by the propulsion system is analyzed to show the feasibility of the system. A goal for the design of this system is that it would utilize no more than 25% of the total volume of the system. Table 2.2 shows the volume of each component and the total volume with respect to the 6U, 12U, and 27U CubeSat frames which are:

- 6U: $0.12 \times 0.24 \times 0.36$ cm

- 12U: $0.24 \times 0.24 \times 0.36$ cm

- 27U: $0.34 \times 0.35 \times 0.36$ cm

Table 2.2: Volume used by components of the air-breathing thruster in the "long" configuration with respect to different sizes of CubeSats

CubeSat	Inlet Volume (cm^3)	Intermediate Channel Volume (cm^3)	Thruster Volume (cm^3)	Total Thruster Volume (cm^3)	Percent Volume Used
3U	Parabolic Inlet				
	408	99	503	1010	34
	Conical Inlet				
	325	"	"	927	31
6U	Parabolic Inlet				
	2×408	"	"	1418	14
	Conical Inlet				
	2×325	"	"	1252	12
12U	Parabolic Inlet				
	4×408	"	"	2234	11
	Conical Inlet				
	4×325	"	"	1902	9
27U	Parabolic Inlet				
	9×408	"	"	4274	9
	Conical Inlet				
	9×325	"	"	3527	8

The table assumes a structure of the thruster much like that shown in Figure 2.15: a simple parabolic or conical type inlet (this choice will be discussed in Chapter 4, a channel connecting the inlet to the accelerator grids, and the accelerator grid space. Obviously the entire accelerator grid will not be 10 cm, but the thruster is portioned out into 1U sections for all three parts. Also note that the volume listed here is not the actual volume of the components but the volume assuming that the internal part of the inlet, channel, and thruster cannot be used for other systems (which they can't). The 3U, as expected, will have the least amount of volume once the thruster is

placed inside of its framework. Even though the thruster only uses ∼30%, the remaining volume may include unusable spaces near the inlet and accelerator grid components. It is likely, on the 6U CubeSat, that with wiring and magnets placed on the various components that the thruster might be closer to 25% of the volume especially if the parabolic inlet is used. The 12U and 27U CubeSats clearly wouldn't struggle to contain a thruster system within their framework. Once again the percent volume used is slightly underestimated by only taking into account the frame of the thruster, but the percent is well below the 25% max that additional volume could be taken up by the thruster components.

If we now consider the volume of the system not including the unusable space, a rough estimate of the volume of the thruster's framework shown in Figure 2.16 is 74 cm^3. The inlet material is approximately 0.1 cm thick which makes its volume ∼12 cm^3. If the channel is a hollow cylinder and the accelerator grid is also a hollow cylinder (with one closed end) that have thicknesses of ∼0.1 cm, their volume together is ∼62 cm^3. Assuming the components are made of aluminum alloy which has a density of 2770 kg/m^3, the mass of 3U thruster system would be 0.21 kg. Table 2.3 summarizes the mass of this proposed system for the 3U, 6U, 12U, and 27U CubeSats using the "long" configuration.

Table 2.3: Mass of the air-breathing thruster systems when applied to various CubeSat sizes

CubeSat	Mass Limit (kg) [*Hevner et al.,* 2011]	# of Inlets	Total Inlet Volume (cm^3)	Total Volume (cm^3)	Mass (kg)
3U	3	1	12	74	0.21
6U	12	2	24	86	0.24
12U	24	4	48	110	0.30
27U	54	6	72	134	0.37

These numbers don't take into account the wiring and other hardware involved, but if we assume those take roughly 2 kg, this leaves the 6U system with ∼10 kg of mass to spare for other subsystems, and the 27U CubeSat with almost 53 kg of available mass to use on other subsystems. The thruster in the 3U CubeSat would use most of the allowable mass.

2.4.4 Summary

The proposed air-breathing thruster is designed to use electrostatic propulsion, in particular applying the concepts of an ion thruster. The system includes an inlet for capturing the incoming neutrals in the ram direction, an intermediate channel for ion confinement, and accelerator grids. The system is modular with each of these three distinct pieces housed in 1U sections.

There are certain efficiencies that must be accounted for, including the efficiency of the ionization process. In the case of this air-breathing system, there will also be an efficiency of the particle capture. This efficiency is discussed in Chapter 3 and analyzed for this system in Chapter 4. Including these efficiencies, Equation 2.8 is now:

$$T = \eta_c \eta_u \epsilon_{ram} \sqrt{\frac{2m_i}{q}} I_b \sqrt{V_b} \tag{2.15}$$

where η_c is the inlet capture efficiency, η_u is the ionization efficiency of the thruster, and ϵ_{ram} is the thrust reduction due to ram drag. The primary goal of this work is to generate a design such that the size and efficiencies of these components generate enough thrust to overcome atmospheric drag.

In Chapter 3, atmospheric composition and drag will be discussed and calculated. The chapter also discusss the principles behind the gas-surface interactions that will occur on the inlet surface that contribute to the inlet capture efficiency; this efficiency is analyzed in Chapter 4 for various inlets. Chapter 5 discusses the ionization efficiency. Finally, Chapter 6 shows that all of these elements provide a thrust that is greater than drag for the 6U, 12U, and 27U systems under certain conditions.

Chapter 3

Atmospheric and Orbital Considerations

This chapter gives an overview of the atmospheric and orbital conditions that must be taken into account when working with RAM-EP systems. The composition of the atmosphere in LEO will be defined. Then a look at key aerodynamics and fluid mechanic attributes will be outlined for this region of space.

3.1   Atmospheric Composition

Earth's atmosphere extends to approximately 10,000 km above the Earth's surface. The atmosphere sees various drops in particle density as altitude is increased with the lowest density of course being at the highest altitudes of the atmosphere. The atmosphere not only works to provide lift to aircraft, but it also works against lift by creating drag. For in-space propulsion, RAM-EP technology struggles with the trade-off between altitude and efficiency. That is, the lower in altitude the higher the density of the atmosphere and therefore the more propellant that is available; however, this also means an increase in drag experienced by the space vehicle. The drag will be discussed in the next section. The question that is necessary to answer in this section is what neutral particles are available for use in the atmosphere in LEO and in what quantity.

For this research the atmosphere is modeled using the NRLMSISE-00 [*Picone et al.*, 2002]. "NRLMSIS" stands for Naval Research Laboratory Mass Spectrometer and Incoherent Scatter Radar. The "E" in the model denotes that the model extends from the surface of the Earth to space. The "00" denotes the year the model was released (2000). The MSIS model was originally

developed by NASA, and the latest 2000 version was developed by the Naval Research Laboratory from the former NASA MSISE-90 model [*Hedin*, 1991]. The 2000 model is the most advanced basis for atmospheric estimation. Another model, the JB2006, was developed from the Jacchia approach and modeling efforts [*Schönherr et al.*, 2015]. The JB2006 and the even more refined JB2008 are the best for modeling the mean atmospheric density, but the MSIS model still remains the go-to model for accuracy in individual particle densities within the Earth's atmosphere [*Schönherr et al.*, 2015].

This model uses the input of the day, month, and year, as well as the solar activity and geomagnetic activity. The solar activity is characterized by the quantity $F10.7$ which refers to the solar radio flux at a wavelength of $\lambda = 10.7$ cm. The solar activity follows an 11-year cycle where the solar activity hits a high and a low during that period. The geomagnetic activity is measured to determine the heat generated by direct collisions of solar wind and air particles. The geomagnetic activity is characterized by the quantity Ap which refers to the daily planetary amplitude. Using data obtained from NOAA [*NOAA*, 2017], the maximum, minimum, and mean solar activity can be determined. Figure 3.1a shows a plot of the data obtained from NOAA from 1991 to 2016. This same data was used to plot the geomagnetic activity as shown in Figure 3.1b.
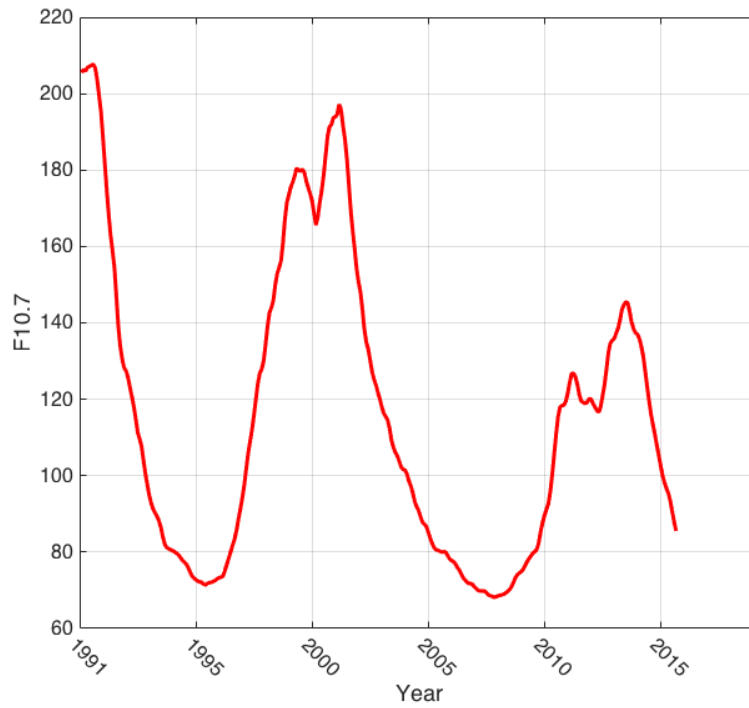
(a)
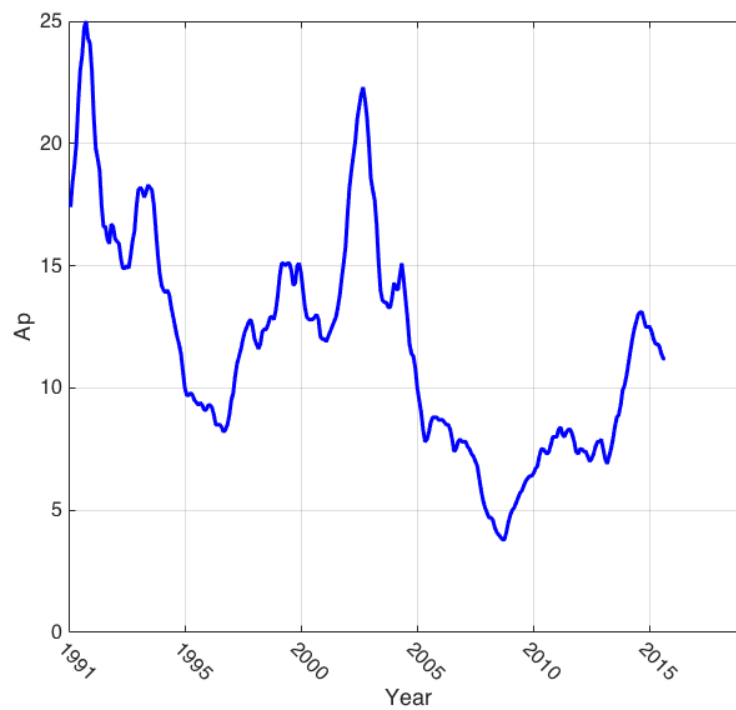
(b)

Figure 3.1: (a) The solar activity plotted between January 1991 and August 2016. (b) The geo-magnetic activity between January 1991 and August 2016.

Schönherr et al. [2015] conducted an analysis of air-breathing ion propulsion, and made the assumptions that the average F10.7 value was 140 and the Ap was 15. This was most likely done to show an ideal scenario where the particle density in the atmosphere was at its highest. However without much difficultly, the maximum, minimum, and average particle composition in the atmosphere can be shown. For this research, the composition between 80 km and 600 km will be observed. Figure 3.2 shows the Earth's atmospheric particle composition between 85 km and 600 km at the average solar activity. Clearly from this graph, it can be concluded that in the lower altitudes N_2 and O_2 will be the primary particles captured by the propulsion system and contributors to spacecraft drag. Argon will also contribute some for altitudes below 100 km, but after that its density drops off quickly, and thus accounting for it in any calculations here will not be done. As the altitude increases there is a steady decline in N_2 and O_2, and at about 150 km, atomic oxygen becomes the dominant particle in the atmosphere. Once again all other particle densities are too small to make a significant contribution to the system until about 500 km in altitude, above which hydrogen and helium dominate the atmosphere's composition. This model is not only essential for determining how much propellant is available for the air-breathing system, but also will allow for an accurate description of thrust available from each constituent of the atmosphere as well as the drag that will be experienced by the system.
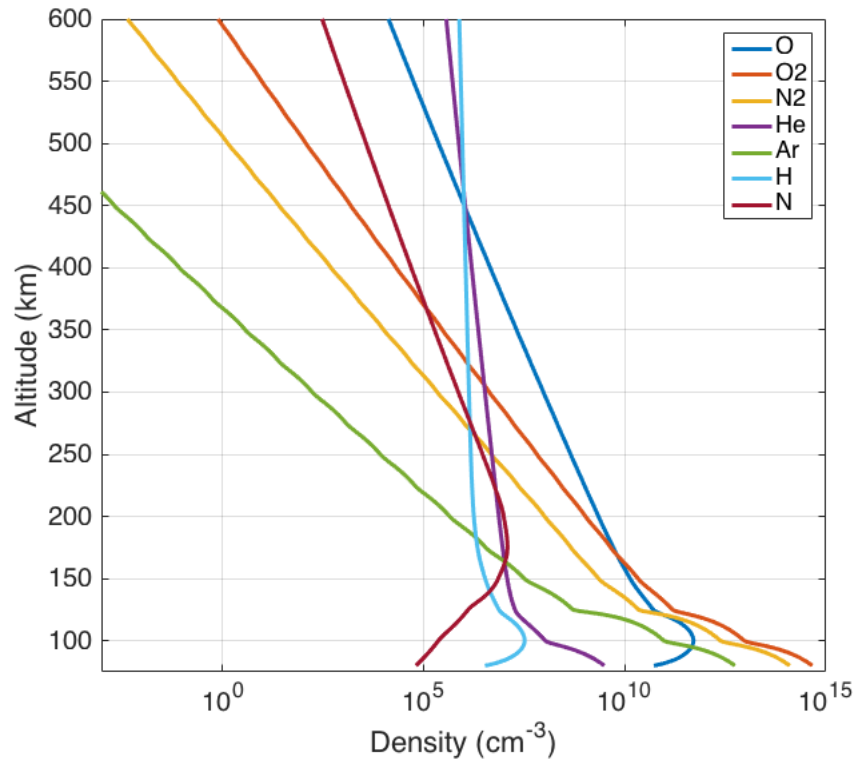
Figure 3.2: Atmosphere particle density composition charted from the NRLMSISE-00 Model at average solar flux and geomagnetic activity from 80 km to 600 km.

3.2   Orbit

As stated earlier, CubeSats are limited in altitude to 600 km. This restriction is primarily due to a CubeSat's inability to deorbit naturally within the required 25-year period at any altitude above 600 km due to the low atmospheric density and thus extremely low drag force on any spacecraft. For this research, the orbital altitudes of interest will remain below 600 km. Another simplifying assumption that will be made in this research is that all orbits are assumed to be circular. Doing so makes the available propellant to the thruster a constant factor. Further performance analysis is necessary regarding the variance in density for non-circular orbits, but that analysis is beyond the scope of this paper. The performance analysis of the CubeSat with an air-breathing system does not lose appreciable accuracy under the assumption of a circular orbit.

It is important to quantify the speed at which the neutrals will enter the inlet of the system with respect to the space vehicle. According to *Romano* [2013] in LEO orbits, the thermal velocity of the neutrals and ions is anywhere between 500 m/s and 1000 m/s. This can be confirmed by:

$$v_{th} = \sqrt{\frac{2kT}{m}} \tag{3.1}$$

where v_{th} is the thermal velocity, k is the Boltzmann constant, T is the temperature, and m is the mass of a single molecule.

Using Equation 3.1, the thermal velocity of neutral particles can be plotted against altitude. As a sample, the thermal velocities of N_2, atomic oxygen, and hydrogen are plotted in Figure 3.3, where the atmospheric temperature profile is taken from the NRLMSISE-00 model.
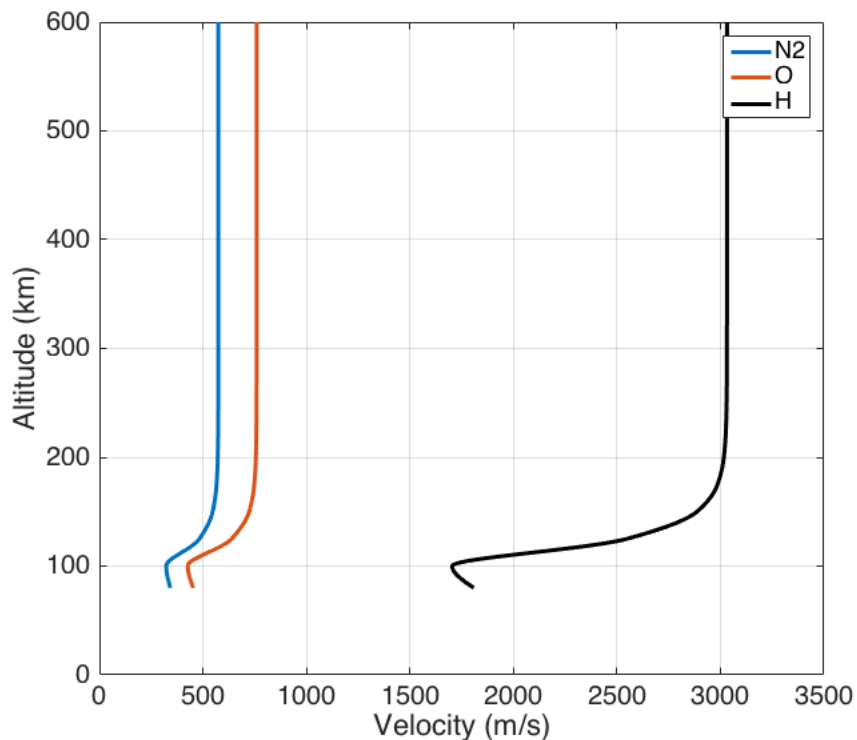
Figure 3.3: Plot of thermal velocity for N_2, monatomic oxygen, and hydrogen.

The velocity of the space vehicle orbiting in LEO can be determined by:

$$v = \sqrt{\frac{GM_e}{R_e + h}} \tag{3.2}$$

where G is the gravitational constant of the Earth, M_e is the mass of the Earth, R_e is the radius of the Earth, and h is the altitude of the orbit.

Using Equation 3.2, the velocity of the space vehicle can be plotted between 85 km and 600 km in altitude. Figure 3.4 shows the orbital velocity at these altitudes along with the mean velocity.
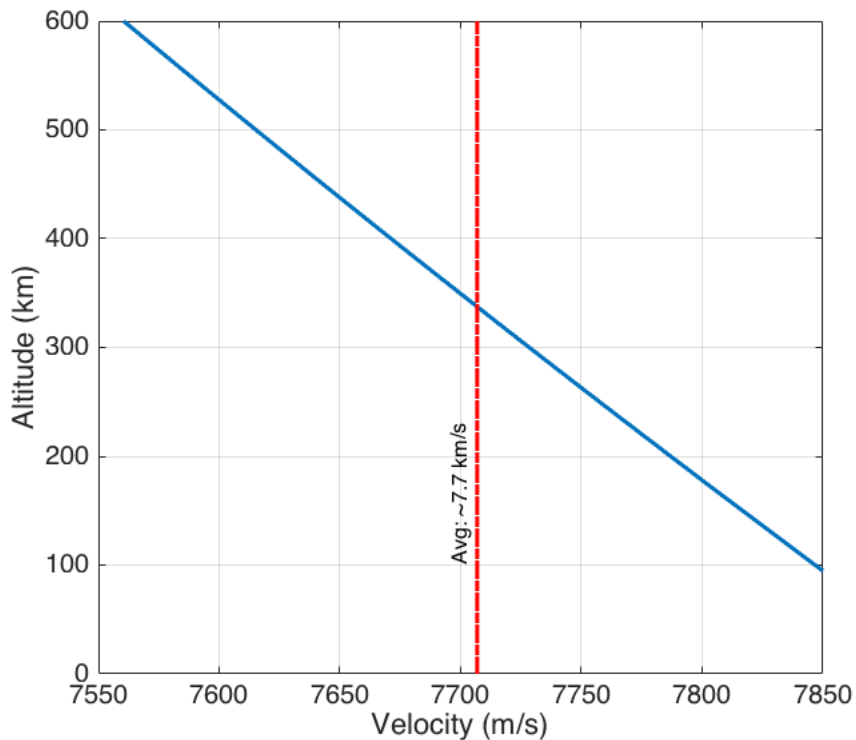
Figure 3.4: The orbital velocity of any satellite in orbits between 80 km and 600 km. The velocity varies by only 300 m/s which is small in comparison to the orbital velocity. The average velocity in this altitude range is 7.7 km/s.

Clearly, the velocity of the space vehicle is much greater than the thermal velocity of the incoming neutrals to the inlet of the system. Even the lightest of the molecules that will be

encountered (hydrogen) are moving at less than half the velocity of the space vehicle. Therefore, relative velocity between the atmospheric particles and the spacecraft will be given by the spacecraft velocity for the purpose of drag and thrust calculations.

3.3   Drag

Drag is the component of force acting on an object that is inside a medium, whether the medium is moving around the object or the object is moving inside of the medium. For orbits below 300 km, the drag is a major factor in the lifetime of the system, and thus why a drag make-up system for these altitudes has become an important topic of research. There is significantly less in-situ data that has been collected in ELEO compared to altitudes above 300 km. If CubeSats can be equipped with thrusters that negate the force of drag at these lower altitudes there will be a cheap option for data collection at these ELEO altitudes. According to a study conducted by the ESA on RAM-EP systems, thrusters of this kind are not "competitive" above 250 km [*Cara et al.*, 2007]. Although often cited, this study does not clearly justify or present its findings, and it is unclear in its definition of "competitive". It is true that above 250 km, the drag on the system is low enough that a degradation of the systems orbit will not occur at a fast enough rate perhaps to justify such a system; however, it could be easily argued that an air-breathing could be used for other applications such as station keep and low-thrust orbit changes. Nonetheless, in the remainder of this work we consider all altitudes from 85 to 600 km.

The drag on the system can be calculated from:

$$D = \frac{1}{2}\rho\, C_D A v^2 \tag{3.3}$$

where ρ is the density of the medium, C_D is the coefficient of drag, A is the area, and v is the velocity. Variations in the coefficient of drag in Equation 3.3 are investigated next.

3.3.1   Coefficient of Drag

The common standard coefficient of drag used in most orbital mechanics calculations is $C_D = 2.2$, which is a good estimate over the range of altitudes considered in this research. This value was originally estimated by Graham Cook for satellites with a compact shape [*Cook*, 1965]. Follow-up research was done on Cook's estimate using the MSISE-90 atmospheric density model to calculate the coefficient of drag on a spherical satellite. As previously discussed in Chapter 2, the accuracy of Dressler's concept was questioned because the coefficient of drag will vary with altitude. Figure 3.5 shows the change in drag coefficient on a spherical satellite due to altitude and solar activity.
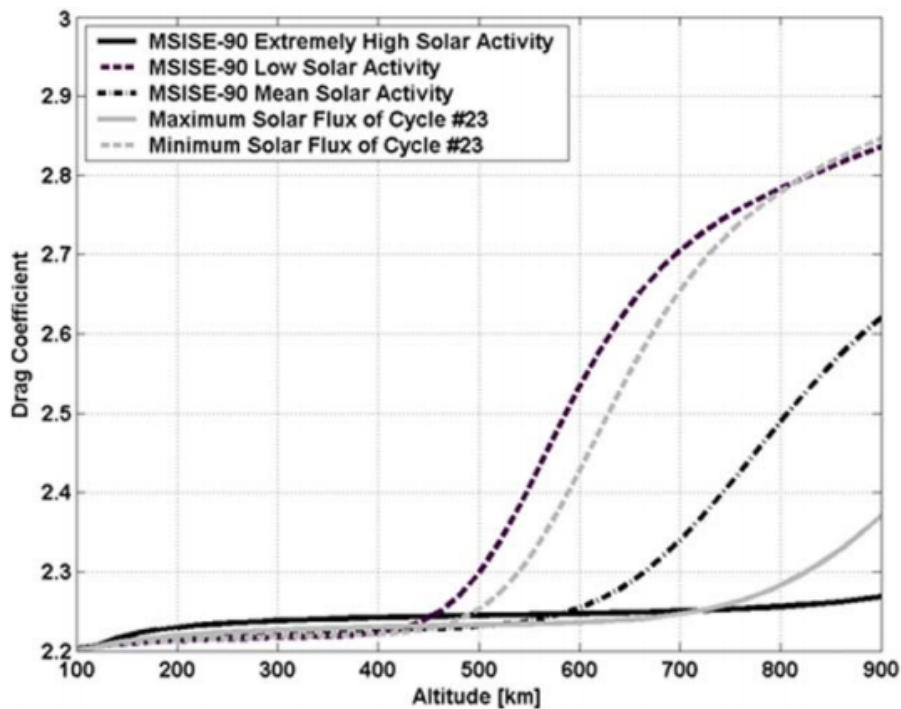
Figure 3.5: Physical drag coefficient for a spherical satellite as a function of altitude and solar activity [*Pardini et al.*, 2006, p. 396].

The work of *Pardini et al.* [2006] here shows that for altitudes below 450 km, a drag coefficient of $2.2 \pm 5\%$ is accurate for a comparable shape. According to *Pardini et al.* [2006], there are two reasons why the drag coefficient increases at higher altitudes. First, the change in atmo-

spheric composition (more helium and hydrogen atoms) leads to lower accommodation values which corresponds with higher drag coefficients. The second is due to a violation of the hyper-thermal flow assumption. The thermal speed of the particles is higher at these higher altitudes, while the satellite's orbital velocity decreases.

Romano [2013] compiled a table for the different efforts to properly define the coefficient of drag for certain shapes. Table 3.1 summarizes those results. For this research, given the focus on CubeSats, a coefficient of drag of 2.2 will be used. This appears to be a safe estimate given the available research done on the subject.

Table 3.1: C_D based on various studies. Adapted from [*Romano*, 2013]

Study	S/C	C_D
Vallado, Finkleman	Compact shape	2.2
Pardini, Tobiska, Anselmo	Compact shape	$2.2 \pm 5\%$
"	D = 1.4 m, L = 1 m	2.35
"	L/D = 5	3.30
Montenbruck, Gill	Spherical shape	2
"	Non-spherical convex-shape	2.0 - 2.3

3.3.2 Knudsen Number

When considering drag, it is commonly assumed that the atmosphere around the object in question is considered a continuum of particles. As defined in fluid mechanics when the size of the flow system (e.g. the object in the flow and the surroundings) is much larger than the than the mean free path of the particles, continuum flow can be assumed [*Kunda and Cohen*, 2008]. In other words, the fluid in question most be composed of a large number of molecules in constant motion and undergoing constant collisions with each other and the flow system. Whether a flow is considered continuum or free molecular flow is based on the Knudsen number, K_n, which is a

function of the length of the object in question and the particle density (not mass density of the particles). The Knudsen number is defined as follows:

$$K_n = \frac{\lambda}{L} \tag{3.4}$$

where L is the characteristic length of the system, and λ is the mean free path of the particles, defined as

$$\lambda = \frac{1}{\sqrt{2}\,\pi d^2 n} \tag{3.5}$$

where d is the diameter of the particle, and n is the particle density.

A flow is considered to be in "free molecular flow" when the Knudsen number is greater than 1. This calculation is important when calculating drag because in the case of free molecular flow, the drag becomes a more complicated function that must account for the dynamic pressure and the surface temperature of the space vehicle [*Romano*, 2013].

In order to determine where this change in flow occurs within the atmosphere, the Knudsen number is plotted in Figure 3.6 with respect to altitude using the NRLMSISE-00 atmosphere model under different solar conditions. Table 3.2 shows the values for used F10.7 and Ap that correspond to the minimum, maximum, and average solar and geomagnetic activity over an 11-year period from 2005 to 2016.

Table 3.2: Solar & Geomagnetic Activity Summary from 2005 to 2016 [*NOAA*, 2017]

	Maximum	Average	Minimum
F10.7	145.5	98.7	68.2
Ap	15.1	8.6	3.8

The Knudsen number is highly dependant on the particle density, and therefore, the solar min and max are also plotted for the respective lengths. The 3U, 6U, 12U, and 27U CubeSats all

have roughly the same length (30 cm for the 3U, and 36 cm for the others), and so for reference the 1U CubeSat Knudsen numbers are shown as well.
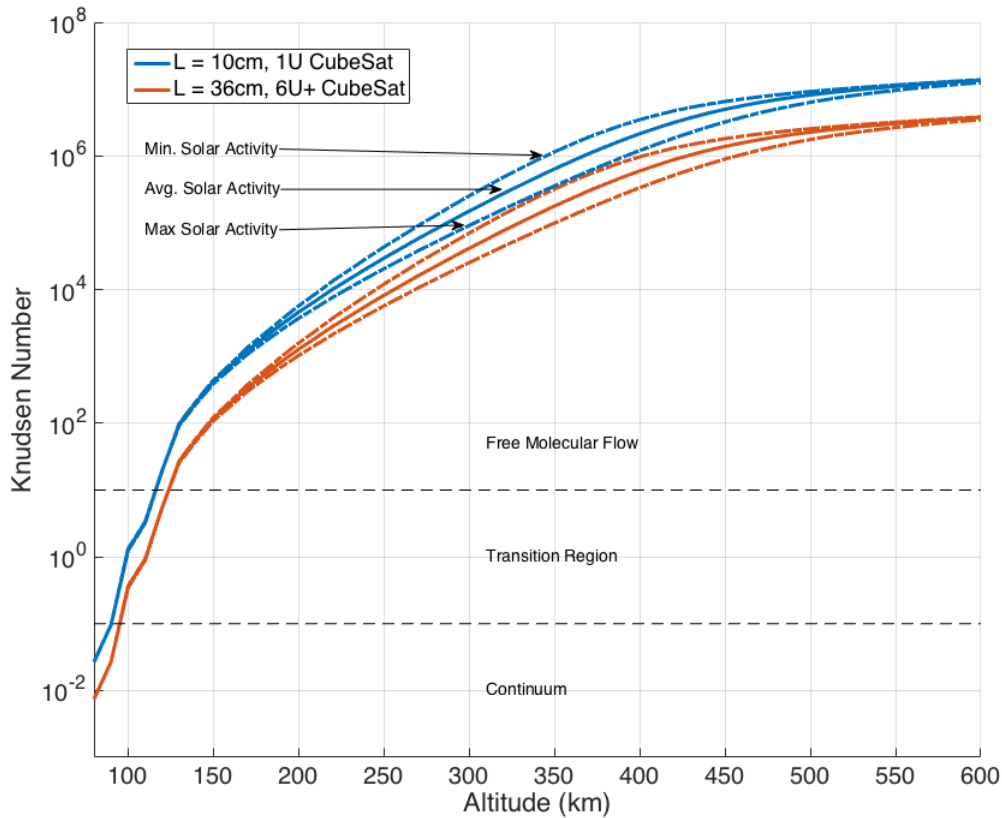
Figure 3.6: A graph of the calculated Knudsen number against altitude for two common lengths for CubeSats. The shorter being for a 1U CubeSat, and the longer being for CubeSats of size 6U and greater.

For drag make-up, the drag experienced by the CubeSat will be both a combination between free molecular flow and continuum flow depending on the CubeSat's initial orbital altitude. The transition region for this research will be modeled as a continuum flow region, but it is important to note that such an assumption is only for simplification in order to obtain a baseline for the data. Further analysis within that transition region would be necessary to accurately define the drag effects on the satellite; however, since that falls out of the scope of this paper, the simplifying assumption is justified.

Another point to note from Figure 3.6 is that the solar activity has a minimal effect at the extrema of the altitude range in question. Even though there is a variance in the Knudsen number particularly around 350 km, it has no effect on the drag calculations since it is clearly in the free molecular flow region. If, however, this variance from the solar activity were positioned across the "boundary" of the free molecular flow and transition region, the problem would become more complicated. This would only occur for very long space vehicles (e.g. a continuous space vehicle of the length of the ISS) which is not the case here.

3.3.3 Drag in Free Molecular Flow

In free molecular flow, the particle density is so small that instead of being a fluid, i.e. a continuous stream of particles, each particle is viewed individually. In short, there is no interaction between the molecules; it is a collisionless environment. However, the interaction between the object's surface and the particle becomes extremely important. In continuum flow, the amount of time an individual particle interacts with the body in question is minimal due to the nature of the flow. However when there is only a single particle involved in the interaction with the surface, the time of interaction goes up; and therefore, a redistribution of momentum and energy occurs instead of a transfer [*Vallado and Finkleman*, 2008]. It is for this reason that drag cannot be viewed as a net force caused by a "collection" of particles, but as the interaction with single particles upon the surface.

According to *Vallado and Finkleman* [2008], accurately solving for drag under these conditions is significantly complicated. Depending on which atmospheric model is used, the parameters of the satellite, the orbit in question, and the orbit propagation methods, the results can be varied. The authors state that:

> A particular set of input conditions (satellite parameters, atmospheric models, use of indices, force models and solution method) will achieve an optimized solution. A different initial set of input conditions will arrive at a different, but equally valid, and potentially better solution to predict into the future. [*Vallado and Finkleman*, 2008]

It is due to this fact that a free molecular flow drag model will not be implemented in this paper. A simplified model could be constructed, but in light of Vallado's research, such an attempt would seem to interject its own inaccuracy unless done with a certain level of complexity. Such complexity to accurately define the drag is outside of the scope of this paper. However for future analysis of this proposed air-breathing system for CubeSats, it might be necessary to construct such a model. For now, it is understood that the drag model used here will overestimate the drag force on the satellite.

3.4 Gas-Surface Interactions

In order to properly construct a model for the inlet of this proposed air-breathing system, it is necessary to understand the added complexity brought about by free molecular flow. As stated before, the gas-surface interaction is no longer like that of the flow of fire hose to a car panel but of a potato gun to a car panel. A redistribution of momentum and energy occurs between the particle and the surface. This means that how the particle will reflect off of the surface is very different from what is commonly expected in a continuum flow.

3.4.1 Particle Scattering

On Earth, in what is considered "continuum flow" for the atmosphere, the kinetic behavior of a body that impacts a surface elastically is referred to as specular reflection. A commonly used example is that of a billiards ball hitting the rail of the table. The rail can be used to make certain shots because the trajectory after impact with the rail can be accurately predicted. Now imagine if the rail in this analogy were jagged like a saw blade but non-uniform. The reflection of the ball off the rail would be highly unpredictable making a precise estimate of the ball's trajectory after hitting the rail almost impossible. This is the case in free molecular flow. Since the flow is characterized by discrete particles, the interaction of the particle with the surface becomes extremely important especially when discussing the capture of particles in the inlet of RAM-EP systems. Figure 3.7 shows an illustration of the difference between specular and diffuse reflection.
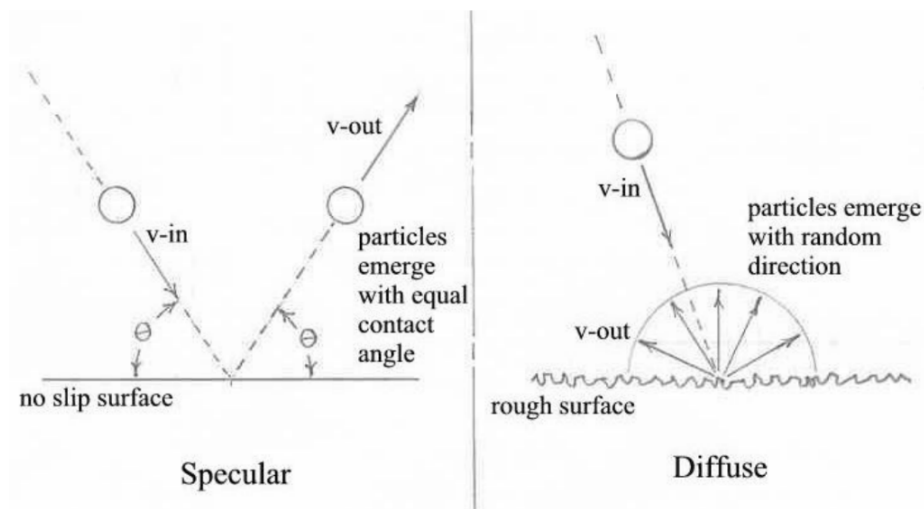
Figure 3.7: Difference between specular and diffuse reflection [*McGuire*, 2001].

In the past 35 years, gas-surface interactions in space have been highly documented. This has led to the discovery that satellite surfaces are coated with "adsorbed" molecules which in turn affect the energy accommodation and reflection of molecules from the surface for satellites in the altitude range of 100–300 km [*Moe and Moe*, 2005]. The term "adsorption" refers to the trapping of atomic oxygen and its reaction products on the satellite's surface. If the surface is clean, or devoid of trapped atoms and molecules, incoming particles will reflect nearly specularly; however, as the surface becomes contaminated with adsorbed atoms and molecules, the incoming particles are reflected more diffusely and in turn lose a large portion of their incident kinetic energy [*Moe and Moe*, 2005]. As altitude increases, the surface coverage of adsorbed atoms and molecules decreases. Referring back to Figure 3.2 this should be of no surprise as we see that the atomic oxygen density is almost five orders of magnitude smaller above 300 km than at its peak near 100 km.

Therefore in reality, the reflections that occur off of the satellites surface will be quasi-specular in nature while the surface is not full contaminated. As the contamination is increased, the fraction of quasi-specular reflections decreases and the diffuse fraction of reflections increases. Figure 3.8 shows a representation of the quasi-specular reflection as an addendum to Figure 3.7. Determining if the reflection is quasi-specular or fully diffuse will be discussed in a Chapter 4 when discussing particle capture.
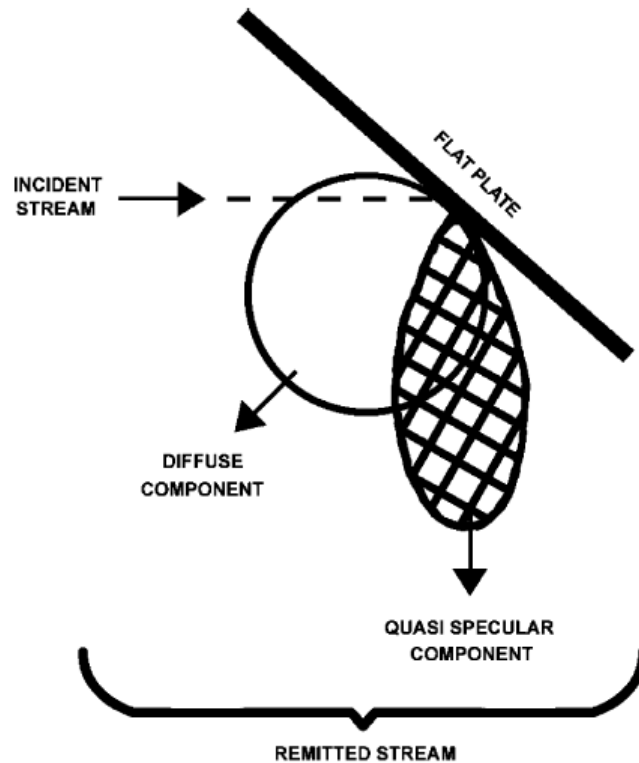
Figure 3.8: Off of a non-contaminated surface the reflection will be quasi-specular, but as the contamination increases the chance of a diffuse remission increases [*Moe and Moe*, 2005].

3.5   Summary

The key assumptions established in this chapter are

- All orbits considered in this work are assumed to be circular.

- The particles are assumed to be stationary compared to the speed of the space vehicle.

- The coefficient of drag for all computations is 2.2.

- The simplified model for drag will be used.

Using these assumptions, the drag experienced by the 3U, 6U, 12U, and 27U CubeSats can be plotted against altitude. This graph assumes a perfectly flat ram-directed surface. This graph will be revisited once the proposed system is defined in the next chapter. The frontal area will actually

be smaller due to the inlet so that the expected drag will be somewhat lower than calculated here.

Figure 3.9 shows the drag profile across the specified LEO altitudes.
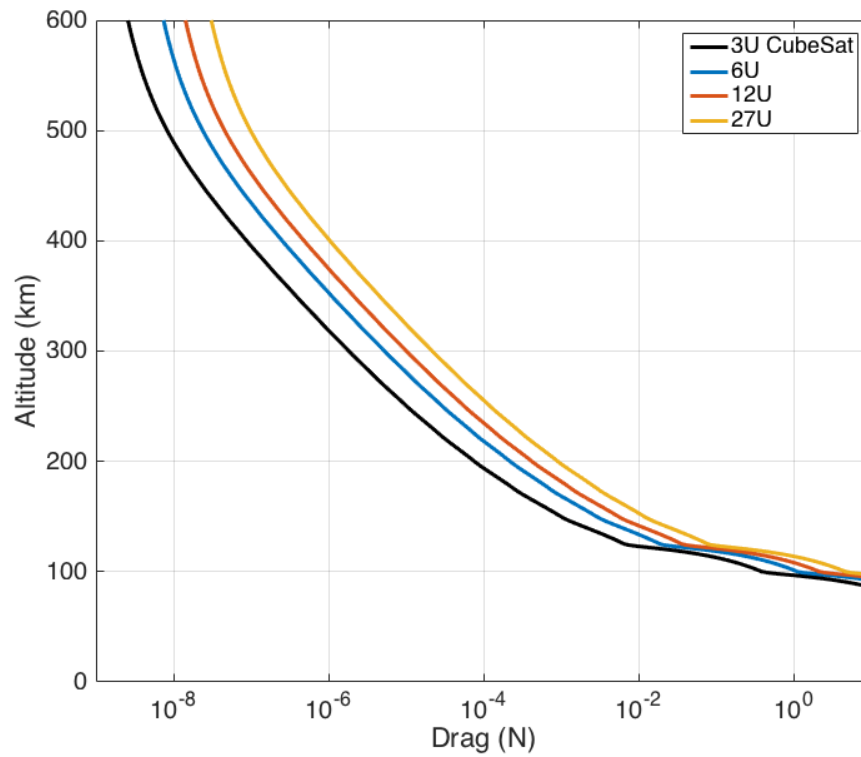
Figure 3.9: This graph shows the magnitude of drag across LEO altitudes for 3U, 6U, 12U, and 27U CubeSats, under average solar conditions.

Chapter 4

Inlet Design

This chapter discusses the proposed design of a CubeSat air-breathing inlet. The inlet shape is analyzed and discussed. The addition of baffles to the inlet's frame is analyzed. A brief discussion of parabolic optics is also included. The analysis in this chapter provides an inlet capture efficiency to be used in Equation 2.8.

4.1   Inlet Design

There are two primary designs existing for optimum particle capture for RAM-EP systems: Nishiyama's collimated design [*Nishiyama*, 2003] and McGuire's conical scoop [*McGuire*, 2001]. Neither Nishiyama's nor McGuire's designs were able to capture more than 50% of the incoming particles [*Singh and Walker*, 2015]. Both also confirm that smaller inlets are more effective in particle capture [*Singh and Walker*, 2015].

Nishiyama's collimated design is strongly based on the work of *Clausing* [1971] who showed that rarefied gas flow through long, narrow tubes results in fewer reflections than of tube where the radius is equal to or greater than the length. This is also known as the Clausing effect. By running several long, narrow tubes around the perimeter of the satellite, Nishiyama's design is able to take advantage of this physical phenomenon. This poses less problems for longer satellites, but for CubeSats such a system would take up most of the allowable volume.

The conical inlet proposed by McGuire relies on small shocks that would potentially form at the front of the inlet, in turn compressing the flow. This conical design relies heavily on this assumption even though the author seems to contradict himself on whether the assumption is valid:

> In the upper atmosphere, one cannot assume that the continuum assumption for the flowfield is valid. So one cannot assume shocks will work. It doesn't mean that they don't, but the behavior will be different from a hypersonic flowfield.

McGuire does not go on to justify or explain how they would be different and in turn why he can rely on the shocks for compression. The shock compression on the conical inlet is the linchpin to his research. It might be possible that such shocks could occur in the transition region up to about 250 km, depending on the satellite's size, but beyond that the density of the atmosphere is far too low to produce shocks.

To McGuire's credit though, the rarefied gas regime is still undergoing research and is not as well defined as continuum flow. This presents a significant problem when evaluating the flow through the inlet regarding velocity and mass flow rate. This problem will be discussed later. The following inlet design will, for accuracy and without adding much complexity, assume that the "flow" is considered one particle at a time.

With these two designs in mind, a process was developed to help determine the best shape for an air-breathing CubeSat system. First, three different shapes were tested for their effectiveness in capturing incoming particles: a pyramidal shape, a conical shape, and a parabolic shape were each tested with a feasible length given that this inlet will fit inside of the CubeSat's structure.

4.1.1   Parabolic design

The parabolic shape was defined using the Cubesat's ram face dimensions, the desired length, and a common radius for micro-thrusters. Figure 4.1 shows how the parabolic shape reflects (under specular reflection) particles. If the incoming particles on in line with the axis of the parabola, the particles will be reflected towards the focus (the red dot).
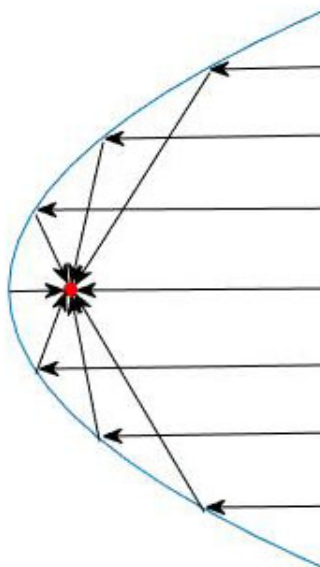
Figure 4.1: Optics of parabola in specular reflection

The inlet radius in these scenarios is 5 cm, and the length of the inlet was varied between 5 cm, 7.5 cm, and 10cm. The outlet aperture size was selected based on common radii for micro-thrusters found in *Wirz et al.* [2001]. An average size for micro-ion thrusters is about 2 cm. As described previously, the open systems by Conley and Dressler would have been more effective with some type of compression. This design therefore condenses the incoming flow into a smaller aperture. This outlet aperture size was also selected to minimize the amount of space the entire system uses. With that, the outlet aperture is designed to have a radius of 1 cm.

To determine the position of the focus, the basic equation for a parabola was used.

$$y(x) = ax^2 \tag{4.1}$$

The two boundary conditions on this parabola are that at $x = 1$ cm (the exit radius of the inlet), the equation of the parabola must be

$$y(1 \text{ cm}) = a \tag{4.2}$$

and at $x = 5$ cm (the entrance radius of inlet) the length must be:

$$y(5 \text{ cm}) = L + a = a(5)^2 \tag{4.3}$$

where L is the desired inlet length. Based on the chosen length, L, the value of the constant a can be solved. By knowing a, the position of the exit aperture is known, and then the focus can be determined by

$$f = \frac{1}{4a} \tag{4.4}$$

The following table shows the position of the focus with respect to the parabola's origin compared to the location of the exit of the inlet which is determined at $x = 1$ cm.

Table 4.1: Inlet parameters

Inlet radius (cm)	L (cm)	a (cm)	focus (cm)
5	5	0.21	1.2
5	7.5	0.31	0.8
5	10	0.42	0.6

Table 4.1 shows that as that the longer the inlet the closer the outlet will be to the focus thus increasing particle capture. Ideally, the focus would be positioned behind the exit, that is the magnitude "a" would be greater than the magnitude of the focus. This would give a 100% specular capture, but the parabola would have to be longer.

4.1.2 Analysis of the Shape

The MolFlow+ application developed by *Kersevan and Pons* [2009] was used to run the analysis on these three shapes. MolFlow+ is an open source software package "that allows the calculation of several physical quantities of interest to vacuum engineers and scientists, such as pressure profiles, effective pumping speeds, adsorption distributions, angle of incidence or effusion

profiles, and more" [*Kersevan and Pons*, 2009]. MolFlow+ uses what is referred to as the "test-particle Monte Carlo" (TPMC) algorithm in order to model rarefied gas flow. MolFlow+ is capable of modeling specular and diffuse (cosine and uniform distributions) reflections. Figure 4.2 shows the parabolic shape being analyzed under diffuse reflection.
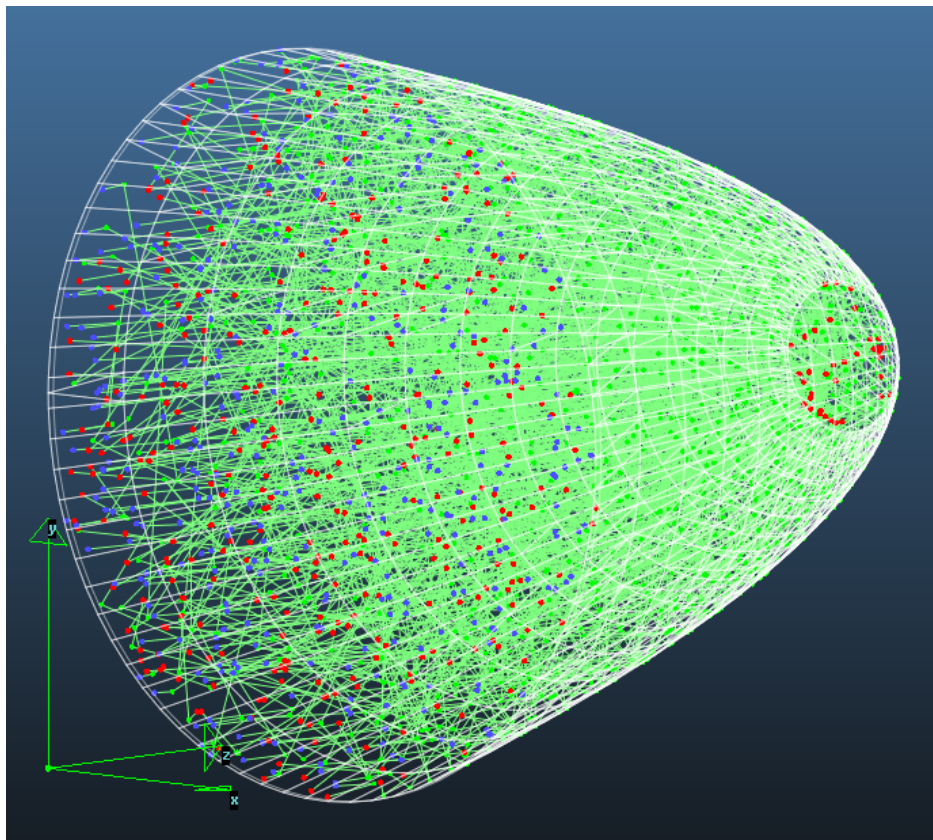
Figure 4.2: Example of MolFlow+ analysis. Red dots show the escapes out of the test volume. Blue dots show entry into the control volume. Green lines show the particle trajectories.

The inlets shapes were tested at three different lengths: 5 cm, 7.5 cm, and 10 cm. It was assumed that the temperatures of all the surfaces were uniform. Figure 4.3a shows a truncated pyramid with a length of 10 cm, an inlet area of 10 cm by 10 cm, and an outlet area of 2 cm by 2 cm. Figure 4.3b show a truncated cone (similar to McGuire's scoop [*McGuire*, 2001]) with a length of 10 cm, an inlet radius of 5 cm, and an exit radius of 1 cm. Figure 4.3c shows the proposed parabolic inlet with a 10 cm length, 5 cm inlet radius, and 2 cm exit radius. MolFlow+ uses the fluid space for simulation and so the actual models used in testing were solid shapes.

(a)

(b)

(c)
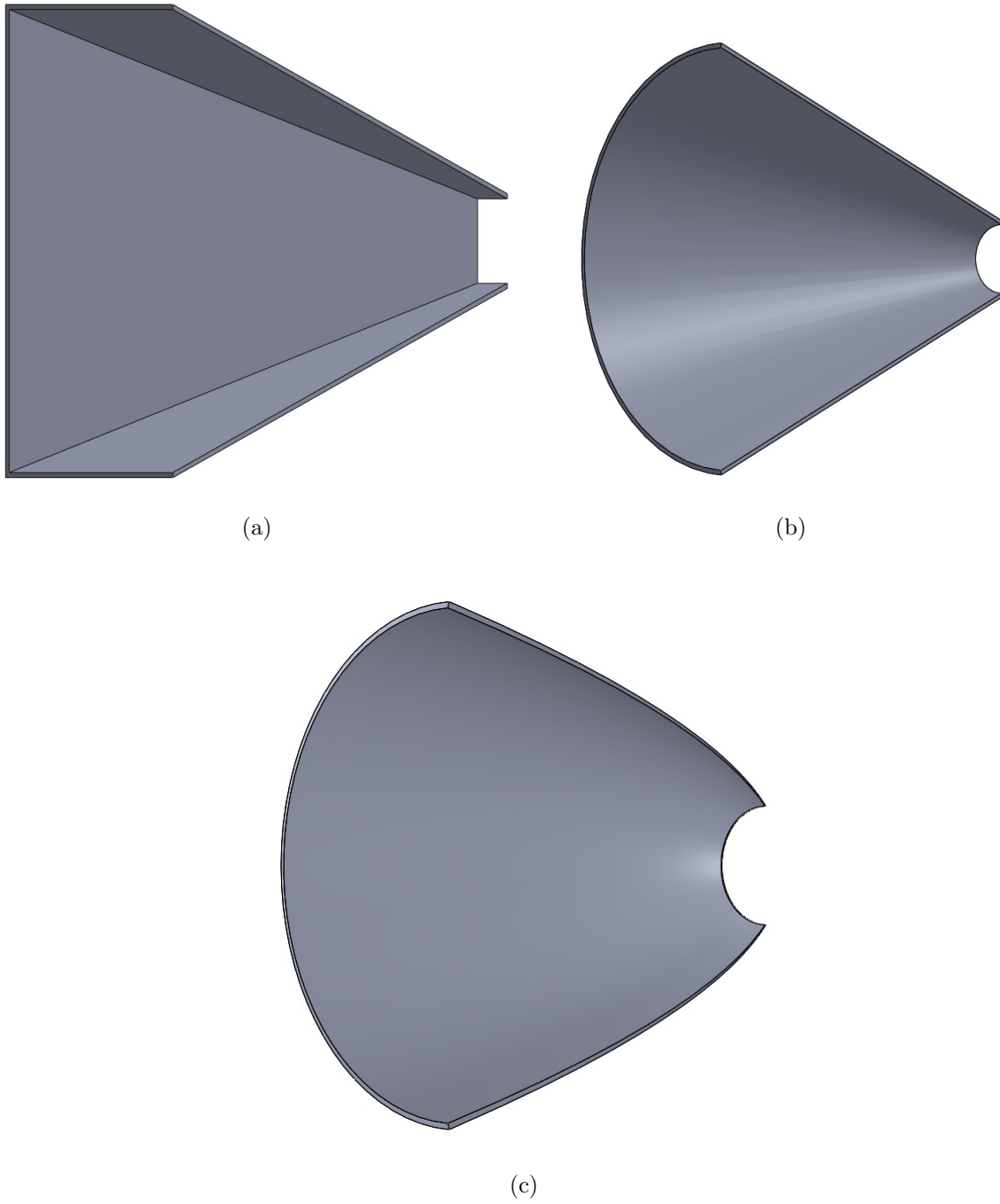
Figure 4.3: Cross section of the tested inlet shapes (a) truncated pyramid (b) conical (c) parabolic
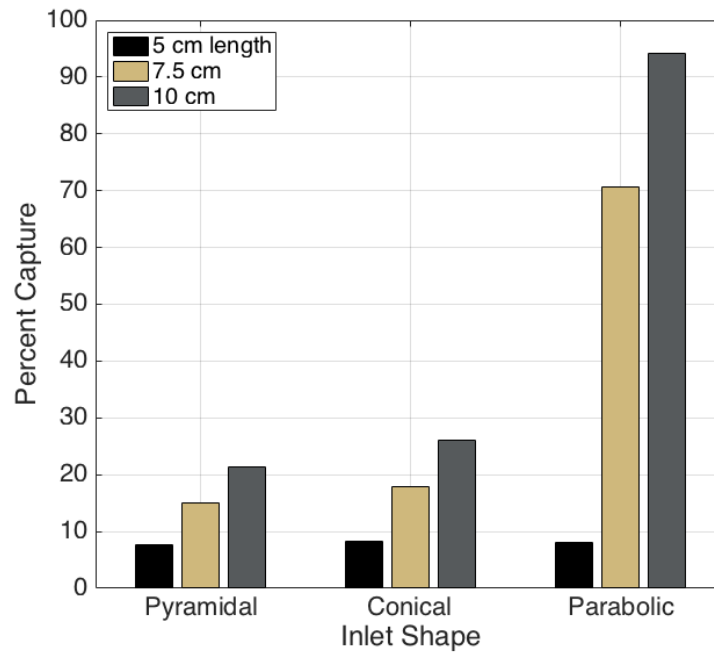
(a)
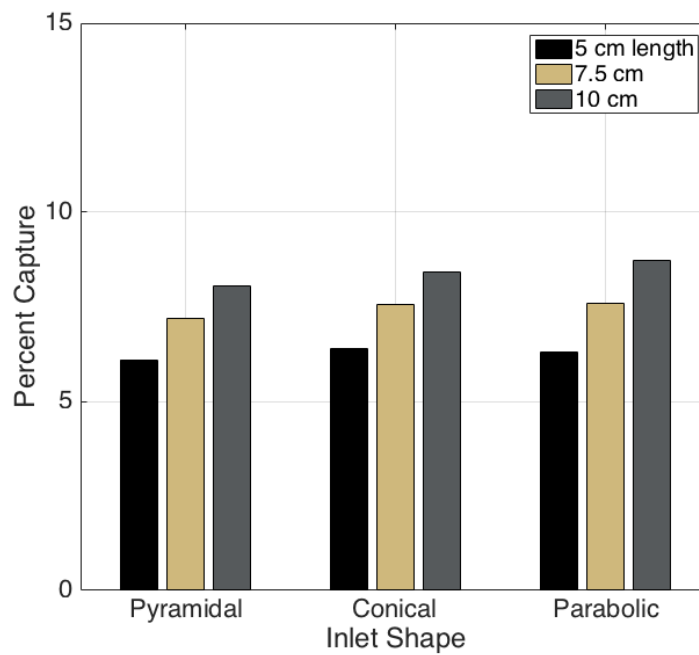
(b)

Figure 4.4: Inlet capture of pyramidal, conical, and parabolic shapes for various inlet lengths for (a) specular reflection (b) diffuse reflection.

The results of the MolFlow+ analysis are shown in Figures 4.4a and 4.4b. Under the ideal scenario of specular reflection, it is clear that the parabolic shape outperforms the other two shapes due to the optics of a parabola. The capture of the parabolic shape is not 100% because the focus actually sits in front of the outlet. Also, the results of the conical shape are well below 50% capture as expected from the research of *Singh and Walker* [2015].

Under diffuse conditions the inlets' performances are nearly identical. Due to the random nature of the reflections from the surface, this is no surprise. However at the longer length of 10 cm, the parabolic shape has a slightly greater capture percentage. From these results, it was concluded that a 10 cm length, and a parabolic inlet shape were the best choice.

Since the 2 cm outlet chosen was rather arbitrarily, the outlet size was varied to test the change in the percentage of captured particles using the MolFlow+ software. The inlet's parabolic curve was redesigned for each of these different outlet sizes instead of simply decreasing the outlet area. As shown in Figure 4.5 the capture percentage increases for diffuse reflection as the ratio outlet area and inlet area of system go to unity which is not surprising. The specular reflection analysis is not shown here because for outlet sizes above 3 cm, the capture is 99.99%.
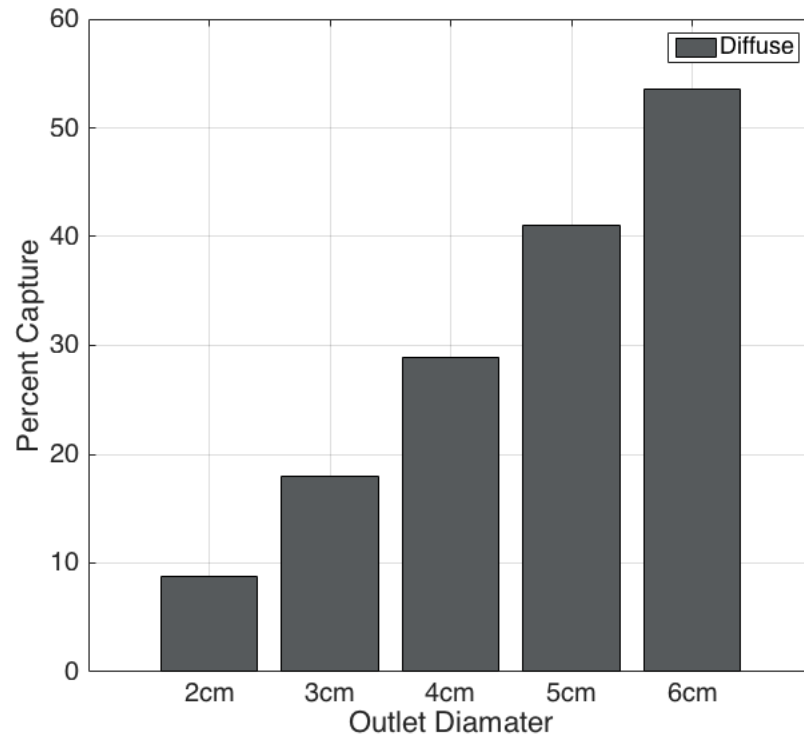
Figure 4.5: Parabolic inlet capture comparison using various outlet sizes for diffuse reflection.

The capture percentage is a mostly linear function, but there is a slight larger increases between the 2 cm and 3 cm outlet apertures. This is due to the location of the parabola's focus. As the inlet to outlet ratio of the parabola goes to unity, the focus becomes positioned farther and farther behind the outlet aperture which increases particle capture and is more easily seen in the specular case. At 2 cm the focus sits in front of the outlet, and only has a 94% capture efficiency while above 3 cm the focus sits behind the outlet aperture. Figures 4.1 and 4.6 explain this phenomena further.
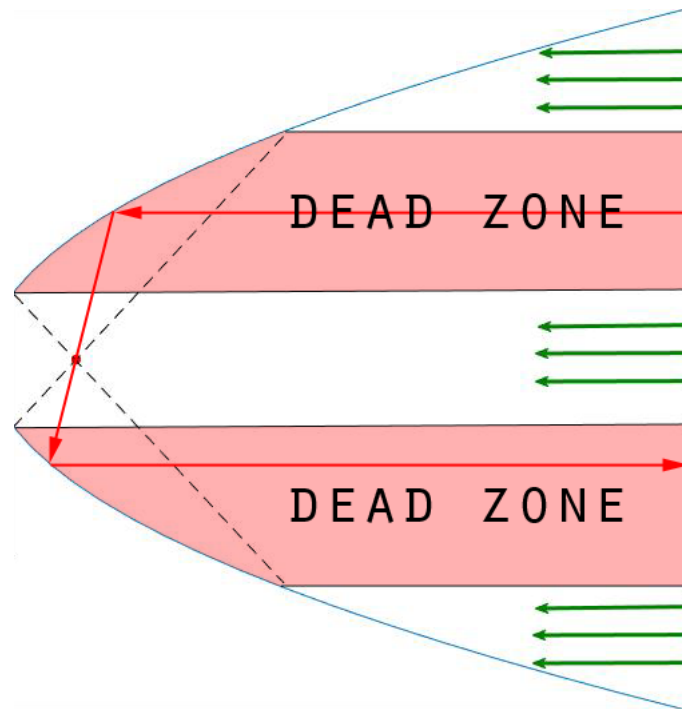
Figure 4.6: Parabolic inlet with outlet behind the focus. If the particle enters the inlet within the dead zone, the particle will reflect back out of the inlet under specular reflection conditions. The size of the "dead zones" are exaggerated for visual purposes.

If the focus is in front of the outlet aperture, there is a volume of incoming particles that will be directed back out of the inlet. If the focus is either in-line with the outlet or is behind outlet, the particle capture will increase specifically for specular reflection.

4.1.2.1   Aligning the Focus

If the parabolic shape is to be used, should the focus be adjusted to maximize particle capture in the specular case? Doing so will inevitably decrease the size of the inlet aperture or increase the length of the inlet, but if the adjustment is produces a net gain in particles captured, it will be worthwhile. There might be fewer particles incoming due to a smaller inlet, but if the particles incoming from a larger inlet reflect back out of the inlet for a certain positions on the inlet, the total number of particles captured could be similar.

Figure 4.1 and 4.6 show the behavior of the focus. If the focus were aligned with the outlet or "behind" the outlet, the dead zone characterized in Figure 4.6 would no longer exist. With this

in mind, it is necessary to determine the volumetric difference if the parabola inlet aperture were changed.

In this scenario, the inlet aperture of the inlet system will decrease, but the size of the outlet aperture needs to stay the same. Using Eq. 4.1 and Eq. 4.4, the value of a where the outlet is aligned with the focus can be solved by setting y to the value of the focus when x is the radius of the outlet:

$$\frac{1}{4a} = y(1 \text{ cm}) = ax^2 \qquad (4.5)$$

This yields a value for a of 0.5. This means the focus is at 0.5 cm from the origin of the parabola. Keeping the length of the inlet at 10 cm, the inlet aperture will be slightly smaller.

Doing a volumetric comparison via CAD modeling in SolidWorks, the inlet with the aligned focus is 349.59 cm^3 whereas the original inlet is 408.42 cm^3. Assuming an altitude of 300 km, the overall particle density is 2.792×10^{-15} g/cm^3. So the inlet with the aligned focus under specular conditions (100% capture), ingests 0.976×10^{-12} g of propellant while the original inlet with ~90% capture efficiency, ingests 1.027×10^{-12} g of propellant. So despite having the aligned focus with a perfect capture percentage under specular reflection, the larger inlet aperture still captures more mass of propellant. This comparison assumes the inlet's are kept at a 10 cm length. If the focus were aligned and the inlet increased in length, the aligned focus would capture more mass of propellant. Once again, the question comes down to the particular mission: the designer must decide whether it is more important for the inlet to ingest more mass thus providing more thrust but use more volume, or to have more volume available for other subsystems.

4.1.2.2   Addition of Baffles

In an effort to improve the diffuse reflection scenario, a baffled design of the parabolic shape was tested. Similar to the concept of having a long narrow tubes, a series of baffles could makes one large inlet seem like many smaller inlets. In an effort to test this, the parabolic shape was

modeled for simulation with 1 baffle, 3 baffles, and 5 baffles. Figure 4.7 shows an example of the parabolic inlet with 3 baffles.
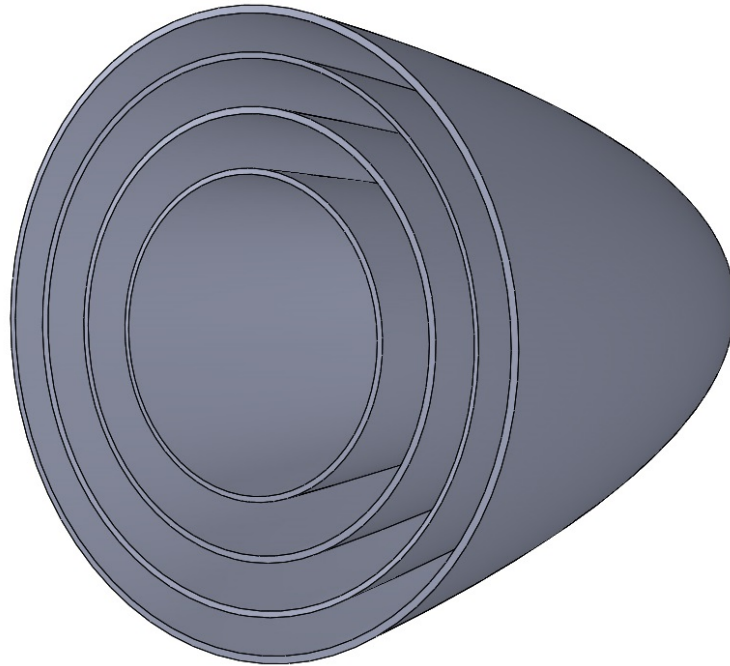
Figure 4.7: 3-Baffled parabolic 10 cm length inlet.

The parabolic curves for the baffles were defined the same way as the outer shell of the original model by dividing the initial aperture into 4 separate flow regions, and thus giving the boundary conditions needed.

Under the same test conditions, the baffled inlets were tested in MolFlow+. Figures 4.8 – 4.10 shows the results of this test. Figure 4.8 compares the performance again for the pyramidal, conical, and parabolic inlet shapes, but this time also includes baffles. The conical and pyramidal shapes perform the best without baffles, but the addition of three baffles to the parabolic inlet actually increases the capture percentage by about ∼40% under diffuse reflection. This isn't a large increase given the density, but with an air-breathing system, any increase to the total mass captured at diffuse conditions is beneficial.
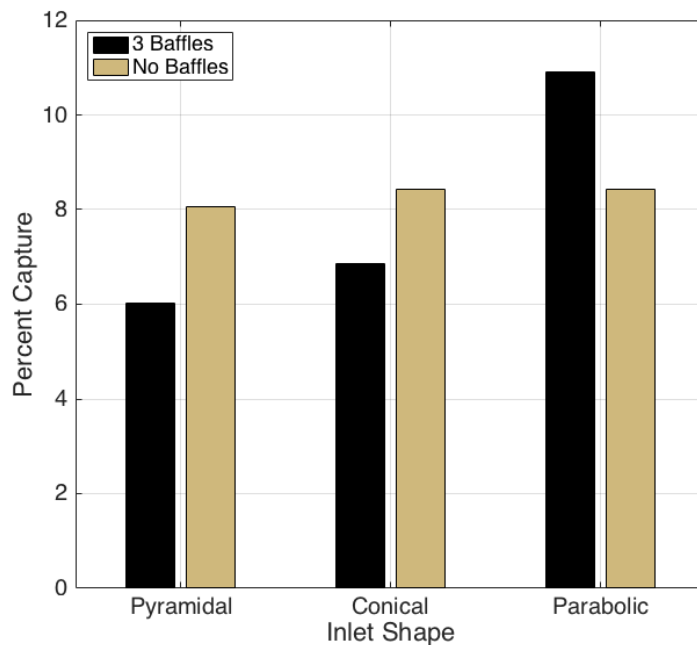
Figure 4.8: Inlet capture percentage comparison for different inlet shape and number of baffles under diffuse conditions.
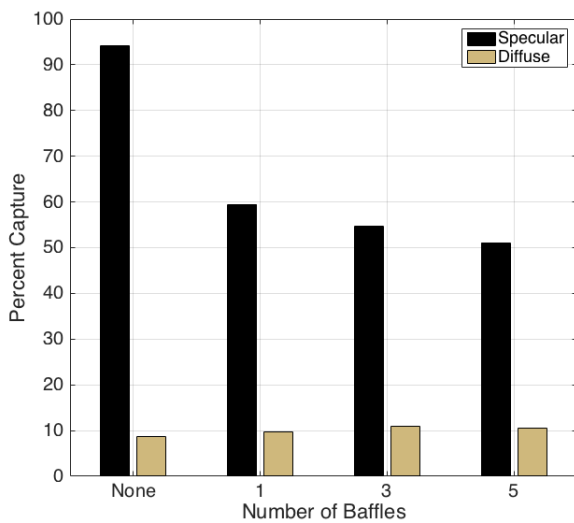
(a)
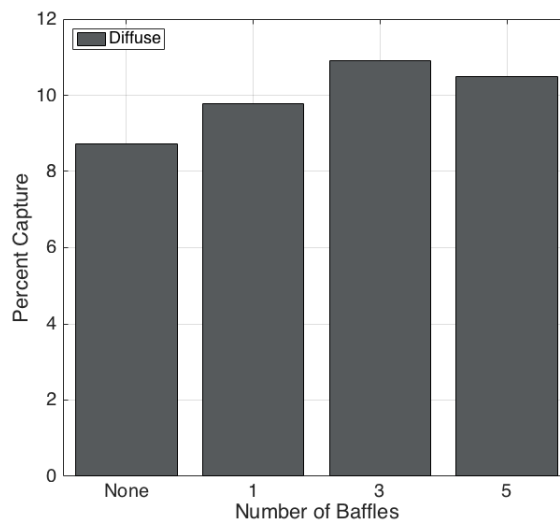
(b)

Figure 4.9: Parabolic inlet capture comparison using various baffles. (a) Specular and diffuse reflection capture percentages (b) Diffuse reflection capture percentages (same as those shown in (a) but zoomed in for clarity).

Figure 4.9a shows that the addition of baffles negatively impacts the specular reflection of the parabolic inlet which is no surprise given that the baffles block each subsequent level from reflecting towards the focus. However in Figure 4.9b, it is clear that that there are diminishing returns on the number of baffles used. Given the size and shape of the inlet, 3 baffles appears to the be optimal number to increase the diffuse capture percentage.
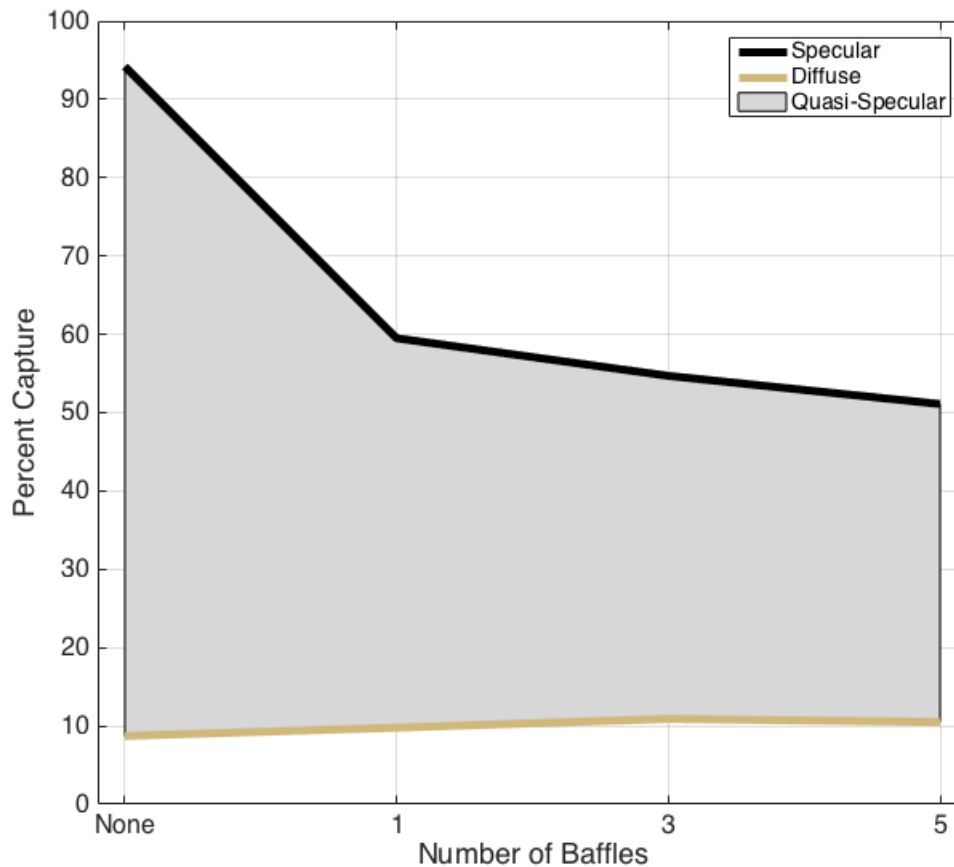
Figure 4.10: Parabolic capture baffles with use of baffles compared to no baffles showing the quasi-specular solution space.

Figure 4.10 shows the range of capture percentages that can be expected depending on the number of baffles used. The space in between specular reflection and diffuse is what is referred to here as the quasi-specular region where the specular and diffuse capture percentages mark the upper and lower bounds of this region. The inlet will largely operate in this region until the inlet surface

reaches full contamination. This region could probably be modeled for any particular scenario as a weighted combination of the upper and lower bounds, but the weights would need to be empirically determined. For the inlet design, the goal would be to increase the diffuse lower limit while keeping the specular reflection upper limit high. The question is then is it better to have a larger range of capture percentages (the inlet with no baffles), or to have an inlet that gives a higher diffuse capture percentage (the 3 baffle inlet) with a lower specular capture percentage? The answer to this question can be determined by knowing the rate of contamination of the surface which is different depending on the material used for the inlet. The answer to this question is out of scope for this paper and is left to future research.

4.2   Further Discussion

4.2.1   The Problem of Rarefied Flow

Today even the world's best super computers have difficulty with numerical calculations based on the Boltzmann equation (an equation proposed in 1872) [*Sharipov*, 2006]. The "model-equations" have been and still are the most used method for the calculations of rarefied gas flows [*Sharipov*, 2006]. These "model-equations" are simplifying methods in order to make the calculations of rarefied gas flow more obtainable, but their outputs are limited.

The common assumptions made for any rarefied gas flow in a pipe or in a conical duct are that the length of the tube or duct is much, much greater than the the width or largest area of the pipe. This is the same principle expressly used by *Nishiyama* [2003] for his design. If the length of the pipe is significantly greater than the width (or radius), the end conditions can be ignored and the flow can be considered one-dimensional. That is not the case for any inlet in this study.

4.2.2   Compression of Rarefied Flow

The next step in air-breathing systems is to increase compression. To rely on shocks is out of the question, and conventional fluid properties that would cause compression (flow through

a variable area tube, etc.) are more likely, it still stands that compression of the "individual" particles into a more tightly packed cluster, would result in greater thrust. The methods on how to accomplish this though are outside of the scope of this paper; however ion containment is one possible way to accomplish this, and it will be discussed briefly in the next chapter.

4.2.3   Decontamination

As stated before, the primary source of contamination (aka. accommodation) of the inlet surface is due to atomic oxygen. Oxygen is "sticky", and readily attaches and stays attached to metallic surfaces. This interaction produces the fully diffuse gas-surface interactions that will decrease the efficiency of the inlet over time. This gas-surface interaction will vary with the material used, and will affect how the oxygen molecules will attach (as a cluster or in a disordered pattern). Although out of scope for this paper, it will be necessary to determine a metal that is capable of a low adsorption rate in order to keep the inlet capture efficiency as high as possible for the lifetime of the mission. Another proposed solution is to determine a way to "de-adsorb" the inlet. This currently seems to be either out of the realm of possibility or the ability to do so has not yet been discovered.

Chapter 5

Ionization and Ion Confinement

This chapter discusses potential methods of ionization for the proposed thruster along with methods of ion confinement that could be employed. This chapter is more theoretical in scope than the inlet or the thruster analysis, and therefore will speak generally about possibilities and solutions to this problem. A proposal for further research is outlined in Chapter 7.

5.1   Plasma Generation

As outlined in Chapter 2, there are several methods commonly employed for ionization. The simplest method is the hollow cathode tube inside of a chamber comprised of magnets used for ion confinement. For this air-breathing thruster, there are two possible configurations that could be used within the 3U, 6U, 12U, and 27U frameworks. The first configuration has the thruster running the length of the CubeSat (using multiple inlets, in some cases, with a single accelerator grid set), and the second configuration consists of multiple thrusters (inlets and accelerator grids. Both configurations will be discussed as each poses a unique problem to plasma generation.

5.1.1   The Long Configuration

A cross section of the proposed thruster running the length of the CubeSat, what we refer to as the "long" configuration, was previously shown in Fig. 2.15. By using a reasonable sized acceleration grid (see *Wirz et al.* [2001]) and a 10 cm inlet, there would need to be a length of tube connecting the inlet to the thruster.

Normally the propellant for an electrostatic thruster is ionized inside of the chamber that is located immediately behind the accelerator grids (see Figure 2.2a). In Chapter 4, the capture percentage under diffuse conditions was determined to only be ~10%. Using a similar model but including a 15 cm tube to the end of the inlet in our Monte Carlo modeling brings the capture efficiency down to roughly 4% for diffuse reflection. Therefore if the incoming neutrals are not ionized until they're close to the accelerator grids, the number of particles lost due to further gas-surface interactions will increase, dropping the number of captured particles in half from an already low capture percentage.

If a modified ion confinement method could be utilized along the length of this uniform tube leading from the exit of the inlet to the accelerator grids, the ionization could potentially occur at the exit aperture of the inlet. The Penning trap is able to confine ions in the axial and radial direction by use of electrodes and permanent magnets. Figure 5.1 shows the layout of a Penning trap.
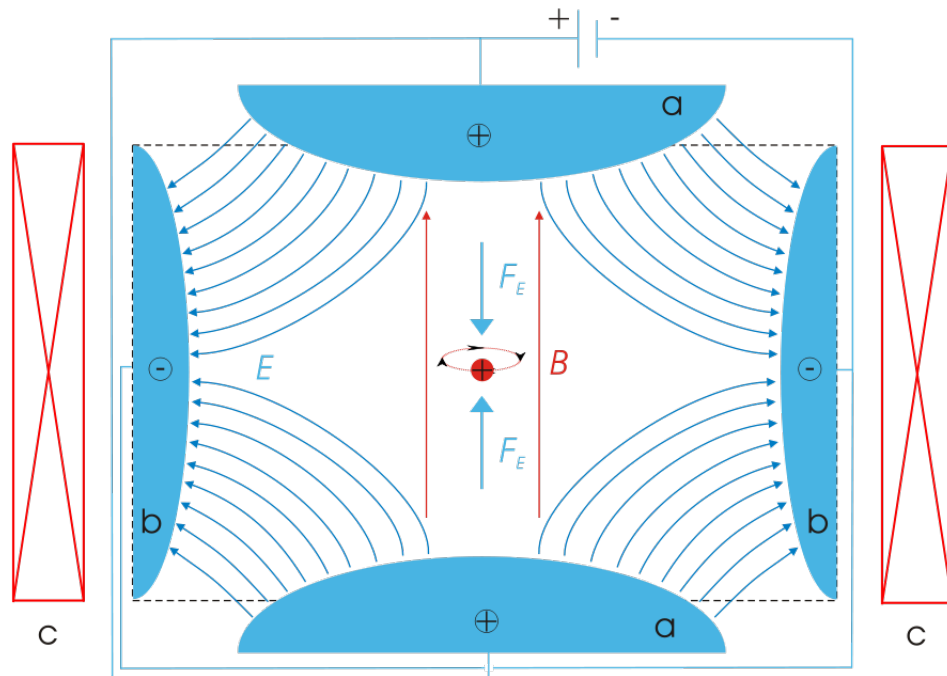

Figure 5.1: Diagram of a Penning Trap [*Kriesch*, 2006].

The Penning trap consists of an axial magnetic field to radially confine particles and a quadrupole electric field for axial confinement. In such a system, the ions would be trapped in a circular cyclotron motion. If applied to the problem at hand, the ions would not impact the channel leading to the accelerator grids; however, they would lose all axial velocity needed to carry them through the channel. Assume the configuration shown in Figure 5.1 is applied to the long channel leading to the accelerator grids, and the figure is a cross section of channel looking towards the accelerator grids. If an electric field were applied across the plane of channel, a force would be applied along the length of the channel (via $\vec{E} \times \vec{B}$), hence accelerating the particles towards the accelerator grids but preventing interactions with the surface of the channel.

5.1.2   The Short Configuration

The "short" configuration would allow for multiple thrusters to be placed within the framework of a CubeSat. Positioning this air-breathing system in an abbreviated position where the inlet would be closer to the accelerator grids would remove the need for ion confinement. The neutral particles could be ionized shortly before the accelerator grids, and simple magnetic confinement (see Figure 2.8a) alone would guide the ions through the accelerator grid. This configuration would have no impact on the 27U's thruster design as its frame is a cube unless the inlet was lengthened.

Depending on the size of the CubeSat, the inlet length could be increased, and as was shown in Chapter 4, the longer the inlet the higher the capture percentage. Assuming the accelerator grids along with any other hardware take up only 0.5U, the inlet could be as long as 25 cm for the 27U CubeSat.

Since the fuel source in an air-breathing system is no longer the limiting factor, the degradation of the plasma generator becomes more of an issue depending on which type of generator is used. However with regards to air-breathing systems, plasma generation for low particles densities can present a problem depending on what type of plasma generator is chosen. It becomes a balance between longevity of the plasma generator and ability to ionize at low densities.

The DC-discharge method is advantageous for low density applications. The number of electrons produced by the cathode could be increased for this application in order to mitigate ignition issues caused by the low density of the incoming neutrals. However, cathode erosion would be a problem for long-term operations, and the breakdown of the cathode would limit ionization during the life-time of the CubeSat.

The other option would be the microwave discharge which only uses electromagnetic fields for ionization. This eliminates any issues with life-span for plasma generation; however as stated before, this system is sensitive to frequency and low plasma densities. If it were possible to specifically calibrate this type of generator for air-breathing applications, it would be the most reliable.

The RF discharge system does require more initial care such as shielding the RF antenna or building the thruster body out of an insulting material. The RF system might also require a spark generator in order to increase the number of electrons in the discharge chamber before the ionization process begins. The RF system also has lower efficiencies, but it uses less power and it doesn't use a cathode.

5.2   Performance

5.2.1   Fundamentals

The mass (or propellant) utilization efficiency reflects the number of incoming particles that are ionized by the plasma generator which can be defined as:

$$\eta_m = \frac{\dot{m}_i}{\dot{m}_p} \tag{5.1}$$

for singly charged ions where $\dot{m}_i$ is the ion mass flow rate and $\dot{m}_p$ is the neutral mass flow rate.

The performance of the plasma generator is commonly characterized by looking at the discharge loss against the mass utilization efficiency [*Goebel and Katz*, 2008]. The discharge loss is

primarily the cost of producing ions; it accounts for the amount of power used to ionize the neutrals against the resulting beam current that is produced by the ionization efforts. It can be defined by:

$$\eta_d = \frac{P_d}{I_b} \tag{5.2}$$

where P_d is the power to produce ions. In totality, the discharge losses account for producing ions and excited neutrals, ions that hit the grid instead of becoming part of the beam, and heating the electrons that are lost to the walls [*Goebel and Katz*, 2008].

The more efficient the mass utilization the greater the discharge losses become and vice versa [*Goebel and Katz*, 2008]. Figure 5.2 shows an example of this comparison for an RF ion thruster.

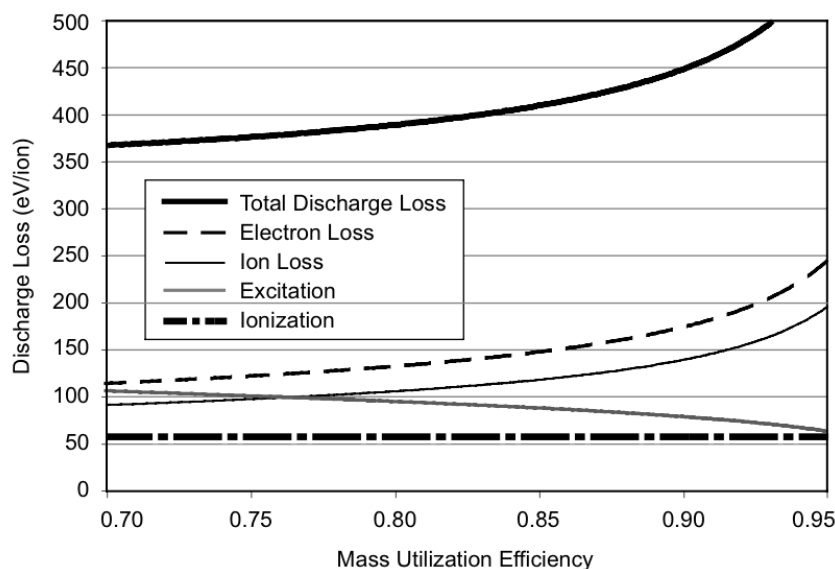Figure 5.2: Mass Utilization Efficiency to Discharge Loss for an RF Ion Thruster [*Goebel and Katz*, 2008].

5.2.2   Application

The primary issues with selecting a plasma generator lies within current technological limitations. Traditional thermionic cathode emission sources, which operate well within noble gases, cannot operate within oxygen-containing species, and despite this knowledge, there is been little

effort to develop technology to overcome this [*Singh and Walker*, 2015]. A non-thermionic emission source prototype has been designed, but it has not been developed or tested. As far as RF or microwave cathodes, no tests have been conducted on atmospheric constituents [*Singh and Walker*, 2015].

The mass utilization efficiency is another issue for air-breathing systems. While current ionization methods are capable of high efficiencies for xenon, this not translatable to atmospheric constituents [*Singh and Walker*, 2015]. According to *Wirz et al.* [2001], a micro-ion thruster of comparable size to the one that would be used in the system proposed in this paper, has a propellant efficiency of 50% (as high as 82%) using a DC discharge system. However according to *Pilinski* [2008], the DC discharge ionization efficiency for neutral atmospheric particles is much lower. The Drag and Atmospheric Neutral Density Explorer (DANDE) satellite ingests neutral atmospheric particles for analysis and ionizes them. The research on the DANDE showed that an expected ionization efficiency of these low density neutral particles is 0.1% [*Pilinski*, 2008]. *Shabshelowitz* [2013], whose research focuses specifically on ionization for air-breathing thrusters using RF discharge, makes an estimate of 10% efficiency. A white paper by *Matney* [2013], that bases its work on *Conley* [1995], is optimistic that 100% ionization of the incoming particles is possible given the proper chamber design.

In *Shabshelowitz* [2013], the conclusion is that an RF plasma generator can increase ionization for a HET thruster; and even though air-breathing propulsion is feasible for smaller satellites, there needs to be further study of the ionization of the atmospheric constituents. In general, the ionization of atmospheric gases for use in electrostatic thrusters will require further research before a consensus can be reached on ionization efficiencies. It is possible that new methods of ionization might need to be explored in order for the atmospheric constituents to reach the same efficiencies as xenon propellant [*Singh and Walker*, 2015]. For this research, 10% ionization efficiency will be assumed, but an analysis of how ionization impacts the performance of this proposed system will be conducted in Chapter 6.

Chapter 6

Thrust Analysis from Acceleration Grid

In this chapter, the expected thrust and performance of this proposed air-breathing electric thruster is analyzed given the capture percentage of the inlet and the ionization efficiency outlined in Chapters 4 and 5. The effects of voltage and solar activity on the thrust are quantified. The thrusters performance compared to the drag on the various CubeSat sizes is discussed. The power requirements of the system are also outlined, along with the power-limited effects on the performance of the thruster.

The analysis of this concept thruster was run with respect to the 6U, 12U, and 27U CubeSat sizes as well as an assessment of its use in a 3U system. The following performance characteristics and assumptions were assumed throughout unless otherwise noted:

- The beam voltage and the total voltage are considered equal since the numbers of particles effecting the electric field are small. It is assumed that there is one particle at a time passing through the field due to the low densities. The voltage used therefore is 700V when running these calculations (unless otherwise stated). This number is considered a good estimate of performance based on similar systems [see *Wirz et al.*, 2001].

- Average F10.7 and Ap values were used. As shown in Table 3.2, the average value over the past 11 years for F10.7 was 98.7, and the average Ap was 8.6.

- The 3U, 6U, 12U, and 27U CubeSats dimensions are as follows:

    3U: $0.10 \times 0.10 \times 0.30$ cm

6U: $0.12 \times 0.24 \times 0.36$ cm

12U: $0.24 \times 0.24 \times 0.36$ cm

27U: $0.34 \times 0.35 \times 0.35$ cm

- All drag calculations are calculated in the ram direction (that is, the drag on the smallest face of the CubeSat). If the broad-side is used to calculate drag, it is noted.

- Based on the results in Chapter 4, the maximum capture percentage of the parabolic inlet is rounded to be 90%, and the minimum capture percentage of the inlet is rounded to be 10%. All values in-between are considered quasi-specular reflections.

- The ionization efficiency of the system is assumed to be about 10% which is an estimate made from *Shabshelowitz* [2013]. For these calculations, it is assumed that the grid transparency is accounted for within this efficiency percentage. If one were to assume a 12% ionization efficiency and an 80% grid transparency, the total efficiency would be about 10%.

- The system is assumed to be ionizing a combination of atomic oxygen, O_2, N_2, and hydrogen. Argon, atomic nitrogen, and helium are not used in these calculations because argon's and nitrogen's densities are low relative to the other particles, and helium's first ionization potential is very high relative to the other particles making it much less likely to ionize.

- As described in Chapter 4, the same sized inlet is used for each CubeSat configuration; however, the number of inlet's used varies based on the configuration. The 6U CubeSat uses 2 parabolic inlets, the 12U uses 4 parabolic inlets, and the 27U CubeSat uses 9 parabolic inlets in the "long" configuration. This means that the density of the propellant is multiplied by the number of inlets for the thrust calculation depending on the configuration in question.

- Conservation of mass is used to estimate the density increase due to variable area nature of the inlet. That is:

$$\rho_1 A_1 \cancel{v} = \rho_2 A_2 \cancel{v} \qquad (6.1)$$

where any losses in speed experienced by the incoming neutrals are assumed to be negligible such that the velocity is constant across the length of the inlet.

6.1   Particle Contribution

The contribution to thrust was analyzed to show which particles have the greatest effect on thrust at different altitudes. Figure 6.1 shows the overall thrust following asymptotes bound by hydrogen above approximately 450 km, atomic oxygen between 450 km and about 175 km, and N_2 below 175 km.
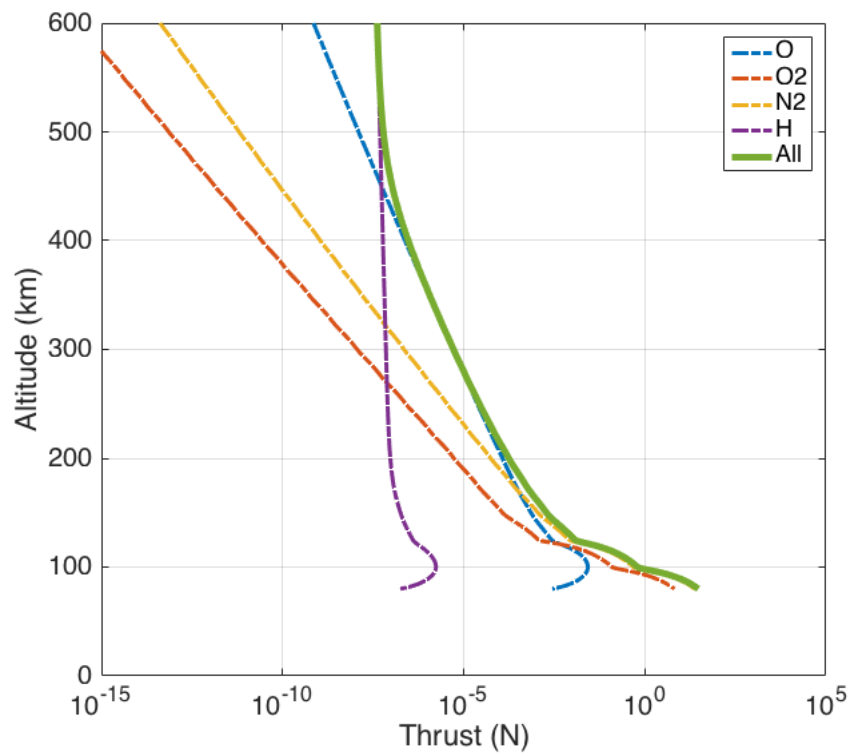

Figure 6.1: Particle contribution to thrust at various altitudes at 90% inlet efficiency for a 3U system

6.2   Thrust vs. Voltage

The voltage potential between the screen grid and the acceleration grid impacts the performance of the ion thruster. An analysis of this effect was examined at an altitude of 125 km and 300 km at both 90% inlet efficiency and 10% inlet efficiency assuming an average solar activity.

Figure 6.2a indicates that a 6U CubeSat at 125 km equipped with 2 inlets in the ram direction can output a little less than 0.1 N of thrust under specular reflection. Figure 6.2b shows this same 6U system, but at a higher altitude where the neutral particle population is much less dense. The thrust obtainable with specular reflection is in tens of μN range. Figure 6.2c shows a 12U CubeSat at 125 km equipped with 4 inlets in the ram direction, and the thrust range is double that of the 6U as expected. Figure 6.2d shows the decrease in thrust due to the particle density where the thrust range is in the tens of μN. Figure 6.2e shows a 27U CubeSat at 125 km equipped with 9 inlets in the ram direction outputting ∼4.5 times the thrust of the 6U thruster. Figure 6.2f shows the same CubeSat at 300 km where once again the thrust is considerably less due to the particle density. These results shows that the voltage is a critical component to the performance of the thruster. The thrust performance only appears to vary linearly with the change in voltage as Equation 2.8 clearly shows that thrust is proportional to the square root of voltage.
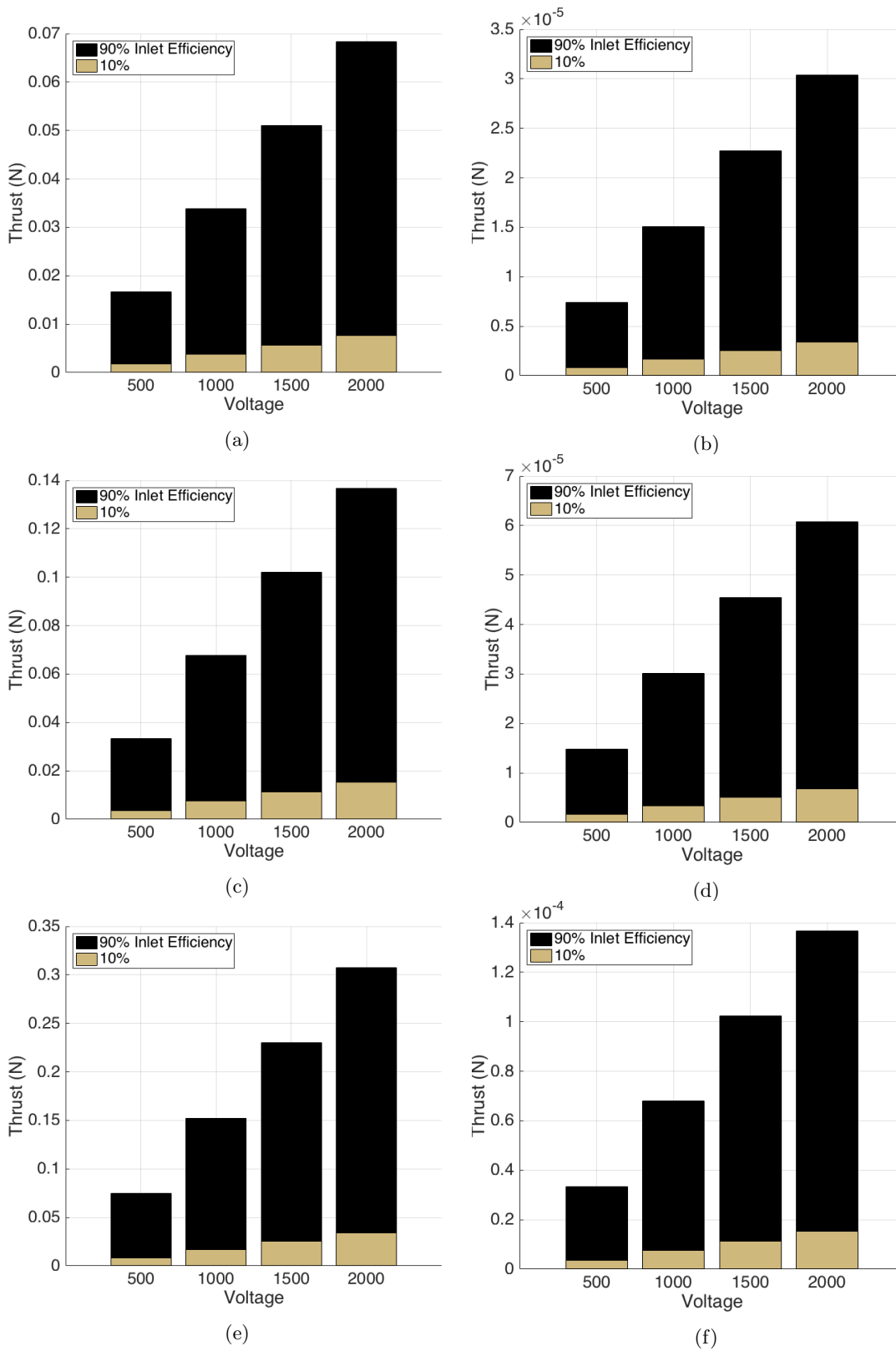
Figure 6.2: Magnitude of Thrust when voltage is varied for (a) a 6U system at 125 km (b) a 6U system at 300 km (c) a 12U system at 125 km (d) a 12U system at 300 km (e) a 27U system at 125 km (f) a 27U system at 300 km

6.3   Thrust vs. Solar Activity

As highlighted in chapter 3, the solar activity will affect the particle density of the atmosphere. Naturally, this will affect thrust. An analysis of this effect was examined at altitudes of 125 km and 300 km at both nearly specular and diffuse conditions assuming an operating voltage of 700V. Refer to Table 3.2 for the values used for F10.7 and Ap for max, min, and average solar activity.

Figure 6.3a and 6.3b shows the thruster performance of a 6U CubeSat (with 2 inlets) varying with solar flux at 125 km and 300 km respectively. Figure 6.3c and 6.3d shows the thruster performance of a 12U CubeSat (with 4 inlets) varying with solar flux at 125 km and 300 km respectively. Figure 6.3e and 6.3f shows the thruster performance of a 27U CubeSat (with 6 inlets) varying with solar flux at 125 km and 300 km respectively. At the lower altitudes the solar flux has little impact on the overall thrust which is directly correlated to the density remaining fairly consistent with variations in the solar flux at this altitudes. The real difference is experienced at higher altitudes, and the difference in the thrust increases between solar max and solar min as the altitude increases. At an altitude of 300 km, the thrust is already an order of magnitude different between minimum and maximum solar flux.

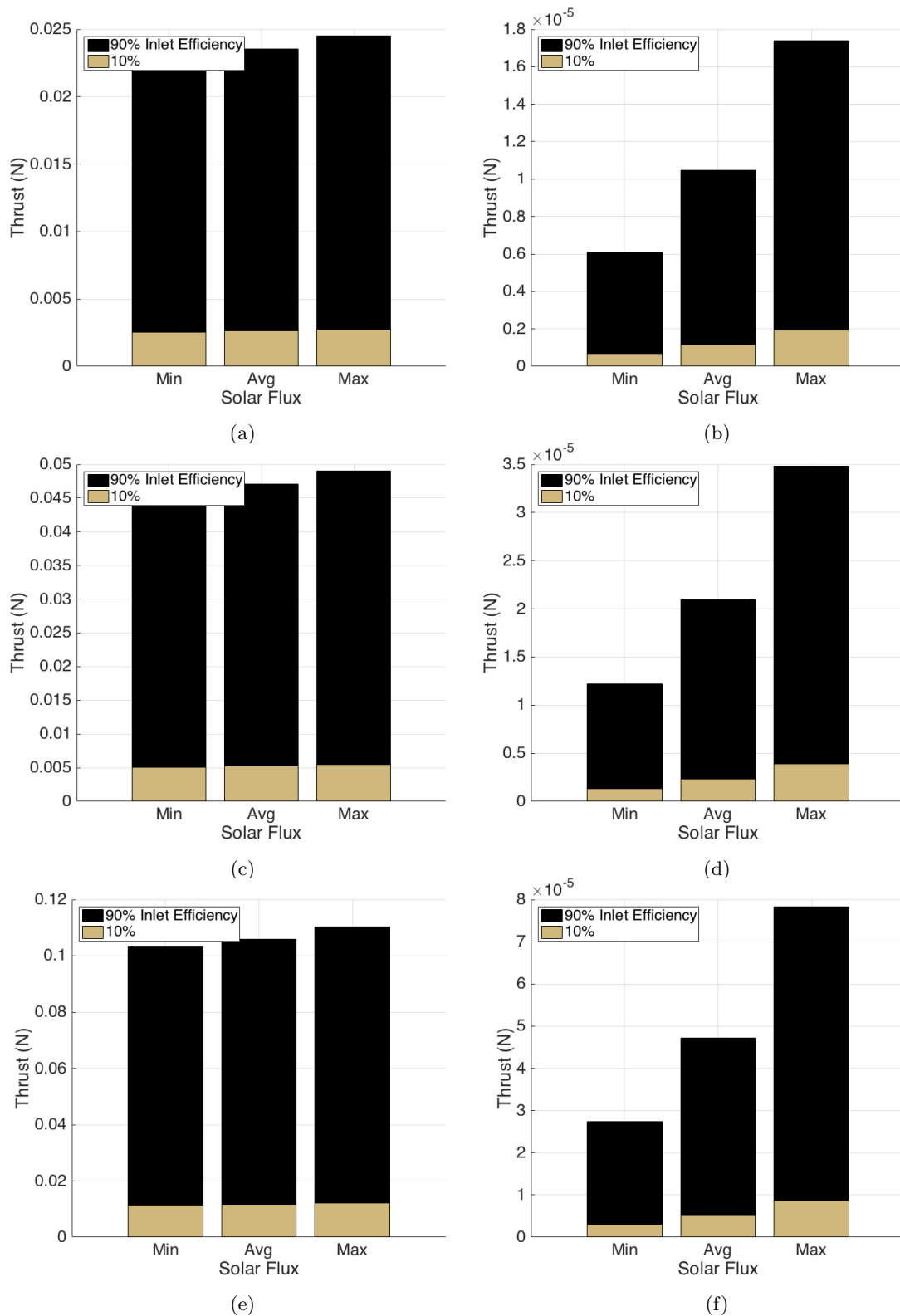Figure 6.3: Magnitude of Thrust at max, min, and average solar activity at an operational voltage of 700V (a) for a 6U system at 125km (b) for a 6U system at 300km (c) for a 12U system at 125km (d) for a 12U system at 300km (e) for a 27U system at 125km (f) for a 27U system at 300km

6.4   Thrust vs. Drag

One of the primary goals of this research is to analyze the ability of this proposed air-breathing thruster to overcome drag. This section evaluates the current performance taking into consideration solar flux and the system's power limitations. The thrust and drag are also analyzed with regard to the different configurations discussed in Chapter 2.

6.4.1   Solar Activity

Running analysis of a 3U system (single inlet, single thrust system) under specular and diffuse conditions each at the min, max, and average solar conditions is displayed in Figures 6.4a, 6.4b, and 6.4c. The red lines show thrust at minimum, maximum, and average solar flux when the inlet has a capture efficiency of 90% and 10%. The thrust shown is for a 3U system which has 1 inlet and 1 set of accelerator grids. If the inlet efficiency stays above ~70%, the thruster will be able to counteract drag in a 3U system; however if this single thruster is used in a 6U system, the inlet efficiency will need to stay at 90% in order to match drag at ~300 km. Its also important to note that the solar conditions clearly effect drag more than they do thrust even though they are both dependant the atmospheric density. The "bumps" seen in the lower altitudes are due to the significant changes in density that are projected in the NRLMSISE-00 model. The model was constructed to run in 25 km steps, and below 125 km, the density changes rapidly (about 2 orders of magnitude every 25 km).

(a)   (b)

(c)
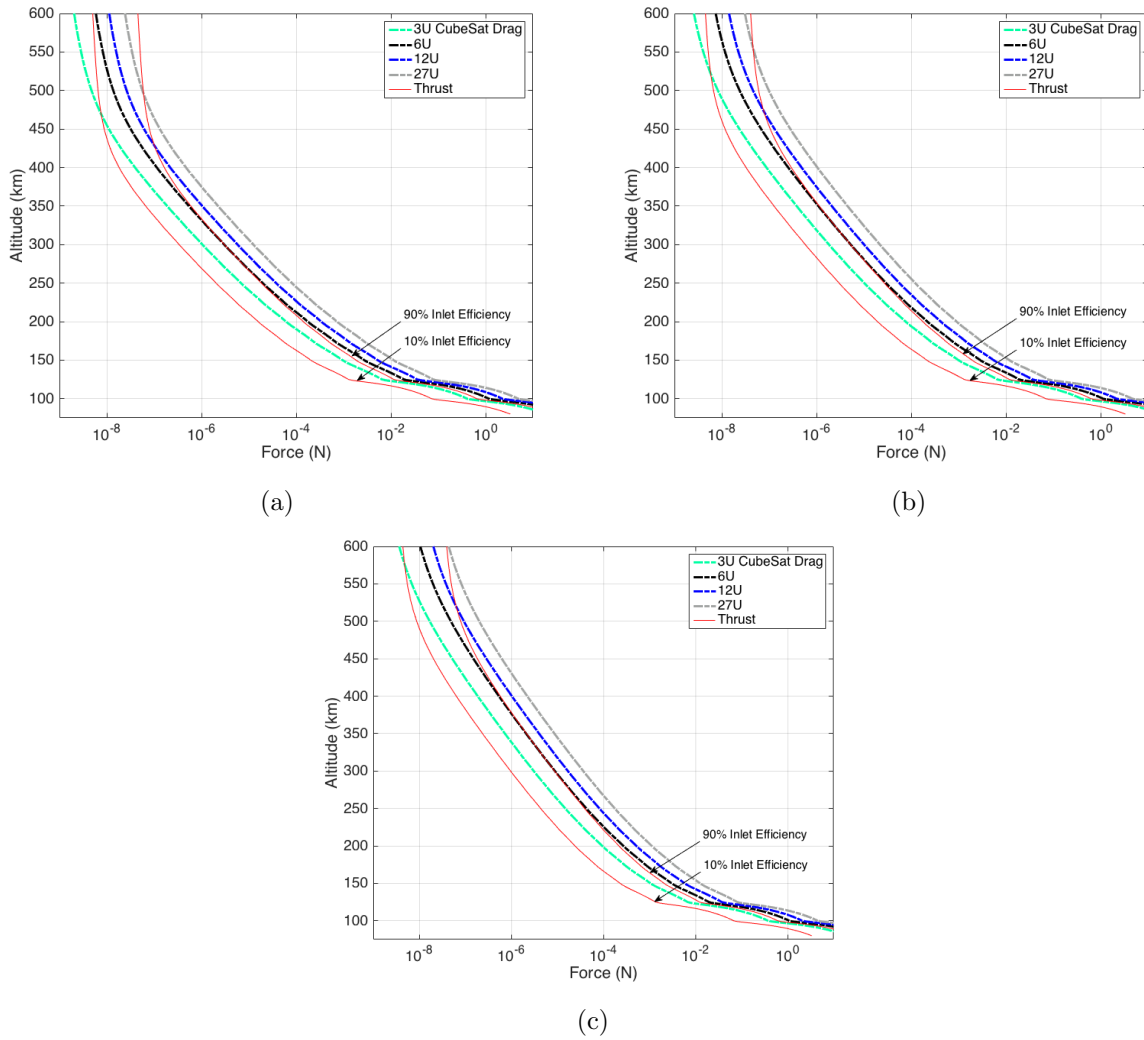
Figure 6.4: Drag versus Thrust plot at min (a), average (b), and max (c) F10.7 for nearly specular and diffuse capture for a single inlet thruster

6.4.2   Power-Limited Thrust

As stated previously, electric thrusters are power-limited, and in the case of the CubeSat using an air-breathing system, power is most definitely the single largest limitation. Busek Space and Propulsion Systems makes CubeSat thrusters that on average require around 25W and at most 75W [*Busek Space Propulsion and Systems*, 2014]. Obviously, the solar panels, power supply and power requirements of other subsystems would vary based on the mission.

Using the mass flow rate, the exit velocity of the ionized particles, and an efficiency of conversion into exhaust kinetic energy which is commonly between 0.4 and 0.9 *Kantha* [2017], the power requirements of the system are considered across the LEO altitudes for 1 to 6 thrusters.
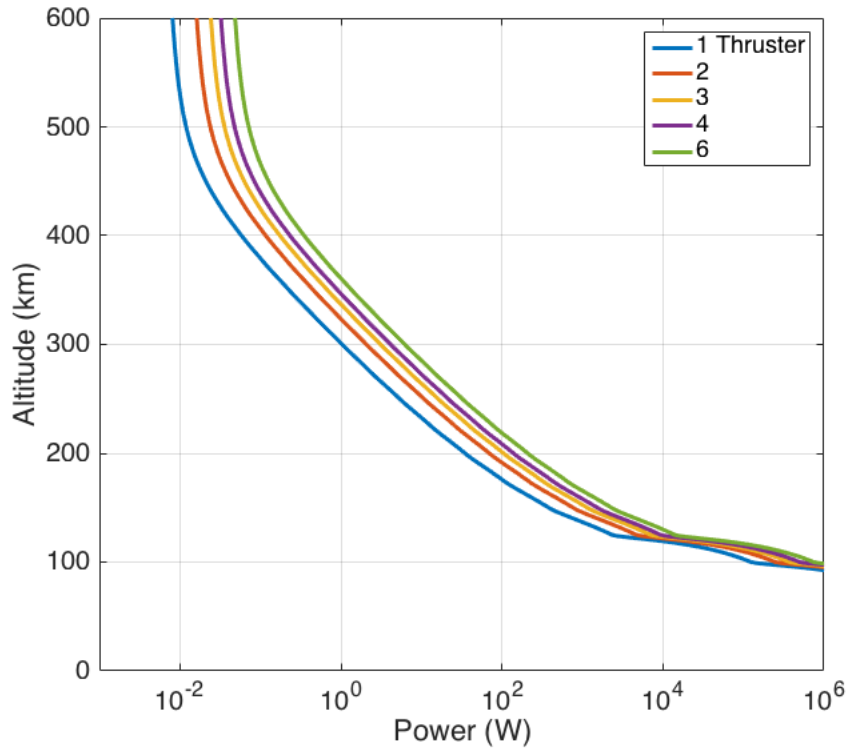
Figure 6.5: Power vs. altitude for a single thruster at max inlet efficiency

Figure 6.5 shows the power required for 1–6 of the proposed thrusters under average solar flux conditions. The power necessary to operate this system is in the tens of kilo-Watts below 125 km, and the power consumption increases exponentially below 125 km. This increase in power consumption occurs because the number of neutrals begin utilized as propellant increases due to the increase in density. This figure doesn't account for the change in beam voltage that would occur due to the increased density or the additional consumption of power for more ionization. As stated in Chap 2, EP systems are power-limited unlike chemical rockets which are energy-limited (by the propellant).

Here it is assumed that the CubeSat's thruster is limited to 10 W or 100 W. Figure 6.6 shows the power-limited thrust versus drag for a single inlet thruster at 10% and 90% inlet capture efficiency at an average F10.7 and Ap.
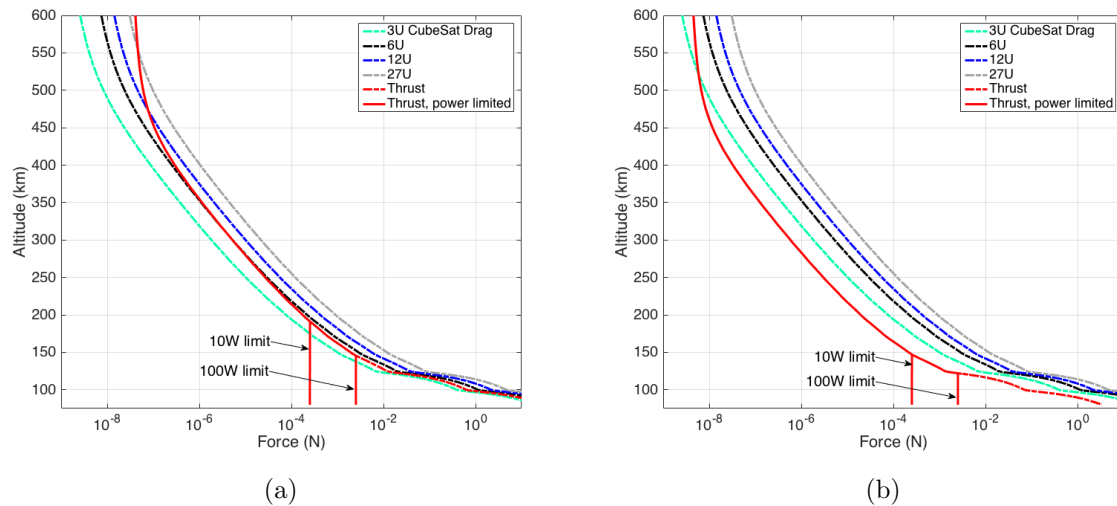
Figure 6.6: Thrust versus drag showing a 3U power-limited system at average F10.7: (a) Power limited at 90% inlet capture efficiency at an operational voltage of 700V (b) Power limited at 10% inlet capture efficiency at an operational voltage of 700V

Figures 6.6a shows the thrust for a power-limited 3U thruster system at 100 W and 10 W with 90% inlet capture efficiency. Figures 6.6b shows the thrust for a power-limited 3U thruster system at 100 W and 10 W with 10% inlet capture efficiency. The power limitation of the system makes the air-breathing thruster far less effective at lower LEO altitudes especially when the inlet is fully contaminated. A 3U system with 90% inlet efficiency would only be able counteract drag above ∼175 km at 10 W and above ∼145 km with 100 W. As before, any inlet efficiency below ∼70% would not be able to match drag. This power limitation will be used for all further thrust calculations using 10 W as a power limit for the system. It's also important to note that with 10 times the available power, the 3U system using 100 W is only able to operate 25–50 km lower in altitude from the 10 W system. This shows that the returns by increasing power are small, and in order to reach lower altitudes massive amounts of power would have to be employed.

6.4.3 Multiple Inlets

By varying the number of inlets used, the thruster can be increased based on the size of the CubeSat. This is the advantage of the long configuration discussed in Chapter 2. The CubeSat could operate on only one set of accelerator grids with multiple inlets feeding into the ion confinement channel. Table 6.1 gives a summary of the potential number of inlets per CubeSat size.

Table 6.1: Maximum number of inlets per CubeSat in the long configuration

CubeSat Size	Inlets
3U	1
6U	2
12U	4
27U	9

The following figures show the thrust against drag over this range of inlets. Drag is determined using atmospheric density from the NRLMSISE-00 model discussed in Chapter 3, and then using the basic drag equation as shown in Equation 3.3. Thrust is calculated from the beam voltage, beam current, and the electric field generated between the accelerator grids as detailed in Equation 2.15. The thrust curves displayed range from 90% efficiency to 10% efficiency of particle capture in the inlet.

Figure 6.7a shows the thrust of a 6U system with inlet efficiency from 90% to 10% with a power limit of 10 W. Figure 6.7d shows the thrust to drag ratio for the same system at inlet efficiencies of 90%, 50%, and 10%. Figure 6.7b shows the thrust of a 12U system with inlet efficiency from 90% to 10% with a power limit of 10 W. Figure 6.7e shows the thrust to drag ratio for the same system at inlet efficiencies of 90%, 50%, and 10%. Figure 6.7c shows the thrust of a 27U system with inlet efficiency from 90% to 10% with a power limit of 10 W. Figure 6.7f shows the thrust to drag ratio for the same system at inlet efficiencies of 90%, 50%, and 10%. For the 6U

system the thruster matches drag at about 200 km for inlet efficiencies above 50%. For the 12U and 27U thruster systems, the thrust matches drag between 250 km and 200 km for inlet efficiencies at about 50%. This is within the altitude range where increased atmospheric observation is desired.
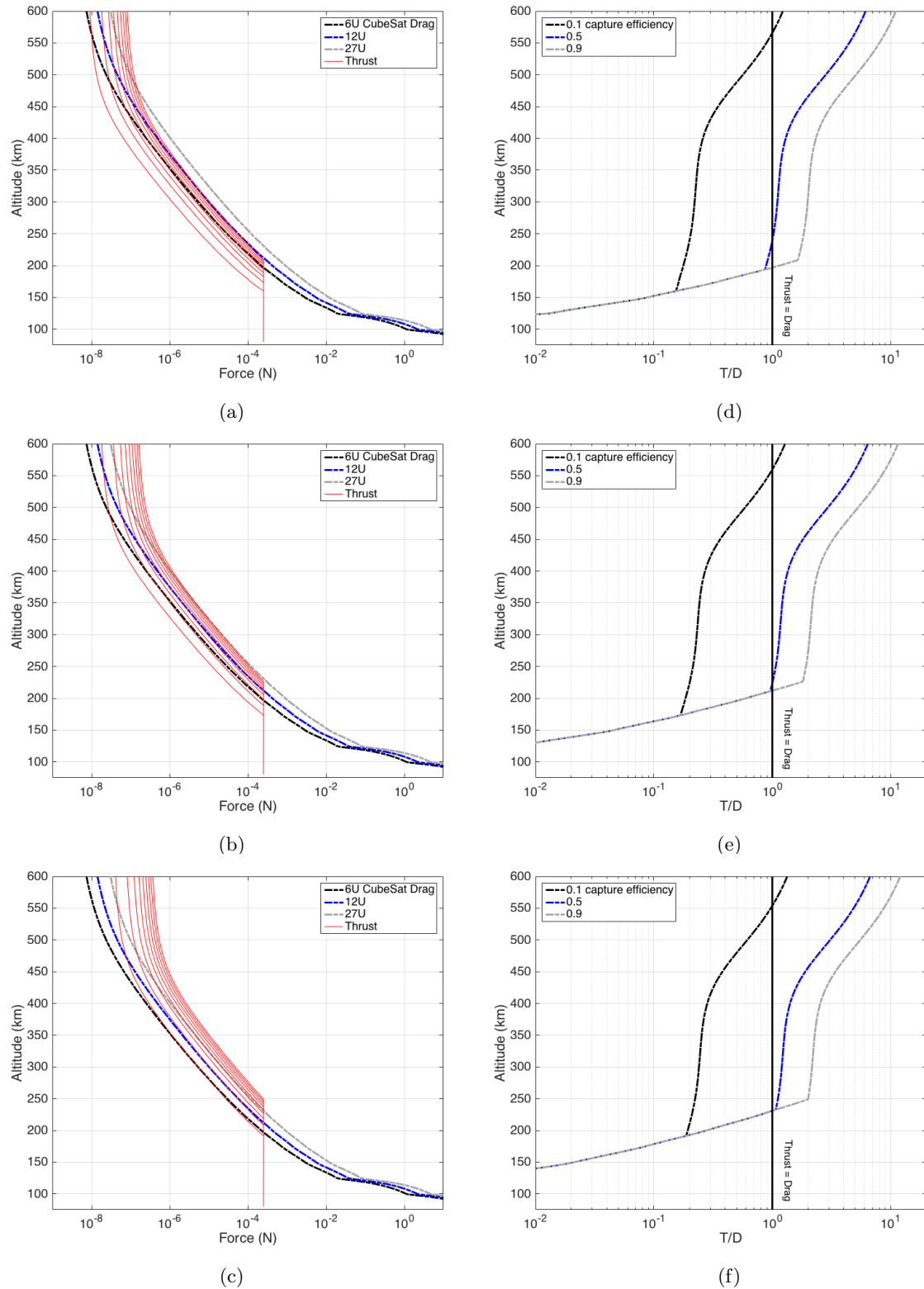
Figure 6.7: The left column shows thrust versus drag from 90% to 10% inlet capture efficiency (a) 6U system with 2 inlets (b) 12U system with 4 inlets (c) 27U system with 9 inlets. The right column shows T/D (d) 6U system (e) 12U system (f) 27U system

These plots show that the thruster is only effective above 200 km for the 6U system, and above about 250 km for the 27U system. As shown in Figures 6.4a through 6.4c, this thruster could produce thrust greater than drag well below 100 km; however, to do so as shown in Figure 6.5, the power would need to be around 10 kW which is completely unreasonable for a CubeSat.

6.5   Thruster Orientation

Running the thruster along the length of the CubeSat system presents a problem. However by using the "short" configuration would allow the inlet to feed ionized particles directly into the acceleration grid. The system would be placed with the inlet of the thruster on the broad side of the CubeSat as demonstrated in Figure 6.8. Instead of increasing the number of inlets, each 1U segment gets an inlet and accelerator grids.
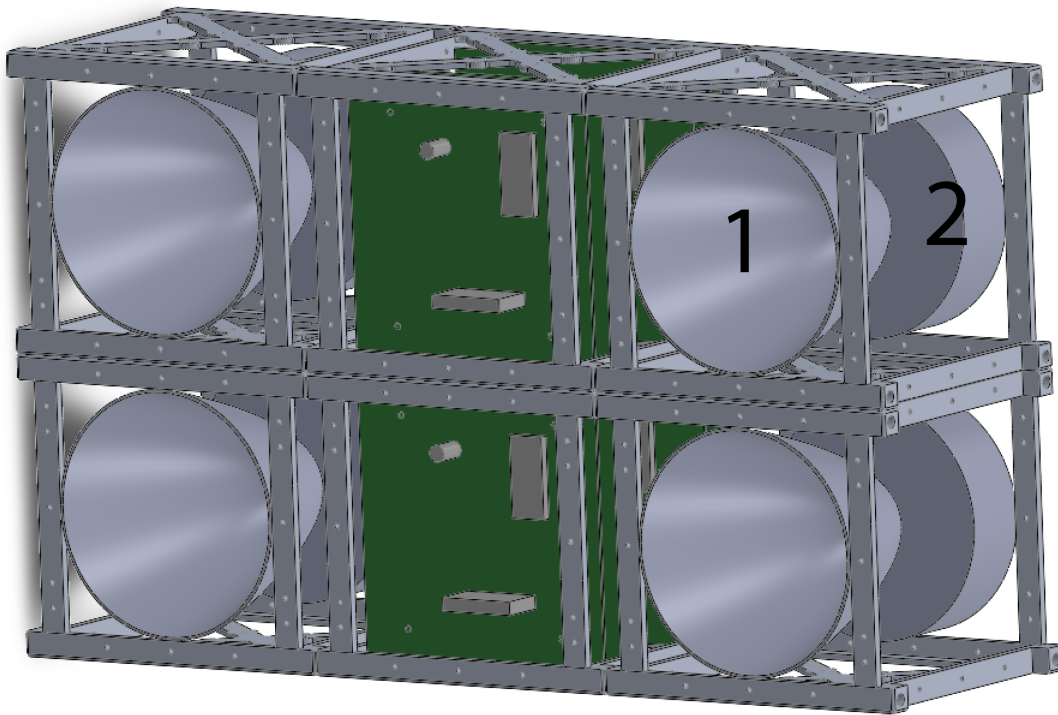
Figure 6.8: 6U CubeSat with four thrusters on the broadside (1) inlet (2) accelerator grids

Depending on the thrust needs of the system, the 6U Cubesat could either use two thruster in the center or four thruster, two at each end of the CubeSat. Naturally in this setup the drag will increase, and require power be supplied to each thruster; however, it is important to note this configuration as a possibility.
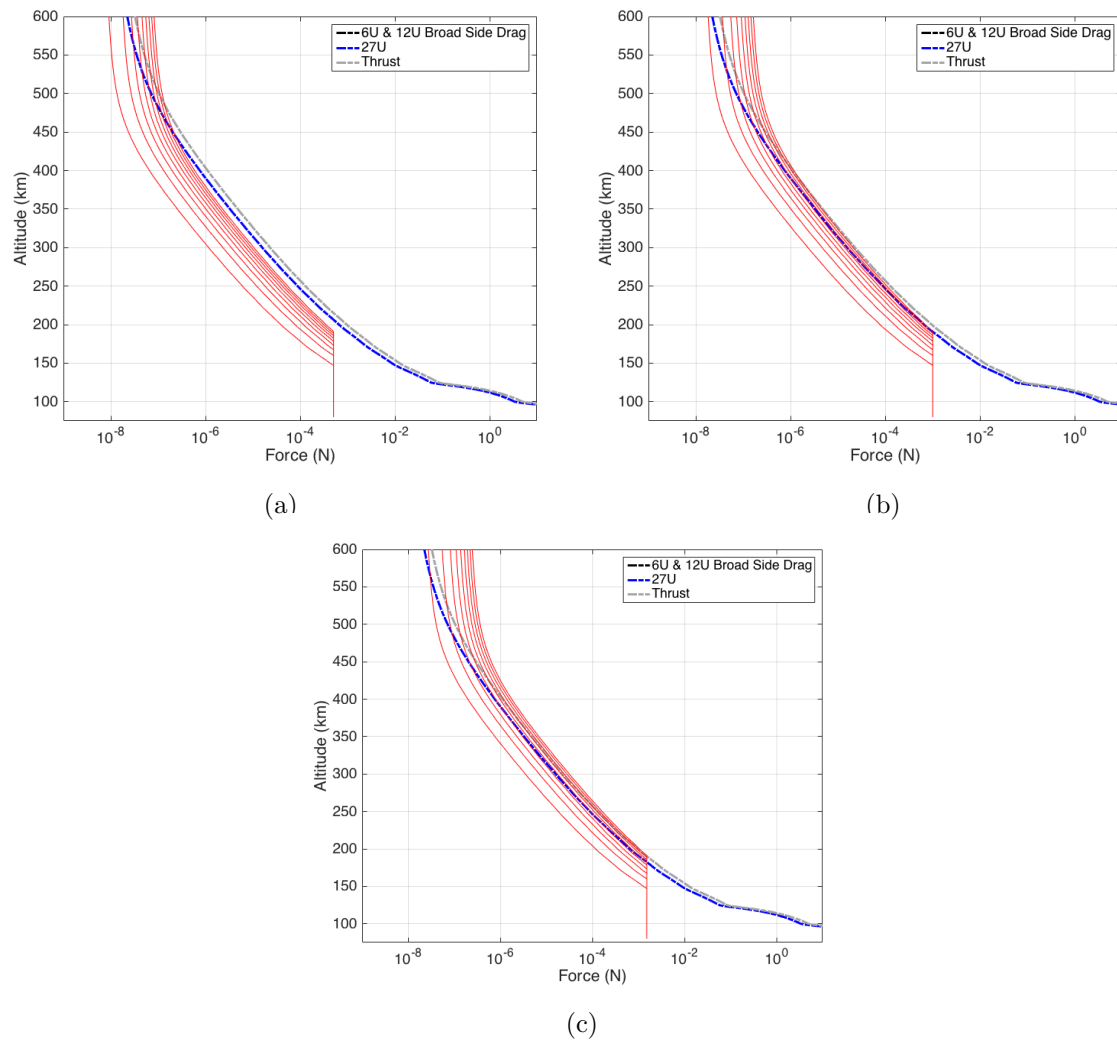
Figure 6.9: Thrust and drag for CubeSat with drag on the broadside (a) using 2 thrusters (b) using 4 thrusters (c) using 6 thrusters

Figures 6.9a through 6.9c show thrust compared to drag using 2, 4, and 6 thrusters respectively in the broadside configuration. The thrust is shown from 90% inlet efficiency to 10% inlet efficiency. Figure 6.9a shows the 6U and 12U systems would only be able to overcome drag above

450 km using 2 thrusters if the inlet efficiency is 90% or greater. With 4 thrusters, the 6U and 12U systems would require operation at 90% inlet efficiency or above to counteract drag down to ~180 km. For the 27U, it is possible to counteract drag down to ~350 km with the 4 thrusters. With 6 thrusters, the 6U and 12U CubeSat could counteract drag down to ~180 km if the inlet efficiency stays above ~50%, for the 27U the inlet efficiency would need to be above ~80%.

The following figures show the thrust to drag ratio against altitude for the variety of thrusters configurations on the 6U, 12U and 27U CubeSats. Figures 6.10c and 6.10f show the thrust to drag ratio for a 6U and 12U CubeSat using 2 and 4 thruster systems respectively with the drag acting on the broadside of the CubeSats (which for the 6U and 12U is the same area). Thrust-to-drag ratio is defined at inlet efficiencies of 90%, 50%, and 10%. Figures 6.10c through 6.10f show the thrust-to-drag ratio using 3, 4, 5, and 6 thrusters respectively at 90%, 50%, and 10% inlet efficiency. Since the 27U CubeSat is essentially a large cube, there is no difference between what has been defined here as the ram and the "broadside" configuration. The 27U CubeSat will always use the "long" configuration of the thruster; however, this graph assumes that several full thruster systems are used and not just several inlets leading into one set of accelerator grids. This is why the maximum of 6 was used because it leaves room for other subsystems and cargo.
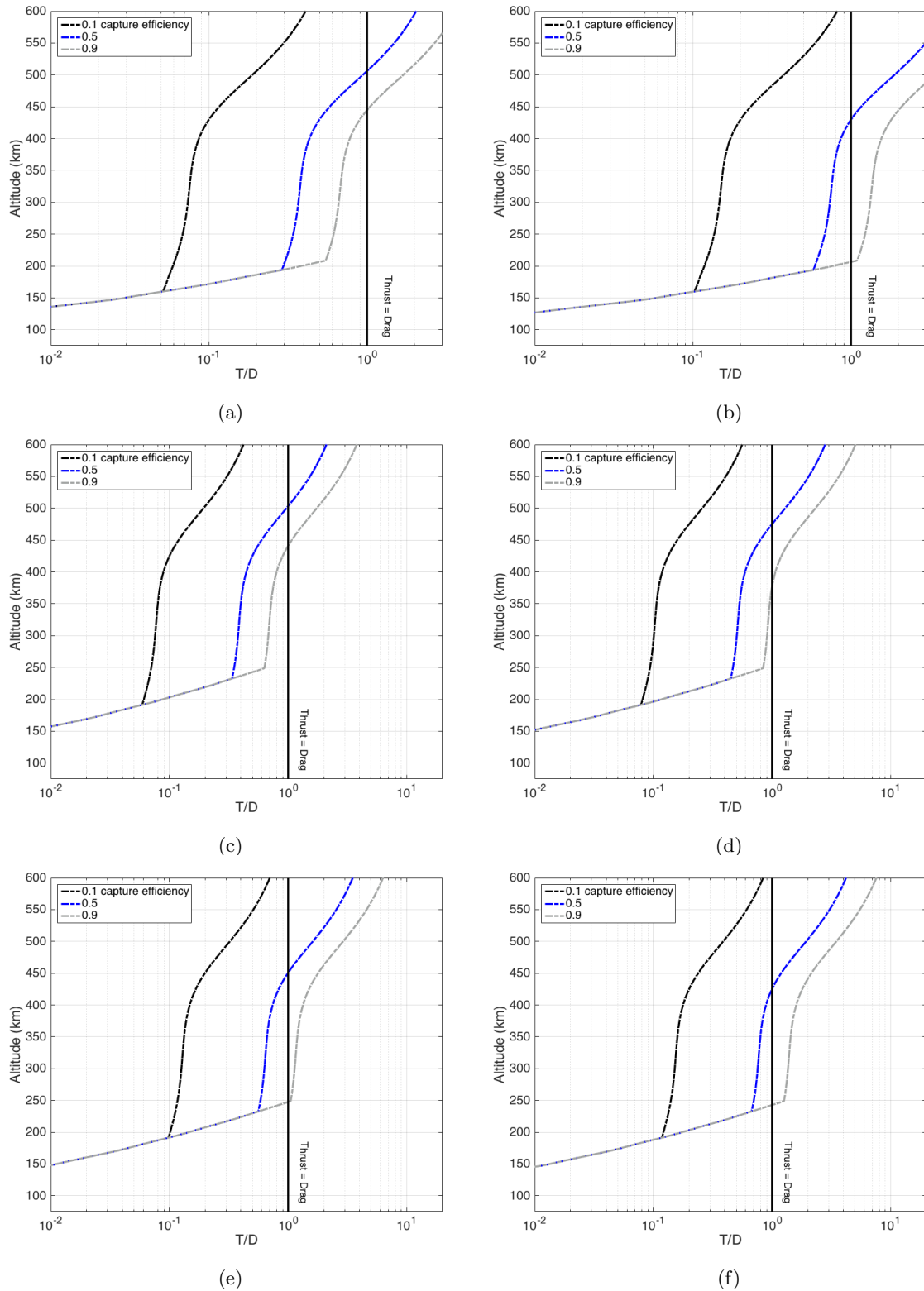
Figure 6.10: Thrust to drag ratio against altitude for CubeSat with drag on the broadside (a) 6U or 12U using 2 thrusters (b) 6U or 12U using 4 thrusters (c) 27U using 3 thrusters (d) 27U using 4 thrusters (e) 27U using 5 thrusters (f) 27U using 6 thrusters

Figures 6.10a through 6.10b show in a different way what was explained in Figures 6.9a and 6.9b. It remains clear that due to the drag increase, the thrusters are less effective in counteracting drag as the inlet contamination increases. However, this configuration is more of a solution to solve ion confinement issues than as a means to increase the thrust to drag ratio. Figures 6.10c through 6.10f show that the 27U system is only capable of counteracting drag below 250 km with 5 or more thrusters is the inlet efficiency remains close to 90%. The ion confinement will remain an issue for the 27U configuration; however, the performance was still analyzed to show the difference between a multiple inlet thruster and a multiple thruster system.

6.6   Thrust vs. Ionization Efficiency

As discussed in Chapter 5, the ionization efficiency used in the previous sections is only an estimate of the performance. The currently limited research into ionization of atmospheric particles has not provided a definitive value for the ionization efficiency of these particles. In fact it may be possible that new technology needs to be developed in order to efficiently ionize atmospheric particles in the upper atmosphere. This section therefore will analyze and discuss the effect that the ionization efficiency has on the performance of this proposed system. Here we consider the 6U CubeSat design, in the "long" configuration, with an operating voltage of 700 V, and varying the inlet capture efficiency between 10%, 50%, and 90%. The performance is analyzed at ionization efficiencies of 50%, 10%, 1%, and 0.1%.
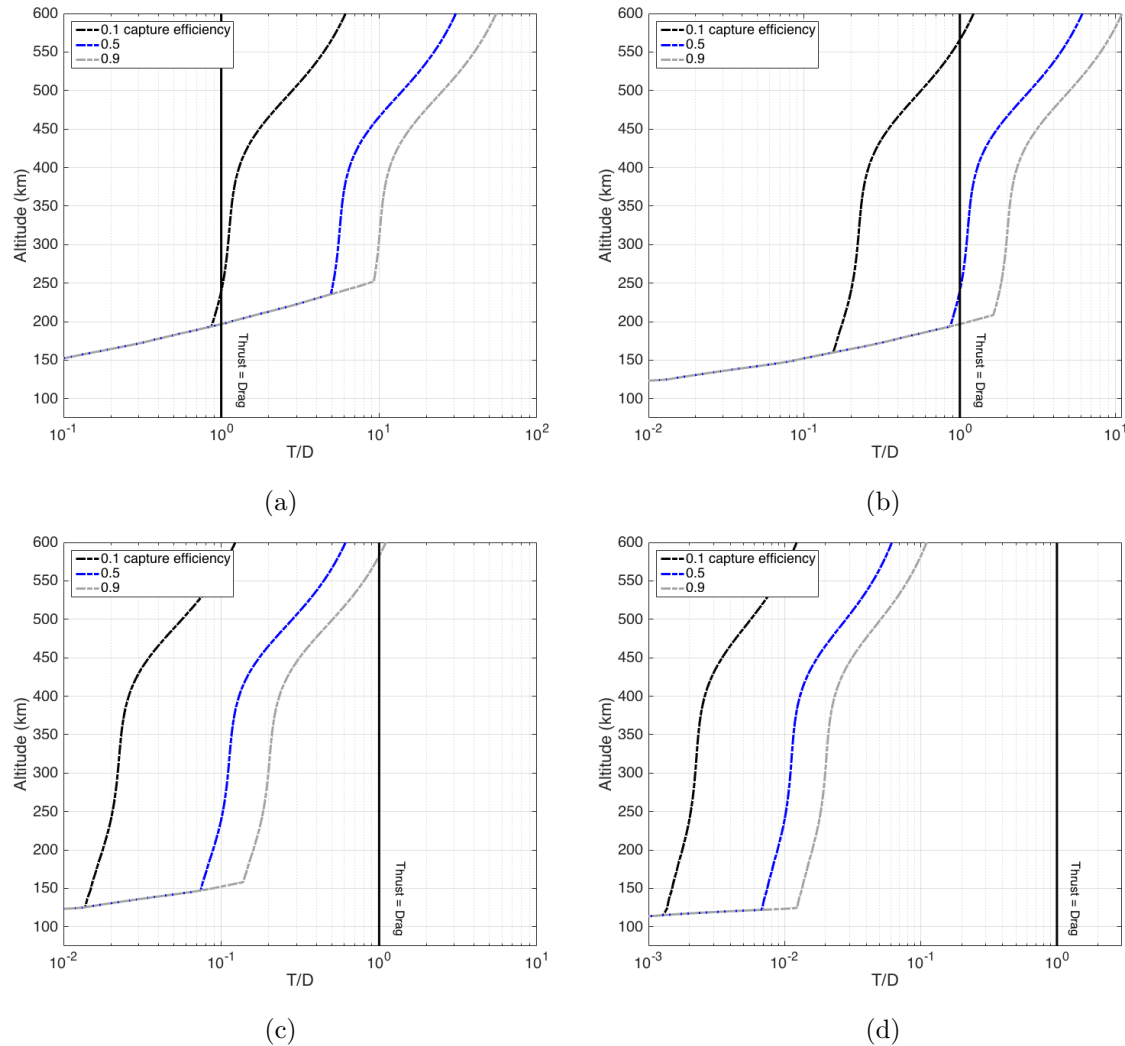
Figure 6.11: Thrust versus Drag for a 6U CubeSat for various ionization efficiencies (a) 50% ionization efficiency (b) 10% (c) 1% and (d) 0.1%

Figure 6.11a shows the thrust versus drag with 50% ionization efficiency. Here the inlet efficiency has minimal impact on the thrusters ability to overcome drag. Figure 6.11b shows the thrust versus drag with 10% ionization efficiency. At this ionization efficiency, the thruster is only effective above 200 km for drag make-up if the inlet is capable of at least 50% particle capture. Figure 6.11c and 6.11d show the thrust versus drag for 1% and 0.1% ionization efficiency. The thruster at these ionization efficiency is no longer a viable drag make-up solution for LEO orbits.

For ionization efficiencies between 10% and 50%, it can be seen that the inlet efficiency becomes an important factor in the thruster's ability to overcome drag. If the thruster is able to

ionize as well as the MiXi thruster by *Wirz* [2015] (50% ionization efficiency), the thruster will be effective from 225 km to 600 km in altitude. For ionization efficiencies greater than 50%, the inlet efficiency does not impact the thrusters ability to overcome drag, but the power will limit the altitude at which the thrust matches drag. Below a 10% ionization efficiency, this proposed thruster design will be entirely incapable of overcoming drag in LEO orbits.

6.7   Summary

The proposed air-breathing thruster system is capable of counteracting drag between 225 km and 600 km depending on the power input to the system and the ionization efficiency of the plasma generator. The ionization efficiency is the key for this proposed system to counteract drag in LEO. As the ionization efficiency decreases, the efficiency of the inlet becomes a crucial factor in counteracting drag.

At 10% ionization efficiency, this proposed air-breathing thruster is only effective between 200 km and 600 km requiring an inlet capture efficiency of no less than 50% using the "long" configuration. The total efficiency of these two system (ionization and inlet) can be no less than 5% in order for the system to be viable. Using the "short" configuration, only the 6U with 4 thrusters and the 27U with 6 thrusters are able to operate between 200 km and 600 km with less than 90% inlet efficiency. In this case, the combined efficiency of the ionization and inlet cannot be less than 9%. The power supplied to the system could increases this performance, but as shown, 10 times the power only amounts to 25–50 km in gained altitude. Obviously given Figure 6.5, that increase is not a linear trend, and power demands exponentially increase the lower in altitude operation of the thruster goes.

Chapter 7

Summary and Suggestions for Future Work

As stated at the outset of this paper, the goal is to determine the capabilities and feasibility of air-breathing systems for drag make-up in LEO when applied to CubeSats, and for an internally housed system, what the best design would be. The inlet design was addressed in Chapter 4 where a Monte Carlo based simulation was used to determine the "capture" efficiency of a nozzle. Chapter 5 addressed the intermediate step of ionizing and ion confinement to prevent degradation of the capture and ionization efficiencies. Chapter 6 took the inlet and ionization efficiencies and applied it to the overall analysis of thrust when using a CubeSat sized thruster. In this concluding chapter we discuss the results as a whole, identify the major contributions to the current knowledge base, and offer suggestions for future work.

7.1   Contributions

As an overarching achievement of this paper, analytical calculations of air-breathing thrusters for CubeSats have been provided. The amount of experimental data on air-breathing systems is limited, and so any additional data captured either by experimental means or analytical means is an improvement. The design of this thruster is also unique, and adds to further discussion on the topic how best to build an air-breathing electric thruster.

The research described in this paper provides a baseline for further analytical methods of study for air-breathing electric thrusters. This was a major objective for this paper to provide an analysis of the capability of smaller air-breathing thrusters since most applications suggested they

may only apply to larger satellites. The simple calculations for this micro-thruster system shows that the atmosphere provides enough density to overcome drag at lower altitudes for the larger CubeSat sizes. The largest limiting factor and unknown for this type of system is the ionization efficiency. Depending on the ionization efficiency, the inlet efficiency will play a crucial role. The other limiting factor to this system as stated before is the power.

The study of the inlet design showed that a parabolic shape has a capture efficiency between ~10% and ~90%. This provides the best capture percentages within the range of specular to diffuse reflection behavior for this proposed system. The ability of the parabolic shape to optically focus the incoming particles into a central point that can be varied based on length of the inlet and x^2 term modifier allow for some control of the incoming particle's behavior. The mission of the CubeSat will dictate whether it is necessary to align the focus, but the study here has focused on the optimizing the inlet while keeping it within a 1U framework.

It could be argued that under diffuse conditions, the majority of the capture is obtained from particles directly in-line with the outlet aperture of the inlet; and therefore, the additional complexity of parabolic shape outweighs those gains. However in an air-breathing system, any small increase in available particles for the system to accelerate is a gain to the performance. The gains of not having a limited on-board propellant source far outweigh these design complexities.

The addition of baffles for the parabolic shape does in fact improve the performance of the parabolic shape when the reflections are diffuse. This improvement, however, is small and the design causes degradation of the efficiency under specular reflection. The baffles increase capture efficiency by 25–38% under diffuse behavior. The question then is one of mission. The baffles would add mass, but if the mission is going to be longer, and hence experience diffuse particle behavior for a greater percentage of the CubeSat's lifespan, the increased capture efficiency might be worth the added design cost and mass of the inlet.

Previous analysis of the *Nishiyama* [2003] and *McGuire* [2001] inlets came to the conclusion that the smaller the inlet the better the capture efficiency [*Singh and Walker*, 2015]. The parabolic design discussed in this paper shows that the ratio of inlet entrance to inlet exit can be significantly

greater than one while capturing more particles than the conical design which relied on a shallow angled scoop.

Most of the previously conceived ideas for air-breathing systems have focused on externally attached or deployable air-breathing modules. The design of this proposed air-breathing thruster was built with the consideration of scalability for various sized CubeSats and hence with 1U units in mind for the components, specifically the inlet. This gives this particular air-breathing system the added benefit of modularity unlike other systems today. It should also be noted that the individual components do not use the entire 1U of volume which still leaves room for other subsystems to be placed around the components of the thruster. The modularity means versatility for the mission designers because as discussed in Chapters 5 and 6, the number of inlets can be varied or the number of full systems can be increased in order to meet thrust requirements for the mission. As noted though with any EP system, the implementation is power-limited. By how much is a question of time since the power capacity of CubeSats will increases as their need for different missions grows.

The results show that the ionization efficiency is crucial to the thruster's ability to overcome drag in LEO. A 3U version of this system would only be able to match drag above approximately 300 km if the combined efficiency of the inlet and ionization was greater than or equal to 9%. The 6U, 12U, and 27U systems in the "long" configurations are capable of counteracting drag at 200 km if the combined efficiency of the inlet and ionization remains roughly at or above 5%. Using the "short" configuration, the 6U/12U with 2 thrusters at best can counteract drag at or above 450 km if the inlet efficiency is 90%. The 6U/12U with 4 thrusters, the performance is slightly increased allowing drag make-up from ∼225 km to ∼425 km if the combined efficiency of the inlet and ionization is above 5%. For the 27U "short" configuration, the results are similar with only the 5 thruster and 6 thruster systems capable of drag make-up at or around 200 km; however, this is only if the combined efficiency of the inlet and ionization is roughly 9%.

If the ionization efficiency is 50%, the performance is greatly improved with the 6U "long" configuration system capable of matching drag at ∼200 km with only 10% inlet efficiency. If the

ionization efficiency is less than or equal to 1%, the thruster becomes unable to counteract drag in LEO orbits, and therefore, not a viable solution for CubeSat applications.

This proposed systems shows promise as an air-breathing electric CubeSat thruster; however, this is strictly dependant upon the ionization efficiency of plasma generator and the contamination rate of the inlet surface. Further research into ionization of atmospheric particles will determine if this system truly is a viable CubeSat propulsion system.

7.2   Future Work

Giving all that was accomplished here in this work, there is still plenty of work to be done regarding this subject, and especially as it relates to this concept that will only make its use more feasible for future missions.

7.2.1   Ion Confinement

The ion confinement was briefly discussed in this paper partially due the complexity of the topic in general. There are many ways to manipulate ions and plasmas. The Penning trap proposed in this paper with the additional electric field is a simple answer to perhaps a complex issue. Questions arise on how exactly to implement this idea. The inlet was the first critical piece of the design to study, but this in no way diminishes the importance of the ion confinement. As stated before without the ion confinement, the particle capture within the channel leading to the accelerator grids would degrade significantly. As such if the work were to continue and this design built, a proper analysis of the electric/magnetic field structure would need to be completed. Also it is entirely possible that the proposed solution may in fact be less practical than other methods of ion confinement. In which case, other means would need to be analyzed with the one proposed here.

There is in fact work being done on ion thrusters that use electrostatic ion confinement strictly as a means of ion acceleration, a unique approach that does not require accelerator grids

Miley and Murali [2014]. Further analysis of this technology might lead to a revised design of the proposed system or air-breathing systems in general.

7.2.2   Compression of the Propellant

The literature review on this topic shows that compression will advance the air-breathing electric thruster technology. The past 20 years of research in this area has not seemed to address this, and although a limited form of compression is assumed to occur within this system due to the nature of the inlet, there is room for improvement. The answer is perhaps tied to the ion confinement within the channel. If the ions can be not only radial confined, but perhaps, radially compressed by way of the magnetic fields, there would be an increase in thruster performance. As noted by [*Singh and Walker*, 2015]:

> Turbopumps are major components of liquid rocket engines and have similar design features to turbomolecular pumps. However, an integrated compression and lique-faction system which can reliably and efficiently operate completely in space-like conditions, survive launch loads, and provide the necessary level of compression remains to be demonstrated.

7.2.3   Gas-Surface Interactions

To advance this research further, it will be necessary to characterize the rate at which the surface of the inlet becomes contaminated with oxygen. A study of the materials used for the inlet (and possible the other systems as well) would have allowed for a timeline of thrust to be shown, and performance of the system over time to be derived. It is simple enough to state that the parabolic inlet shape will improve capture over other shapes, but it is desirable that the system stay within the quasi-specular region for as long as possible if contamination is going to occur. This rate of contamination could be mitigated by using the proper materials and/or surface coatings.

7.2.4   Surface contamination

Obviously, a major issue the air-breathing electric thruster system faces is the ability to control the propellant source. Although readily available, it's in a difficult state to capture its full potential so to speak. The issue of diffuse reflection on the inlet surface is just another issue of control. The oxygen contamination of the surface leads to the diffuse reflections. Although there may not be an immediate or foreseeable solution to this problem, for the sake of science, it feels necessary to suggest that further study should be done into a way to decontaminate a surface of oxygen. This in itself would definitely comprise an entire body of research, and would not lend itself to being coupled to the area of air-breathing systems. The solution to this problem alone would have far-reaching effects to the aerospace sciences.

7.2.5   Atmospheres of Other Planets

For the moment, the concern of air-breathing electric thrusters is how they operate in Earth's atmosphere. It most definitely would be advantageous to characterize this system with respect to Mars and other planets. Perhaps in doing so it would lead to solutions and improvement that would not have been considered by only looking at this system for Earth-centric applications.

Bibliography

Burkhardt, H., M. Sippel, G. Krille, R. Janovksy, M. Kassebom, H. Lübberstedt, O. Romberg, and B. Fritsche (2002), Evaluation of propulsion systems for satellite end-of-life de-orbiting, in *38th AIAA/ASME/SAE/ASEE Joint Propulsion Conference & Exhibit*, no. 4208 in 2002.

Busek Space Propulsion and Systems (2014), Ion thrusters, website, doi:March2017, `http://www.busek.com/technologies__ion.htm`.

Cara, D. D., J. G. del Amo, A. Santovincenzo, B. C. Dominguez, M. Arcioni, and I. R. A. Caldwell (2007), Ram electric propulsion for low earth orbit operation: an esa study, in *The 30th International Electric Propulsion Conference*.

Choueiri, E. Y. (2004), A critical history of electric propulsion: The first 50 year (1906-1956), *Journal of Propulsion and Power*, *20*(2), 193–203.

Clausing, P. (1971), The flow of highly rarefied gases through tubes of arbitrary length, *Journal of Vacuum Science & Technology*, *8*(5), 636–646.

Conley, B. R. (1995), Utilization of ambient gas as a propellant for low earth orbit electric propulsion, Master's thesis, Massachusetts Institute of Technology.

Cook, G. E. (1965), Satellite drag coefficients, *Planetary and Space Science*, *13*, 929–946.

Diamant, K. D. (2010), A 2-stage cylindrical hall thruster for air breathing electric propulsion, in *46th AIAA/ASME/SAE/ASEE Joint Propulsion Conference & Exhibit*, no. 6522 in 2010.

Dressler, G. (2006), Spacecraft propulsive device using ambient upper atmospheric constituents for reaction mass, in *42nd AIAA/ASME/SAE/ASEE Joint Propulsion Conference & Exhibit*, no. 4650 in 2006.

Faber, D. (2013), Nanosatellite deorbit motor, in *27th Annual AIAA/USU Conference on Small Satellites*, 2013.

Goebel, D. M., and I. Katz (2008), *Fundamentals of Electric Propulsion: Ion and Hall Thrusters*, JPL Space Science and Technology Series, John Wiley & Sons, Inc.

Hedin, A. E. (1991), Extension of the msis thermosphere model into the middle and lower atmosphere, *Journal of Geophysical Research*, *96*, 1159–1172.

Hevner, R., W. Holemans, J. Puig-Suari, and R. Twiggs (2011), An advanced standard for cubesats, in *25th Annual AIAA/USU Conference on Small Satellites*, 2011.

Institute for Space Travel Systems, University of Stuttgart (2016), Magnetoplasmadynamische triebwerke, website, doi:March2017, `http://www.irs.uni-stuttgart.de/forschung/elektrische_raumfahrtantriebe/triebwerke/mpd-tw/fremdfeldbeschl-tw/mpd-afmpd.html`.

Ito, T., N. Gascon, W. S. Crawford, and M. A. Cappelli (2006), Further development of a micro hall thruster, in *42nd AIAA/ASME/SAE/ASEE Joint Propulsion Conference & Exhibit*, no. 4650 in 2006.

Kantha, L. (2017), *Rocket and Spacecraft Propulsion*, TBD, TBD.

Kersevan, R., and J.-L. Pons (2009), Introduction to molflow: New graphical processing unit-based monte carlo code for simulating molecular flows and for calculating angular coefficients in the compute unified device architecture environment, *Journal of Vacuum Science & Technology A: Vacuum, Surfaces, and Films*, *27*(4), 1017–1023.

King, S. T., M. L. Walker, and S. G. Chianese (2014), Atmospheric electric propulsion mission performance tool, *Journal of Spacecraft and Rockets*, *51*(3), 931–937.

Kriesch, A. (2006), Pennig trap, website, doi:March2017, `https://en.wikipedia.org/wiki/Penning_trap#/media/File:Penning_Trap.svg`.

Kunda, P. K., and I. M. Cohen (2008), *Fluid Mechanics*, 4th ed., Academic Press.

Lücking, C., C. Colombo, and C. McInnes (2012), Solar radiation pressure augmented deorbting from high altitude sun-synchronous orbits, in *The 4S Symposium*, 2012.

Matney, M. (2013), An electric propulsion shepherd for active debris removal that utilizes ambient gas as propellant.

McGuire, T. J. (2001), Aero-assisted orbital transfer vehicles utilizing atmosphere ingestion, Master's thesis, Massachusetts Institute of Technology.

Miley, G. H., and S. K. Murali (2014), *Inertial Electrostatic Confinement(IEC) Fusion*, Fundamentals and Applications, Springer.

Moe, K., and M. M. Moe (2005), Gassurface interactions and satellite drag coefficients, *Planetary and Space Science*, *53*, 793–801.

NASA (2014), Launch services program program level dispense and cubesat requirements document, download from vendor site, doi:December2016, `https://www.nasa.gov/pdf/627972main_LSP-REQ-317_01A.pdf`.

NASAexplores (2013), Propulsion systems of the future, website, doi:April2017, `https://www.nasa.gov/vision/space/travelinginspace/future_propulsion.html`.

Nishiyama, K. (2003), Air breathing ion engine concept, in *54th Inernational Astronautical Congress of the International Astronautical Federation, the International Academy of Astronautics, and the International Institute of Space Law*, 2003.

NOAA (2017), *Recent Solar Indices*, doi:March2017, `ftp://ftp.swpc.noaa.gov/pub/weekly/RecentIndices.txt`.

Oltrogge, D. L., and K. Leveque (2011), An evaluation of cubesat orbital decay, in *25th Annual AIAA/USU Conference on Small Satellites*, 2011.

Pardini, C., W. K. Tobiska, and L. Anselmo (2006), Analysis of the orbital decay of spherical satellites using different solar flux proxies and atmospheric density models, *Advances in Space Research*, *37*, 392–400.

Pekker, L., and M. Keidar (2012), Analysis of airbreathing hall-effect thrusters, *Journal of Propulsion and Power*, *28*(6), 1399–1405.

Picone, J. M., A. E. Hedin, D. P. Drob, and A. C. Aikin (2002), Nrlmsise-00 empirical model of the atmosphere:statistical comparisons and scientific issues, *Journal of Geophysical Research*, *107*, 1468.

Pigeon, T. D., and R. B. Whitaker (2004), Analysis of a near-vacuum hall thruster, in *42nd AIAA Aerospace Sciences Meeting and Exhibit*, no. 127 in 2004.

Pilinski, M. (2008), Analysis of a novel approach for determining atmospheric density from satellite drag, Master's thesis, University of Colorado Boulder.

Romano, F. (2013), System analysis and test bed for an air-breathing electric propulsion system, Master's thesis, University of Stuttgart.

Schönherr, T., K. Komurasaki, F. Romano, B. Massuti-Ballester, and G. Herdrich (2015), Analysis of atmosphere-breathing electric propulsion, *IEEE Transactions on Plasma Science*, *43*(1), 287–294.

Shabshelowitz, A. (2013), Study of rf plasma technology applied to air-breathing electric propulsion, Ph.D. thesis, University of Michigan.

Sharipov, F. (2006), Rarefied gas dynamics and its applications to vacuum technology.

Singh, L. A., and M. L. Walker (2015), A review of research in low earth orbit propellant collection, *Progress in Aerospace Sciences*, *75*, 15–25.

Slough, J., and D. Kirtley (2015), Pulsed plasmoid propulsion: The elf thruster, in *The 31st International Electric Propulsion Conference*.

Vallado, D. A., and D. Finkleman (2008), A critical assessment of satellite drag and atmospheric density modeling, in *AIAA/AAS Astrodynamics Specialist Conference*.

Voss, H. D., J. F. Dailey, W. A. Bauson, and B. Chapman (2015), Nano-satellites and harp for student learning and research, in *122nd ASEE Annual Conference & Exposition*, 2015.

Wirz, R., J. Polk, C. Marrese, J. Mueller, J. Escobedo, and P. Sheehan (2001), Development and testing of a 3cm electron bombardment micro-ion thruster, in *International Electric Propulsion Conference*, 2001.

Wirz, R. E. (2015), Miniature ion thrusters: A review of modern technologies and mission capabilities, in *Joint Conference of 30th ISTS, 34th IEPC and 6th NSAT*, 2015.